Leveraging the Power of Droplet Microfluidics to Profile the Epigenome

by

Gloria Diaz

A dissertation submitted in partial fulfillment
of the requirements for the degree of
Doctor of Philosophy
(Chemistry)
in the University of Michigan
2023

Doctoral Committee:

Professor Ryan C. Bailey, Chair
Professor Julie Biteen
Professor Robert T. Kennedy
Associate Professor Kristin Koutmou

Gloria E. Diaz

gleldiaz@umich.edu

ORCID iD: 0000-0002-4164-6567

Dedication

This dissertation is dedicated to the little girl that wasn't afraid to ask where we could find the spoons.

Acknowledgements

I thank my committee members for their guidance through these projects. I would also like to thank the Rackham Graduate School for awarding me the Rackham Merit Fellowship, which funded me for the first two and a half years of graduate school (tuition and monthly stipend), as well as the travel grants that allowed me to attend Pittcon and the Bioanalytical Sensors Gordan Research Conference. Being awarded these fellowships was a significant accomplishment for me. I would also like to thank the financial support from the National Science Foundation through Grant 1921677 for the epigenetic projects I worked on.

I would like to express my appreciation to my advisor Prof. Ryan Bailey. You have challenged me, and I am a stronger scientist for that. I would also like to thank the other members of my committee, Professor Robert T. Kennedy, Professor Julie Biteen, and Associate Professor Kristin Koutmou. I am also very thankful to Assistant Professor Kaushik Ragunathan, previously at the University of Michigan and now Brandeis University, for all his contributions to the DropCUTT project, but also all his guidance and advise in my development as a scientist.

Many thanks to past and present Bailey lab members. Dr. Yi Xu, thank you for your early guidance and friendship. Your mentorship had meant so much; if it weren't for you, I wouldn't have rediscovered my love for anime. Dr. Cole Chapman, thank you for being desk mates with me and for listening to all my research woes as well as other dramatic stories throughout the years. Dra. Mari Cardenosa, Dr. Heather Robinson, and Dr. Steven Doonan, I am thankful to you all for helping me grow and mature as a scientist and individual**.** I can't thank the current Bailey lab members enough. Nico, I couldn't have done this without you. Thank you for always being

willing to answer. Even when I felt silly asking, you welcomed them. Claire, thank you for always having my back. More than anything, I appreciate your friendship. I will miss game nights with you and Jack. Krista, you are beyond brilliant, and I am so thankful to have learned so much from you. Also, thanks for being the best #GRCRoomie ever! Marina, I could not be more grateful for all our random conversations over the last two years and how you were always willing to listen to me be excited about the silliest things. Thank you for all your sarcastic humor. Nick, you are a rock, and I am inspired by how nothing phases you. I will miss discussing the latest Marvel movies with you. Sam, not going to lie; you are my favorite undergrad.

To my CSUSM professors – While there is an incredible number of individuals from Cal State San Marcos that were always supportive, three professors deserve special mentions. In my junior year of college, I had Dr. Steven Tsui as my physics professor. He saw that I was passionate about learning, maybe not specifically physics, but he appreciated my work ethic. Dr. Tsui, thank you for introducing me to Rachel and for helping me take the beginning steps forward in my chemistry career. Iafe, words cannot express my gratitude. Thank you for believing in me so much that I started to believe in myself. Working with you was my introduction to research. I wouldn't have gotten this far without your guidance, support, and all the cathartic axe throwing. While I did pursue a Ph.D. in organic chemistry, I still carry a lot of your initial lesson, whether that be lab etiquette or how to hold yourself in a professional setting. I am thankful you saw so much potential in me. Next, Elinne. Before meeting you, I had a very narrow view. I only wanted to pursue chemistry as my career and nothing else. You showed me another way. Thank you for expanding my views as a scientist and challenging me to be more. Thank you for inspiring me daily at Zymo and pushing me to apply to Ph.D. programs. Thank you to these three professors for cultivating my direction.

To my family - I love you all. Thank you for putting up with me through high highs and low lows. Mamá, gracias por todo. Desde que era chiquita me dijiste ‘estudia’ y bueno aquí estoy todavía estudiando. Gracias por todas las pláticas, gracias por simpre tener una casa a la que puedo ir a estar en familia. Gracias por siempre recordarme que no importa cuánto tiempo tome, lo que importa es terminar. Papá, gracias por todo tu cariño. Gracias por siempre apoyarme en todos mis sueños y recordarme que si puedo. Gracias a los dos por ser un ejemplo de lo que es salir adelante. To my brother Jesus, we have grown so much as individuals in the last five years. I'm genuinely jealous of how much you have traveled the world in that time; I have to catch up. Thank you for your support, for believing in me, and for doing everything in your power to be there in person. Thank you to you and Andrea for being an example of what it means to be responsible adults and happy parents. To my niece Aria, it's crazy to think how much you can love a human for simply existing. To my partner Mark. I definitely did not make things easy for you. You definitely met me at a crazy time in life, and probably one of my most insecure periods. I thank God and the world that you didn't give up on me. I hate the idea of having to go through graduate school without you. Thank you for all your love, compassion, and patience. And of course, the food. My pallet of tastes has expanded immensely because you have shown me to experience food differently. I love you. I can't wait to go wine tasting with you in California and drink coffee with you in France once this is all over. Sokka, while I know you love Mark more than me, thank you for letting me hold you when I needed kitty snuggles.

Thank you to all of you for understanding that this career path is an investment.

Table of Contents

List of Tables

List of Figures

List of Equations

List of Appendices

Abstract

The human epigenome is a vast genome-wide body of proteins, chemical structures, and nucleic acids that orchestrate mechanistic gene regulation. Monitoring epigenetic modifications as biomarkers can be beneficial in clinical settings to track disease development and diagnose patients with certain conditions. Conventional methods for surveilling the epigenome are chromatin and epigenetic profiling assays that probe for chromatin segments where specific epigenetic modifications are localized. These assays incorporate next-generation sequencing (NGS) which outputs a wealth of information. While epigenetic assays are clinically relevant and generate large sets of data, their utility is mostly constricted to research settings because they require skilled technicians to perform the intricate steps as well as an abundant cell population, rendering them impractical for profiling in small, or rare, clinical samples. In order for screening of the epigenome to be systematically implemented in clinical and diagnostic settings, profiling assays must become automated to be reliable, reproducible, and operatable by non-experts. Herein, we describe work completed to automate three profiling assays, ChIP-Seq, CUT&RUN, and CUT&Tag.

Chromatin Immunoprecipitation with sequencing (ChIP-seq) is the gold standard for identifying loci associated with a specific target of interest, such as transcription factors or histone tail modifications. In collaboration with the Mayo Clinic's Epigenetic Translation Program, this thesis presents consecutive droplet microfluidic modules that address different sections of the conventional protocol to automate ChIP-Seq. Our initial microfluidic module simultaneously lysis whole cells, enzymatically digests chromatin to nucleosomal length, and

delivers antibody functionalized magnetic beads that target the epigenetic mark of interest. The second microfluidic module focuses on washing the magnetic beads with the bound target of interest through a co-flow of four distinct wash buffers. Our current work is aimed at demonstrating the versatility of the droplet integrated ChIP system by optimizing the workflow to profile a diverse range of histone tail modifications. Using quantitative polymerized chain reactions (qPCR) and calculating ΔΔCt for a positively and negatively associated gene, we demonstrate effective enrichment of histone tail modifications through our droplet integrated ChIP system.

Enzymatic tethering assays, CUT&RUN and CUT&Tag, identify genomic sequences associated with targets of interest, such as chromatin proteins and histone tail modifications. Low-cost, high-resolution methods, like CUT&Tag, are the techniques needed in clinical and medical research. However, improved automation would allow for higher throughput processing. This thesis presents droplet microfluidic platforms for CUT&RUN and CUT&Tag (DropCUTT), capable of permeabilizing whole cells, extracting nuclei, attaching magnetic beads, and assembling a multi-unit immunoprecipitation construct to identify genetic regions of interest, all in droplets. This expands our lab's droplet microfluidic toolbox by reconfiguring a previously published microfluidic module to condense incubation steps and decrease the amount of manual pipetting steps, all reducing user variation. This semiautomated procedure supports a range of whole-cell inputs (250K-10K cells per sample) while yielding quality tagmented DNA fragments. Preliminary sequencing data confirms accurate genomic profiling of the target of interest, H3K27me3, using the condense assay.

Taken together, the work described in this thesis begins to solve some of the main challenges for integration of epigenetic assays into clinical settings. We fully automated the

conventionally manual ChIP-Seq procedure and developed microfluidic platforms for CUT&RUN and CUT&Tag that decrease the required cell inputs and condenses protocol steps. In summary, this work expands the epigenetic profiling field by providing methods and microfluidic modules to decrease user variation and required sample input.

Chapter 1 : Introduction

1.1 Epigenetics

The term ***epigenesis*** dates back in the English language to the 17th century. In this word, the initial idea of cell differentiation is established[1]. It wasn't until the 1940s that C.F. Waddington coined the word ***epigenetics***[2], but the term in its modern meaning wouldn't begin to surface until half a century later[3]. In December of 2008, in a meeting at Cold Spring Harbor, a definition for epigenetics was finalized[4] - "An epigenetic trait is a stably heritable phenotype resulting from changes in a chromosome without alterations in the DNA sequence." The word epigenetic includes the prefix 'epi', meaning in addition to[5], demonstrating that this field goes beyond the genome to explain phenotypic differentiation. DNA exists as a double-stranded helix that coils around a histone octamer (H3, H4, H2A, and H2B) to form the nucleosome[6]. The basic packaging unit is often described as 'beads on a string'[7] due to the visual of string-like DNA wrapped around and connecting many bead-like histones. The repeated nucleosome units continue to stack onto one another to form chromatin, and through additional folding, the familiar chromosome[8] is constructed. This hierarchical folding is what allows 6.5 feet of DNA to be folded into the nucleus of the eukaryotic cell.

Chromatin can either be packaged into heterochromatin or euchromatin. Heterochromatin is characterized by dense folds that are transcriptionally inactive. Conversely, euchromatin is characterized by loosely packaged folds with frequent opportunity for transcriptional activity[9]. Despite the degree of folding, epigenetic modifications persist throughout the genome to regulate gene expression. The epigenome is a genome-wide body of proteins, chemical structures, and

nucleic acids that modify chromatin without changes to the genomic sequence. These modifications facilitate an array of functionalities and consist of DNA methylation, histone tail modifications, nucleosome positioning/chromatin accessibility, chromatin structure, and non-coding RNAs. Cellular identity is powered by the epigenetic code these modification construct.

Epigenetic modifications serve as biomarkers to monitor and understand disease development and patient diagnostics within clinical and medical settings. There is a growing understanding that alterations to the epigenome along with chromatin abnormalities can be associated with cancers[10], such as prostate[11], and disorders, such as post-traumatic stress disorder[12]. Epigenetic modifications are attractive as biomarkers because they connect the gap between lifestyle and environment to disease development on a molecular level[13]. They can be detected reliably and with pronounced sensitivity in individual cells as well as populations. The most reliable epigenetic biomarker is CpG methylation due to the reliability and robustness of bulk DNA methylation assays[14]. This specific modification occurs within DNA sequences where cytosines are followed by guanine in a repeated pattern and the cytosines are methylated to form 5-methylcytosine. The FDA approved a colorectal cancer screening test that identifies CpG methylation at gene promoter sites (vimentin (VIM)[15], BMP3[16], NDRG4[16], and septin (SEPT9)[17]) in stool and blood samples. Additionally, in individuals with Type 2 Diabetes and obesity, monitoring of CpG methylation in adipose tissue revealed a change in more than 7,000 genes after participating in a 6-month exercise program[17]. While there is extensive research into DNA methylation as a biomarker, histone tail modifications have been recently identified as a reliable epigenetic biomarkers[18].

Histone tail modifications (HTMs) are a post translational modification (PTM) that occurs on the N-terminal tails of the core histones. PTMs can also occur on the

surface of the nucleosome and influence structural fold when in contact with chromatin [19]. Various HTMs exist, but the commonly studied ones include methylation[20], acetylation[21], phosphorylation[22], and ubiquitination[23]. Dysregulation of HTMs can affect gene expression and play a role in tumorigenesis[24]. For example, in diffused intrinsic pontine gliomas (DIPG), aggressive brain tumors located at the base of the brain, nucleotide alterations result in H3.3K27M modifications, that is a methylation occurring at the 27th lysine of histone 3, leading to further decreases in H3K27me3 HTM and increases in H3K27ac[25] HTM. Identifying the connection between HTM and tumorigenesis has allowed for the development of new screening techniques and methodologies. For instance, HTMs are being used for cancer profiling using circulating free cell nucleosomes[26]. When cells undergo apoptosis, they release nucleosomal DNA fragments into the bloodstream. In advanced cancer patients, higher amounts of circulating free cell nucleosomes are present, and through HTM patterns, cell type origin can be identified[27]. Specifically, decreases in H3K27me3 and H4K20me3 have been observed in advance cancer patients. Through HTM profiling, there is potential to seize the use of invasive biopsy extraction.

1.2 Profiling the Epigenome

Chromatin and epigenetic profiling assays yield insight into the various epigenetic modifications orchestrating transcriptional regulation. A plethora of diverse genome-wide profiling assays exist and predominantly utilize Next-generation sequencing (NGS) for analysis.[28] NGS assays are highly sensitivity, provide enhanced resolution between target regions and produce an abundance of insightful information that has changed the types of questions being asked. While there is a variety of assays to profile different epigenetic modifications, these assays follow a standard routine of (1) gaining access to the genome by enzymatic or chemical means, (2) separating the chromatin segments of interest, and (3) detection through NGS to identify genomic fragments associated with the epigenetic target of interest[29]. The increased utility of these assays within research has brought about data congregations like NIH Roadmap Epigenetic Mapping Consortium[30], ENCODE Consortium[31], BLUEPRINT epigenome project[32], and International Human Epigenome Consortium[33]. Initial iterations of profiling assays required large cellular input amounts and current research has progressed towards lowering cellular inputs. This is crucial because large cell amounts are not amenable to all clinical settings. This limitation motivates the development of assays that function at lower cellular amounts. Next, we will survey four epigenetic targets of interest commonly utilized in epigenetic research and their accompanied profiling assays.

DNA Methylation: A direct chemical modification to DNA structure is the addition of methyl functional groups to the 5' position of cytosines. DNA methylation affects chromatin activity by repressing gene transcription when methylation is located on the gene promoter[34]. The addition of methylation to DNA is added by DNA methyltransferases (DNMT)[35] while removing these functional groups is done through the ten-eleven translocation enzyme (TET)[36]. Methylation

patterns differ depending on cell identity, and generally, profiling of DNA methylation is done through whole genome bisulfide sequencing[37]. It works by converting unmethylated cytosines to uracil, and uracil is converted to thymine through PCR amplification for sequencing library preparation. After sequencing and alignment to a reference genome, thymines depict unmethylated cytosines, and unconverted cytosine persists as chemical alteration. This profiling method is considered the gold standard and has the advantage over other methods of generating profiles at base pair resolution. Additionally, the input requirement is significantly low, at about 3,000 cells per sample. This demonstrates why DNA methylation is a significantly reliable epigenetic biomarker.

Chromatin Accessibility & Nucleosome Positioning: Transcriptionally active chromatin regions tend to be associated with accessible genome areas where nucleosomes are depleted[38], or chromatin is unwound (nucleosome breathing), [39] giving way to transcriptionally active proteins and polymerases. Profiling of accessible segments started by using DNase 1 to cut exposed genomic regions (DNase 1 hypersensitive sites). Initially, the analysis method was through southern blotting[40], then RT PCR[41], microarray[42], and finally sequencing[43]. The intensity of DNase 1 cleavage, due to the varied presences of regulatory factor, generated footprints to assess the residency of transcription factors[44] quantitatively. Following the development of DNase-seq, FAIRE-seq[45] (Formaldehyde-Assisted Isolation of Regulatory Elements) was developed to profile accessible regions and access distal regulatory regions DNase-seq could not reach. This is because instead of using an enzyme to digest the genome, it first crosslinks samples and shears chromatin through sonication. Another notable assay is ATAC-seq[46] (transposase accessible chromatin), which is described in chapter four. Lastly, an indirect method that profiles accessible regions but focuses explicitly on profiling nucleosomes is MNase-seq[47]. This assay uses the

endo-exonuclease micrococcal nuclease to digest linker DNA between nucleosomes and yield average nucleosome occupancy. Profiling chromatin accessibility yields insight into transcriptionally active regions genome wide. However, additional insight is required to observe how these regions interact and influence transcriptional regulation.

***Chromatin Architecture*:** Abnormalities in chromatin structure and topology can lead to consequential regulation. Chromatin territories[48], constructed by 3-dimensional folding in the nucleus, consist of both actively and inactively transcribed areas. To observe special formations and interactions, chromosome conformation capture techniques (3C: One-to-one[49], 4C: one-to-many[50], 5C: Many-to-many[51]) can be implemented. Similarly, Hi-C (All-to-all) generate unbiased topological maps of all genome-wide interactions[52]. The procedure for this assay begins by crosslinking cells to enhance interactions and digest chromatin using a restriction enzyme. Fragments with a 5' overhang are biotinylated, isolated using streptavidin beads, and sequencing libraries are constructed. This assay has emphasized the importance of epigenetic topology maps specific to tissue and cell types, as well as throughout different disease states. One step further is the assay ChIA-PET (chromatin interactions mediated by paired-end tag sequencing)[53], focused on identifying interactions of targeted transcription binding sites and promoters. Like Hi-C, cells are crosslinked to strengthen proximal interactions, chromatin is sonicated, and samples are enriched for a target of interest. Biotinylated linkers are then ligated, and interactive segments are isolated using streptavidin. Observing the special organization of DNA within the nucleus advances insight into genomic regulation by identifying and quantifying interactions between distal loci.

Histone Tail Modifications: The benchmark assay for probing genomic regions associated with a specific histone tail modification is chromatin immunoprecipitation with sequencing (ChIP-

seq)[54]. The protocol requires cells to be lysed and digested, followed by target selection via antibody capture, sample washing, and finally analysis through qPCR or sequencing. However, the limitations of ChIP include large cellular input (10^6-10^7 cells), user variability, laborious tasks, and time consumption (at least four days)[55]. In recent years, enzymatic tethering assays have taken center stage for profiling the localization of histone tail modifications. Target specific mapping is provided by genetically engineering a fusion protein to an enzyme, attaching the enzyme to a target of interest, and having the enzyme implement a modification on the surrounding landscape[56]. Unlike ChIP, these enzymatic tethering assays have significant benefits, including flexible sample input (5,000 – 500,000 cells) depending on the target and cell lines used, high signal-to-noise ratio, and minimal background noise. An in-depth explanation of these assays is to follow in chapters three and four.

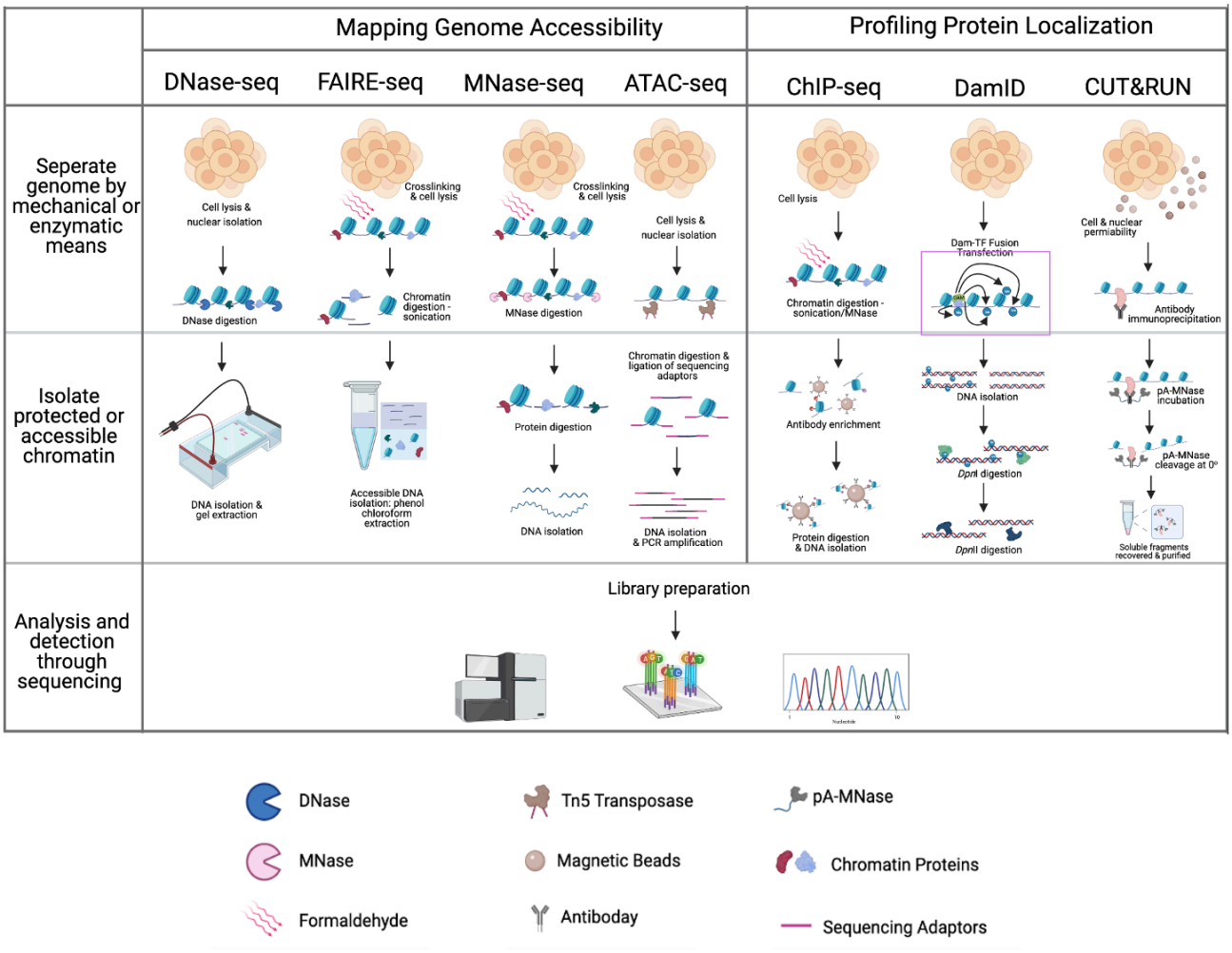

Figure 1.1: Chromatin and epigenetic profiling assays follow a standard assembly procedure (1) gaining accessibility to the genome (2) probing for the chromatin segments of interest (3) analysis through next-generation sequencing (NGS).

1.3 Microfluidics

The field of microfluidics deals with the control and manipulation of fluids within microchannels[57]. This field aims to uncover novel fluidic behaviors and develop innovative miniature devices to understand how fluidic characteristics differ at the sub-milliliter scale compared to macroscale dimensions. First, microfluidic systems have laminar flow because of the low Reynolds number (eq. 1.1), which compares viscous and inertial forces.[58] Developing investigative tools utilizing microfluidics has the benefits of reducing sample volumes, decreasing reagent costs, increasing potential for high throughput parallel processing, and improving uniformity across sample handling.

$$Re = \frac{\rho v \mathcal{L}}{\mu} \tag{1.1}$$

The idea of miniaturizing lab processes onto a microfluidic chip began when Stephen Terry developed a scaled down gas chromatography system onto a silicone wafer[59]. Andreas Manz followed by introducing the concept of a miniature total analysis system (μTAS), which allowed for parallel processing with efficient and fast sample separation through electrophoresis and chromatography[60]. Since then, microfluidic technologies have impacted and even revolutionized research areas like high sensitivity micro reactors[61], single cell analysis[62], drug delivery/screening[63], point of care diagnostics[64], organ mimetics[65], and organic synthesis[66].

Droplet microfluidics is a subsection of this field that breaks the continuous flow of an aqueous stream into droplets using oil as the carrier phase[67] and is stabilized by surfactants[68]. The monodisperse droplets can range in micro to femtometer in diameter and are determined by the capillary number (eq. 1.2), which identifies the proportions between viscosity and interfacial tension[69]. There is high uniformity in droplet formation due to low residence time distribution[70].

Low surface tension yields high capillary action leading to smaller droplets being generated[69]. There are many benefits specific to this field of droplet microfluidics that are in addition to those of microfluidics stated above. In droplets, the surfactants form a barrier at the aqueous and oil interphase which keeps components confined in the discrete, aqueous droplets[68]. This reduces sample loss and decreases the potential for cross contamination. Additionally, droplet microfluidics allows for flexible sample sizes, as flow rates depict the size of droplets and the addition and removal of reagents through additional ports allowing for smaller or larger reaction volumes as need and necessary buffer exchanges. Droplets also have convectional mixing characteristics, increasing reagent interaction and leading to more effective reactions and incubations[70]. Lastly, droplet microfluidic devices allow input independence as they can process large cell amounts and reaction samples without needing to scale device proportions. There is excellent potential for droplet microfluidics, and research has gone into developing double emulsion[71], microbubbles[72], and hollow microcapsules[73].

$$Ca = \frac{\mu_C v}{\gamma} \tag{1.2}$$

1.4 Utilizing microfluidics to profile the epigenome

Automating epigenetic profiling assays by incorporating microfluidics is an advantageous collaboration. Microfluidics allows for flexible liquid manipulation and offers high throughput rapid operation. Additionally, chromatin and epigenetic profiling assays need low input alternatives, and microfluidic adaptation could be the solution. These miniature devices are equipped with small dimensions and offer an opportunity to rework assay protocols by combining and integrating steps to decrease sample loss. Chromatin Immunoprecipitation (ChIP) is a highly pursued assay for microfluidic adaptation. As previously mentioned, ChIP is the gold standard for identifying loci associated with a target of interest (histone tail modification, transcription factor, chromatin protein etc). In the past two decades, microfluidic adaptations have focused on decreasing the amount of cell input and condensing run time. The first version, AutoChIP out of the Quake lab, focused on shortening the immunoprecipitation incubation to two hours[74]. It was fabricated with microvalve control, and the cell amount used was as low as 2,000 cells per sample. SurfaceChIP is an ultra-low input assay translation, using 30 cells per sample, that increases productivity by removing the use of magnetic beads and instead coats the surface of 8 parallel microchannels with antibodies[75]. Microfluidic modules have also been developed to adapt chromatin conformation capture (3C), expanding the capacities of microfluidics to tackle a range of epigenetic profiling assays. The Lu lab at Virginia Tech designed a module with an incubation reservoir between two loading chambers that incorporated on device crosslinking of samples as well as digestion through oscillatory mechanisms[76]. Additionally, microfluidic devices have expanded to DNA methylation detection through bisulfide-based methods. Methylation specific PCR (MS-PCR)[77] looks at hypermethylation in gene promoter regions known to be tumor suppressors[78]. Because it is beneficial to look at

methylation at various tumor promotor regions to increase accuracy this technology has also been multiplexed.[79]

While automation of profiling assays is encouraging and demonstrates a motivation to exploit microfluidics for condensing these protocols and increasing their utility, the current microfluidic iterations have limitations. Various microfluidic profiling assays are dimensionally constructed to operate with a specific amount of input material (cells, fragmented chromatin, etc.). Furthermore, current versions are immensely user dependent due to their elaborate fabrication and controls, requiring high levels of expertise in working with complicated systems. While the incorporation of intricate tools, such as micro values, can be effective, they generate a high learning curve for users. Finally, there needs to be a vast initiative for the multiplexity of fluidic profiling assays. While some microfluidic modules were developed with this motive, a considerable impact would be made within fundamental epigenetic research if microfluidic profiling assays could target more than one epigenetic modification from the same initial sample input. Various microfluidic modules have pioneered the translation of benchtop epigenetic profiling protocol. In order to have full incorporation of automated procedures into clinical landscapes, these constraints must be addressed and built upon.

In summary, microfluidics can aid in the robust and consistent utility of epigenetic profiling assays in research settings but, most importantly, expand their usage in clinical environments. Incorporating genomic and epigenetic profiling assays for clinical diagnostics is beneficial because they can assist in accurately diagnosing patients with genetic conditions, disorders, diseases, and cancers that would otherwise be challenging to identify. This would allow for appropriate medical interventions, and because epigenetics bridges lifestyle and environment choices to disease, clarity of cause could be examined. Droplet microfluidic is a

promising field that can be utilized to automate profiling assays and address the limitations that initial adaptations face. First, they would enhance analytical efficiency because droplets support input independence and uphold a broader range of cell amounts for use. Moreover, they decrease the need to incorporate ornate microvalves for microchannel sectioning because droplets can act as individual reaction vassals without needing a physical partition. Finally, high-throughput experimentation and multiplexing can be achieved through the field of droplet microfluidics. Leveraging buffer and antibody formulation along with precise control and manipulation of droplets multiplexing of more than one target from one sample input could be accomplished. Droplet microfluidics is an evolving technique with immense potential, and because of its many benefits, it is our chosen tool to demonstrate the automation potential of epigenetic profiling assays.

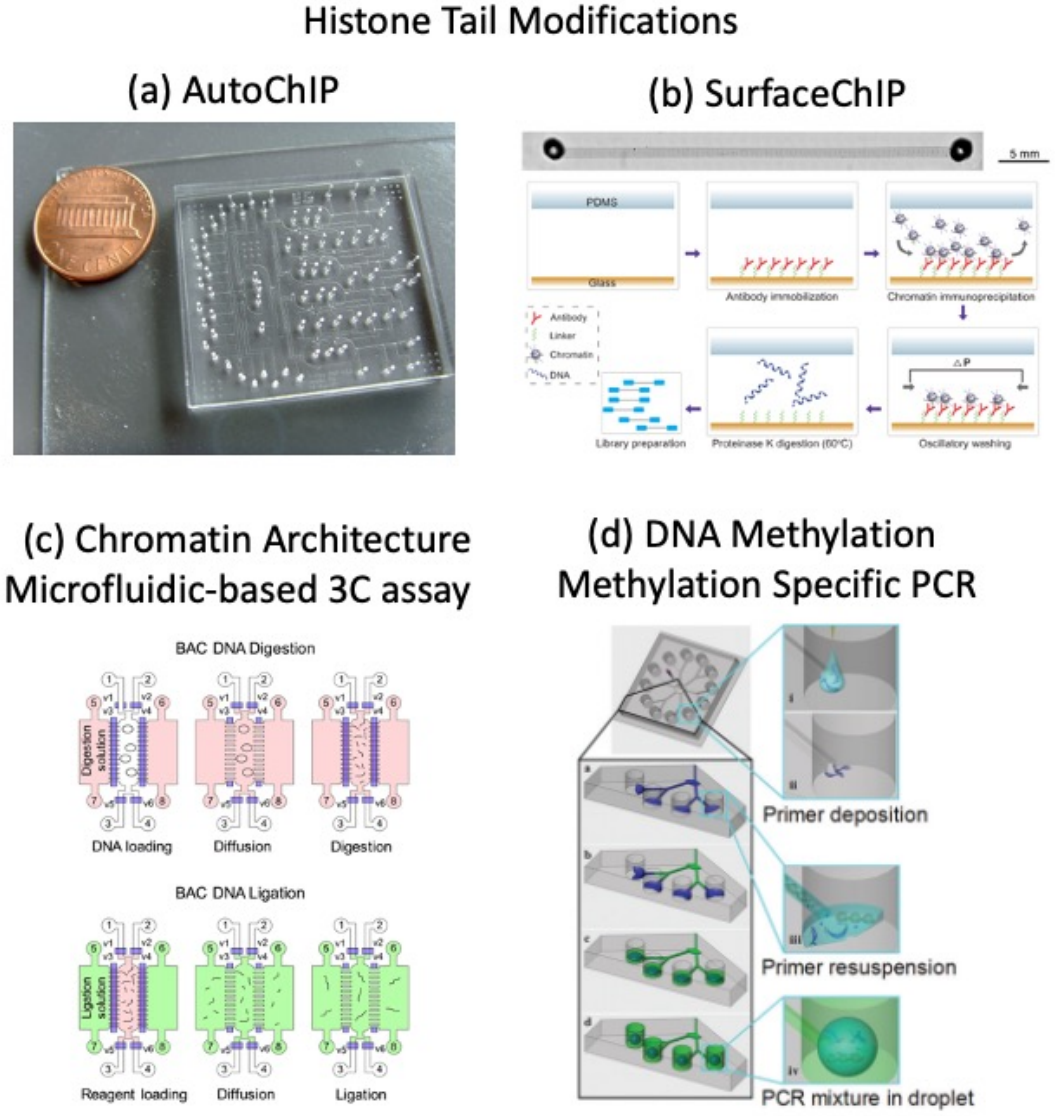

Figure 1.2: Assorted selection of microfluidic modules developed to profile distinct epigenetic modifications – histone tail modifications, DNA methylation, chromatin architecture. (a) AutoChIP, is an elaborate module fabricated with microvalve, that decreases the immunoprecipitation incubation to two hours on device. Reprinted from reference 74 (b) SurfaceChIP, is a unique adaptation of the ChIP protocol as it discards the use of magnetic beads and instead tethers the capture antibodies to the microchannel. Reprinted from reference 75 (c) Microfluidic chromosome conformation capture assay, that utilizes oscillatory mechanisms for sample crosslinking and digestion. Reprinted from reference 76 (d) Multiplexed methylation specific PCR identifies hypermethyation within gene promotor regions. Reprinted from reference 79.

1.5 Dissertation Overview

Projects to harness the potential of droplet microfluidics to automate chromatin profiling and novel enzymatic tethering assays are discussed in this thesis. Chapter two focuses on translating the ChIP assay to a droplet microfluidic format through two Bailey lab microfluidic modules. Chapters three and four expand the microfluidic droplet toolbox by tackling enzymatic tethering assays to profile histone tail modifications. Chapter three begins with condensing procedural portions of CUT&RUN and addressing challenges that arise when translating benchtop protocol. Chapter four expands into CUT&Tag by adapting previously addressed variables and expanding the amount of targeted histone tail modifications. Preliminary results for clinical samples are also discussed as a broader application for our droplet integrated CUT&Tag protocol. Lastly, Chapter five discusses how to further translate the latter portion of the CUT&Tag protocol to a microfluidic format, additional targets to profile, and future work to further the accomplishments of this thesis.

References

(1) William, H. *De generatione animalium*. London: Printed by James Young. 1653.

(2) Waddington, C.H. The epigenotype. 1942. *Int J Epidemiol*. **2012**, *41* (1), 18–20.

(3) Moore, D.S. *The Developing Genome: An Introduction to Behavioral Epigenetics*. Oxford University Press. 2015.

(4) Berger, S.L.; Kouzarides, T.; Shiekhattar, R.; Shilatifard, A.; An operational definition of epigenetics. *Genes & Development*. 2009, **23** (7), 781–3.

(5) "Epigenetics." *Merriam-Webster.com*. Merriam-Webster, 2022.

(6) Luhar, K.; Mäder, A.W.; Richmond, R.K.; Sargent, D.F.; Richmond, T.J. Crystal structure of the nucleosome core particle at 2.8 A resolution**.** *Nature*. **1997**, 389(6648), 251-60.

(7) Thoma, F.; Koller, T.; Klug, A. Involvement of histone H1 in the organization of the nucleosome and of the salt-dependent superstructures of chromatin. *The Journal of Cell Biology*. **1979**, 83, 403–427.

(8) Kornberg, R.D. Chromatin structure: a repeating unit of histones and DNA. *Science*. **1974**, 184(4139), 868-71.

(9) Kornberg, R.D.; Lorch, Y. Chromatin structure and transcription. *Annu Rev Cell Biol*. **1992**, 8, 563-87.

(10) Berdasco, M.; Esteller, M. Aberrant epigenetic landscape in cancer: how cellular identity goes awry. *Dev. Cell*. 2010. **19**, 698–711.

(11) Kahl, P., Gullotti, L., Heukamp, L.C., Wolf, S., Friedrichs, N., Vorreuther, R., Solleder, G., Bastian, P.J., Ellinger, J., Metzger, E., et al. Androgen receptor coactivators lysine-specific histone demethylase 1 and four and a half LIM domain protein 2 predict risk of prostate cancer recurrence. *Cancer Res*. **2006**, 66, 11341–11347.

(12) García-Giménez, J.L.; Seco-Cervera, M.; TollefsboL , T.O.; Romá-Mateo, C.; Peiró-Chova, L.; Lapunzina, P.; Pallardó, F.V. Epigenetic biomarkers: current strategies and future challenges for their use in the clinical laboratory. *Crit. Rev. Clin. Lab. Sci*. **2017**, 54, 529–550.

(13) Ned, R. M.; Melillo, S.; Marrone, M. Fecal DNA testing for colorectal cancer screening: the ColoSure™ test. *PLOS Curr*. **2011**, 3, RRN1220.

(14) BLUEPRINT consortium. Quantitative comparison of DNA methylation assays for biomarker development and clinical applications. *Nat. Biotechnol.* 2016**34**, 726–737 (2016).

(15) Imperiale, T. F.; Ransohoff, D. F.; Itzkowitz, S. H. Multitarget stool DNA testing for colorectal-cancer screening. *N. Engl. J. Med.* **2014**, 371, 187–188.

(16) Lamb, Y. N.; Dhillon, S. Epi proColon® 2.0 CE: a blood-based screening test for colorectal cancer. *Mol. Diagn. Ther.* **2017,** 21, 225–232.

(17) Tina Rönn, Petr Volkov, et al. A six month exercise intervention influences the genome-wide DNA methylation pattern in human adipose tissue. *PLOS Genet.* **2013**, 9, e1003572.

(18) Gezer, U. et al. Histone methylation marks on circulating nucleosomes as novel blood-based biomarker in colorectal cancer. *Int. J. Mol. Sci.* **2015**, 16, 29654–29662.

(19) Kouzarides, T. Chromatin modifications and their function. *Cell.* 2007, 128, 693–705.

(20) Eissenberg J.C.; Shilatifard, A. Histone H3 lysine 4 (H3K4) methylation in development and differentiation. *Dev Biol.* **2010,** 339, 240–9.

(21) Otterstrom, J.; Castells-Garcia,A.; Vicario, C.; Gomez-Garcia, P.A.; Cosma, M.P.; Lakadamyali, M. Super-resolution microscopy reveals how histone tail acetylation affects DNA compaction within nucleosomes *in vivo*. *Nucleic Acids Research*, **2019**, 47 16, 8470–8484.

(22) Nowak, S.J.; Corces, V.G. Phosphorylation of histone H3: a balancing act between chromosome condensation and transcriptional activation. *Trends Genet.* **2004**, 20, 214–20.

(23) Zhang, Y. Transcriptional regulation by histone ubiquitination and deubiquitination. *Genes Dev*. **2003**, 17, 2733–40.

(24) Yoo, C.B.; Jones, P.A. Epigenetic therapy of cancer: past, present and future. *Nat Rev Drug Discov*. **2006**, 5, 37–50.

(25) Piunti, A.; Morgan, M.; et al. Targeted inhibition of Ezh2 and Bet bromodomain proteins for the treatment of diffuse intrinsic pontine gliomas. *Neuro Oncol*. **2017**, 19, 196.

(26) Holdenrieder, S.; Stieber, P. Clinical use of circulating nucleosomes. *Crit. Rev. Clin. Lab. Sci*. **2009**, 46, 1–24.

(27) Snyder, M. W.; Kircher, M.; Hill, A. J.; Daza, R. M.; Shendure, J. Cell-free DNA comprises an in vivo nucleosome footprint that informs its tissues-of-origin. *Cell,* **2016**, 164, 57–68.

(28) Sarda, S.; Hannenhalli S. Next-generation sequencing and epigenomics research: a hammer in search of nails. *Genomics Inform*. **2014**, 1, 2-11.

(29) Tsompana, M.; Buck,M .J. Chromatin accessibility: a window into the genome. *Epigenetics & Chromatin*. **2014**, 7, 33.

(30) Bernstein, B. E. et al. The NIH Roadmap Epigenomics Mapping Consortium. *Nat. Biotechnol*. **2010**, 28, 1045–1048.

(31) Davis, C.A.; Hitz, B.C.; et al. The Encyclopedia of DNA Elements (ENCODE): data portal update. *Nucleic Acids Res*. **2018,** 46, D794–D801.

(32) Adams, D., Altucci, L., Antonarakis, S. *et al*. BLUEPRINT to decode the epigenetic signature written in blood. *Nat Biotechnol*. **2012**, 30, 224–226.

(33) Stunnenberg, H. G. et al. The International Human Epigenome Consortium: a blueprint for scientific collaboration and discovery. *Cell*. **2016**, 167, 1145–1149.

(34) Laird, P. Principles and challenges of genome-wide DNA methylation analysis. *Nat Rev Genet*. **2010**, 11, 191–203.

(35) Lyko, F. The DNA methyltransferase family: a versatile toolkit for epigenetic regulation. *Nat Rev Genet*. **2018***,* 19, 81–92.

(36) Parker, M.J.; Weigele, P.R.; Saleh, L. Insights into the Biochemistry, Evolution, and Biotechnological Applications of the Ten-Eleven Translocation (TET) Enzymes. *Biochemistry* **2019**, 58, 6, 450–467.

(37) Cokus, S., Feng, S., Zhang, X. *et al*. Shotgun bisulphite sequencing of the *Arabidopsis* genome reveals DNA methylation patterning. *Nature*. **2008**, 452, 215–219.

(38) Lee, C.-K.; Shibata, Y.; Rao, B., Strahl, B. D.; Lieb, J. D. Evidence for nucleosome depletion at active regulatory regions genome-wide. *Nat. Genet*. **2004**, 36, 900–905.

(39) Li G.; Levitus M.; Bustamante C.; Widom J. Rapid spontaneous accessibility of nucleosomal DNA. *Nat. Struct. Mol. Biol*. **2005**, 12, 46–53.

(40) Wu, C. The 5′ ends of *Drosophila* heat shock genes in chromatin are hypersensitive to DNase I. *Nature*. **1980**, 286 (5776): 854-860.

(41) Giresi, P.G.; Lieb, J.D.; How to find an opening (or lots of them). *Nat Methods*. **2006**, 3 (7), 501-502.

(42) Crawford, G.E.; Davis, S.; Scacheri, P.C.; Renaud, G.; Halawi, M.J.; Erdos, M.R.; Green, R.; Meltzer, P.S.; Wolfsberg, T.G. Collins FS: DNase-chip: a high-resolution method to identify DNase I hypersensitive sites using tiled microarrays. *Nat Methods*. **2006**, 3 (7): 503-509.

(43) Song, L.; Crawford, G.E. DNase-seq: a high-resolution technique for mapping active gene regulatory elements across the genome from mammalian cells. *Cold Spring Harbor Protocols*. **2010**, 2010 (2): pdb prot5384.

(44) Hesselberth, J.R.; Chen, X.; Zhang, Z.; Sabo, P.J.; Sandstrom, R.; Reynolds, A.P.; Thurman, R.E.; Neph, S.; Kuehn, M.S.; Noble, W.S.; Fields, S.; Stamatoyannopoulos, J.A.; Global mapping of protein-DNA interactions *in vivo* by digital genomic footprinting. *Nat Methods*. **2009**, 6 (4), 283-289.

(45) Giresi, P.G.; Lieb, J.D. Isolation of active regulatory elements from eukaryotic chromatin using FAIRE (Formaldehyde Assisted Isolation of Regulatory Elements). *Methods*. **2009**, 48 (3), 233-239.

(46) Buenrostro, J.D.; Giresi, P.G.; Zaba, L.C.; Chang, H.Y.; Greenleaf, W.J. Transposition of native chromatin for fast and sensitive epigenomic profiling of open chromatin, DNA-binding proteins and nucleosome position. *Nat Methods*. **2013**, 10 (12), 1213-1218.

(47) Ponts, N.; Harris, E.Y.; Prudhomme, J.; Wick, I.; Eckhardt-Ludka, C.; Hicks, G.R.; Hardiman, G.; Lonardi, S.; Le Roch, K.G. Nucleosome landscape and control of transcription in the human malaria parasite. *Genome Res*. **2010**, 20 (2), 228-238.

(48) Mavrich, T.N.; Jiang, C.; Ioshikhes, I.P.; Li, X.; Venters, B.J.; Zanton, S.J.; Tomsho, L.P.; Qi, J.; Glaser, R.L.; Schuster, S.C.; Gilmour, D.S.; Albert, I.; Pugh, B.F. Nucleosome organization in the *Drosophila* genome. *Nature*. **2008**, 453 (7193), 358-362.

(49) Dekker, J. Capturing chromosome conformation. *Science*. **2002**, 295, 1306–1311.

(50) Simonis, M.; Klous, P.; Splinter, E.; Moshkin, Y.; Willemsen, R.; de Wit, E.; van Steensel, B.; de Laat, W. Nuclear organization of active and inactive chromatin domains uncovered by chromosome conformation capture-on-Chip (4C) *Nat*. *Genet*. **2006**, 38, 1348–1354.

(51) Dostie, J.; Richmond, T.A.; Arnaout, R.A.; Selzer, R.R.; Lee, W.L.; Honan, T.A.; Rubio, E.D.; Krumm, A.; Lamb, J.; Nusbaum, C.; et al. Chromosome Conformation Capture Carbon Copy (5C): A massively parallel solution for mapping interactions between genomic elements. *Genome Res*. **2006**, 16, 1299–1309.

(52) Lieberman-Aiden, E.; van Berkum, N.L.; Williams, L.; Imakaev, M.; Ragoczy, T.; Telling, A.; Amit, I.; Lajoie, B.R.; Sabo, P.J.; Dorschner, M.O.; et al. Comprehensive mapping of long-range interactions reveals folding principles of the human genome. *Science*. **2009**, 326, 289–293.

(53) Fullwood, M.J.; Liu, M.H.; Pan, Y.F.; Liu, J.; Xu, H.; Mohamed, Y.B.; Orlov, Y.L.; Velkov, S.; Ho, A.; Mei, P.H.; et al. An oestrogen-receptor-α-bound human chromatin interactome. *Nature*. **2009**, 462, 58–64.

(54) Collas, P. The Current State of Chromatin Immunoprecipitation. *Mol Biotechnol*. **2010**, 45(1), 87-100.

(55) Policastro, R.A.; Zentner, G.E.; Enzymatic methods for genome-wide profiling of protein binding sites. *Briefings in Functional Genomics*. **2018**, 17 (2), 138–145.

(56) CUT&Tag Complete Guide – Methods Overview, *Active Motif*, **2021.**

(57) Whitesides, G. The origins and the future of microfluidics. *Nature*. 2006, 442, 368–373.

(58) Squires, T.M., Quake, S.R. *Rev*. Microfluidics: Fluid physics at the nanoliter scale. *Mod. Phys*. **2005**, 77, 977-1026.

(59) Terry, S.C.; Jerman, H.; Angell, J.B.; A Gas Chromatograph Air Analyzer Fabricated on a Silicon Wafer. *Electron Devices, IEEE Trans*. **1980**, 26, 1880–1886.

(60) Manz, A.; Graber, N.; áM Widmer, H. Miniaturized total chemical analysis systems: a novel concept for chemical sensing. *Sensors Actuators B Chem*. **1990**, 1, 244–248.

(61) Dittrich, P. S.; Tachikawa, K.; Manz, A.; Micro total analysis systems. Latest advancements and trends. *Anal. Chem*. **2006**, 78**,** 3887 -3908.

(62) Grünberger, A.; Wiechert, W.; Kohlheyer, D. Single-cell microfluidics: opportunity for bioprocess development. *Curr Opin Biotechnol*. **2014**, 29, 15-23.

(63) Damiati, S.; Kompella, U.B.; Damiati, S.A.; Kodzius, R. Microfluidic Devices for Drug Delivery Systems and Drug Screening. *Genes (Basel)*. **2018**, 9(2), 103.

(64) Pandey, C.M.; Augustine, S; Kumar, S.; Kumar, S.; Nara, S.; Srivastava, S.; Malhotra, B.D. Microfluidics Based Point-of-Care Diagnostics. *Biotechnol J*. **2018**, 13(1).

(65) Wu, Q.; Liu, J.; Wang, X. *et al*. Organ-on-a-chip: recent breakthroughs and future prospects. *BioMed Eng OnLine*. **2020**, 19, 9.

(66) deMello, A. Control and detection of chemical reactions in microfluidic systems. *Nature*. **2006**, 442, 394–402.

(67) Sohrabi, S.; Kassir, N.; Moraveji, M.K. Droplet microfluidics: fundamentals and its advanced applications. *RSC Adv.*, **2020**,10, 27560-27574.

(68) Baret, J.C. Surfactants in droplet-based microfluidics. *Lab Chip*, **2012**,12, 422-433.

(69) Sartipzadeh, O.; Naghib, S.N.; Seyfoori, A.; Rahmanian, M.; Fateminia, F.S. Controllable size and form of droplets in microfluidic-assisted devices: Effects of channel geometry and fluid velocity on droplet size. *Mater Sci Eng C Mater Biol Appl*. **2019**, 109, 110606.

(70) Song, H.; Tice, J.D.; Ismagilov, R.F. A Microfluidic System for Controlling Reaction Networks in Time. *Angew. Chem. Int. Ed*. **2003**, 42 (7), 768-772.

(71) Nisisako, T.; Okushima, S.; Torii, T. Controlled formulation of monodisperse double emulsions in a multiple-phase microfluidic system. *Soft Matter*, **2005**, 1, 23- 27.

(72) Xu, J.H.; Li, S.W.; Wang, Y.J.; Luo, G.S. Controllable gas-liquid phase flow patterns and monodisperse microbubbles in a microfluidic T-junction device. *Appl. Phys. Lett*., 2006, **88**, 3.

(73) Utada, A.S.; Lorenceau, E.; Link, D.R.; Kaplan, P.D.; Stone, H.S.; Weitz, D.A. Monodisperse double emulsions generated from a microcapillary device. *Science*, **2005**, 308, 537- 541.

(74) Wu, A.R.; Hiatt, J.B.; Lu, R.; Attema, J.L.; Lobo, N.A.; Weissman, I.L.; Clarke, M.F. Quake, S.R. Automated microfluidic chromatin immunoprecipitation from 2,000 cells. *Lab on a Chip*, **2009**, 9, 1365–1370.

(75) Ma, S.; Hsieh, Y.; Ma, J.; Lu, C. Low-input and multiplexed microfluidic assay reveals epigenomic variation across cerebellum and prefrontal cortex. *Science Advances*, **2018**, 4, eaar8187.

(76) Sun, C.; Lu, C. Microfluidics-Based Chromosome Conformation Capture (3C) Technology for Examining Chromatin Organization with a Low Quantity of Cells. *Analytical Chemistry*, **2018**, 90, 3714–3719.

(77) Herman, J.G.; Graff, J.R.; Myohanen, S.; Nelkin, B.D.; Baylin, S.B. Methylation-specific PCR: a novel PCR assay for methylation status of CpG islands. *P Natl Acad Sci USA*. **1996**, 93, 9821–9826.

(78) Chan, M.W.Y.; Chan, L.W.; Tang, N.L.S.; Tong, J.H.M.; Lo, K.W.; Lee, T.L.; Cheung, H.Y.; Wong, W.S.; Chan, P.S.F.; Lai, F.M.M; To, K.F. Hypermethylation of Multiple Genes in Tumor Tissues and Voided Urine in Urinary Bladder Cancer Patients. *Clin Cancer Res*. **2002**, 8, 464–470.

(79) Zhang, Y.; Bailey, V.; Puleo, C.M.; Easwaran, H.; Griffiths, E.; Herman, J.G.; Baylin, S.B.; Wang, T.H. DNA methylation analysis on a droplet-in-oil PCR array. *Lab on a Chip*, **2009**, 9, 1059–1064.

Chapter 2 Profiling Histone Tail Modifications Utilizing Droplet Integrated Chromatin Immunoprecipitation

Gloria Diaz,[a] Steven R. Doonan,[a] Claire D. Cook,[a] Yi Xu,[a] Jeong-Heon Lee,[b] Tamas Ordog,[b] and Ryan C. Bailey[a]

Abstract

Histone tail modifications are important because they can serve as biomarkers to observe the development and progression of certain cancers and diseases. Because of this, it is important to profile their prevalence throughout the genome. To study these modifications, the Bailey lab has previously developed two droplet microfluidic modules (MNase and CAR-Wash) that address two of the three procedural portions in the chromatin immunoprecipitation (ChIP) assay. The MNase module processes low-input cell samples for genome-wide nucleosome positioning. By improving the original design, we optimized resistance to fibers and decreased the probability of magnetic bead clogs. Following the operation of the MNase module, the CAR-Wash module performs immunoprecipitation washing. The utility of these two modules enables histone tail modification profiling in segmented droplets.

2.1 Introduction

2.1.1 Epigenetics & Histone Tail Modifications

The human body is composed of a plethora of distinct cells. Within each nucleus-containing cell, there is an identical copy of the genome. However, the phenotypic attributes experienced by each cell differ due to epigenetic factors that aid in determining cell fate[1]. The field of epigenetics deals with structural changes to the genomic landscape through epigenetic modifications that work to regulate gene expression without changing the genetic sequence[2]. Epigenetic modifications include DNA methylation[3], histone tail modifications[4], nucleosome positioning[5], accessible chromatin regions[6], non-coding RNA[7], and overall, three-dimensional chromatin architecture[8].

The nucleosome is the first structural unit of DNA packaging, in which 146 base pairs (bp) of double-stranded DNA wrap around a histone octamer[9]. At approximately 63 Angstroms in diameter, this repeated, fundamental subunit allows the compaction of DNA in the eukaryotic nucleus[10]. Positioning of nucleosomes across the genome has significant importance since it depicts accessibility of genomic regions for transcription as well as compaction of heterochromatin for gene silencing[6]. The DNA between each unit, known as linker DNA, can fluctuate between ~ 20 to 90 bp. Nucleosomes are composed of eight basic histone proteins that exist in dimers. The four-core histones include H2A, H2B, H3, and H4, while histones H1/H5 are linker histones[9]. The core histones have long, N-terminal tails that are the location for post-translational modifications (PTMs)[11]. Many studies of histone tail PTMs focus on histone 3. Nevertheless, efforts continue to expand the discovery and understanding of modifications on histones H2A, H2B and H4. Commonly studied PTMs include methylation, acetylation, ubiquitination, and phosphorylation[4]. Novel PTMs continue to be uncovered – crotonylation[12],

neddylation[13], propionylation[14], and butyrylation[14]. Fundamental data on histone tail modifications concern individual marks, although there is collective work into an underlying histone code, where varying combinations of histone modifications may depict specific meanings[15].

A variety of PTMs occur on both the N-terminal tail as well as the later surface nucleosome core which has contact with DNA[11]. These modifications influence and alter the structural genomic landscape due to changes in the net charge of histones, steric hindrance, and alterations of inter-nucleosomal forces[4]. Methylation, occurring on both lysine and arginine residues, is an informative mark, as mono, di, and tri-methylation all have distinct meanings and outcomes in transcriptional regulation[16]. Transcriptionally active marks include H3K4[17] and H3K36[18], while repressive marks include H3K9[19] and H3K27[20]. Reversibility of modifications is also possible when placed on lysine residues due to lysine demethylase (LSDI)[21]. Similarly, lysine acetylation is also a reversible modification[22]. It is characterized as an active modifier since it neutralizes the positive charge and disassembles the negatively charged DNA backbone from the nucleosome allowing chromatin to open[23].

2.1.2 Chromatin Profiling

Chromatin Immunoprecipitation (ChIP) is the gold standard assay for profiling genomic regions associated with a target of interest. These targets can range from histone tail modifications, chromatin proteins, transcription factors and more[24]. The ChIP procedure begins by harvesting cultured cells, lysing the cellular and nuclear membranes using detergents, and fragmenting the chromatin through either mechanical or enzymatic means. By tethering antibodies to magnetic beads, the specific target of interest can be immunoprecipitated, accumulated, and washed with different salt solutions to remove non-specific chromatin

interactions and debris. Finally, the DNA fragments associated with the mark of interest are liberated by reverse crosslinking, purified, and prepped for downstream analysis[25]. Variations of this conventional protocol have been developed to study native conditions[26], improve sequencing resolution[27], and expand its utility to low input[28]. However, challenges persist across these iterations: the bulk protocol is time intensive (4-5 days), technician dependent (molecular biology skill level), and has limited utility for low-input samples (e.g. biopsies/ rare cell lines)[29].

Utilizing microfluidics to automate the benchtop ChIP procedure can alleviate the persistent challenges across procedural variations. There has already been a decade's worth of research into the translation of ChIP to a microfluidic format. In 2012, the Quake group developed High Throughput ChIP (HTChIP), which has 16 parallel bead reservoirs as well as a dispersion channels that trap antibody-coated agarose beads[29]. Although this module is highly efficient, the complicated flow control and miniature valves require a skilled operator. Surface ChIP, published in 2018 out of the Lu lab, doesn't use the staple antibody coated magnetic beads[30]. Instead, the bottom surface of the 8 parallel, microfluidic channels are coated with antibodies to capture the target of interest. While these modules have progressed the automation of ChIP, they only address a single portion of the protocol.

In this chapter, our goal is to automate the entirety of the ChIP protocol through separate modules that address different portions of the procedure and cohesively work together. We initially altered the previously published MNase module[31] design that prepares nucleosomal length DNA from whole cells. Following these changes, we join it with the CAR wash[32] module to tackle two-thirds of the ChIP procedure. This optimized workflow is employed to profile a diverse set of histone tail modifications to demonstrate the versatility and utility of our system.

Lastly, we touch on the development of a cylindrical heater to automate the later DNA liberation portion.

2.2 Materials and Methods

Buffer Recipes

Cell Lysis Buffer (pH 7.9) contains 10 mM HEPES, 1.5 mM MgCl2, 10 mM KCl, 0.5%(w/v) IGEPAL-CA630. **Nuclei Digestion Buffer** (pH 7.5) contains 20 mM Tris-HCl, 15 mM NaCl, 60 mM KCl, 5 mM CaCl2, 0.15 mM Spermine, 0.5 mM Spermidine. **TE Buffer** (pH 8.1) contains 10 mM Tris-HCl, 1 mM EDTA. **2X EB Buffer from Mayo EDL** (pH 8.0) contains 20 mM Tris-HCl, 20 mM EDTA, 300 mM NaCl, 2% (w/v) SDS. **Low Salt Immune Complex Wash Buffer** (pH 8.1) contains 20 mM Tris- HCl, 2 mM EDTA, 150 mM NaCl, 0.1 % (w/v) SDS, 1.0% (w/v) Triton X-100. **2X STOP Buffer from Mayo EDL** (pH 8) contains 100 mM Tris-HCl, 20 mM EDTA, 200 mM NaCl, 0.2% (w/v) Sodium deoxycholate, 2.0% (w/v) Triton. **LiCl Immune Complex Wash Buffer** (pH 8.1) contains 10 mM Tris-HCl, 1 mM EDTA, 250 mM LiCl, 1.0% (w/v) IGEPAL-CA630, 1.0% (w/v) Sodium deoxycholate. **High Salt Immuno Complex Wash Buffer** (pH 8.1) contains 20 mM Tris-HCl, 2 mM EDTA, 500 NaCl, 0.1% (w/v) SDS, 1.0% (w/v) Triton X-100

2.2.1 Microfluidics Device Preparation

Microfluidic modules were made using standard photolithography and soft lithography methods. A photoresist master was fabricated by first spin coating SU8-2025 (MicroChem Corp, Westborough, MA) onto a silicon wafer (University Wafer, Boston MA) to a 40-μm thickness. A transparent photomask was designed using AutoCAD (CAD/Art Services, Inc.) and used to crosslink the photoresist through UV exposure using a MJB3 mask aligner (SUSS MicroTec). After post baking (Cimarec, Thermo Scientific), the initial layer was developed using propylene glycol methyl ether acetate (PGMEA) (Sigma-Aldrich, St. Louis, MO) and dried with compressed air. For the second layer of the MNase module, SU8-2050 was spin coated to a

thickness of 150 μm, exposed to UV, and crosslinked to the silicon wafer. The master was developed as previously mentioned and surface treated with tridecafluoro-1,1,2,2-tetrahydrooctyl trichlorosilane (Gelest, Inc., Morrisville, PA).

A PDMS mix (RTV615, Momentive, Inc.) was made to a ratio of 10:1 (PDMS: curing agent) and degassed under vacuum. The mixture was poured over the master and baked at 70°C (HeraTherm Oven, Thermo Scientific) for one hour to cure. Cured PDMS stamps were peeled off, shaped, and hole punched. To clean, stamps were sonicated in water for 5 minutes, dried with compressed air, and cleaned with cellulose adhesive (Scotch Magic Invisible Tapes - 3M,St. Paul, MN). PDMS stamps were bonded to clean glass slides (1 mm thickness, 75 mmx 50 mm, Thermo Fisher Scientific) through oxygen plasma bonding (Plasma cleaner PDC-32G, Harrick Plasma, Inc) and baked at 70°C overnight.

2.2.2 Magnetic Bead Functionalization

Protein A Dynabeads (30 μL per in tube sample and 50 μL per on-chip sample) (Invitrogen, Catalog No. 10003D and 10004D, Thermo Fisher Scientific) were washed twice with 100 μL of 1X STOP buffer per sample (50 mM Tris-HCl pH 8, 10 mM EDTA, 100 mM NaCl, 1% triton, 0.1% sodium deoxycholate). Beads were suspended in 100 μL of 1X STOP buffer per sample and incubated with the appropriate amount of antibody dependent on the number of cells used (**H3K4me3** - Catalog No. ab8580, Abcam, **H3K27me3** - Catalog No.9733, Cell Signaling Technology, **H3K27ac** - Catalog No.8173, Cell Signaling Technology, **H3K4me** Catalog No. ab8895, Abcam, **H3K36me3** - Catalog No. 61102, Active Motif, **CTCT** - Catalog No. 3418T, Cell Signal Technology) on a rotator at 4°C for 2 hours. Following functionalization, beads were washed twice with 100 μL of 1X STOP buffer/ sample and resuspended in 60 μL 2X

STOP buffer per sample protease inhibitor cocktails (1μL/100 μL of sample). For on-chip samples, 100 μL of bead solution was emulsified at a time using a flow-focusing droplet generation device. 1% (w/w) F008 (Perfluoropolyether polyethylene glycol block co-polymer, RAN Biotechnologies, Inc. Beverly, MA) in Novec 7500 (3M, St. Paul, MN) was used for droplet generation.

2.2.3 Cell Culture

HeLa cells were cultured in DMEM medium (Gibco DMEM High Glucose, Catalog No. 11965092, Fisher Scientific) supplemented with 10% v/v fetal bovine serum at 37°C with 5% CO_2. To detach from culture flask, cells were treated with 0.5% trypsin-EDTA (Gibco 0.05% Trypsin-EDTA, Catalog No. 25300-054, Fisher Scientific) for 5 minutes at 37°C. Trypsin was quenched using complete growth media, then cells were transferred to a conical tube and pelleted by spinning at 600 x g for 5 min at 4°C. Cells were washed twice with cold PBS (Lonza™ BioWhittaker™ Phosphate Buffered Solution, Catalog No. BW17516F12, Fisher Scientific) and resuspended in 30% OptiPrep – PBS (OptiPrep™ Density Gradient Medium, Catalog No. D1556-250ML, Millipore Sigma) to a concentration of 7 million cells per mL.

2.2.4 Microfluidic Device Operation

MNase Module Device: Operation of microfluidic chip was visualized using high speed camera (Phantom Miro Ex2 or PhantomVEO 640L) connected to a stereoscope (Leica M80 or DMi8). Prior to use (24 hrs-1hr) chips were treated with Aquapel (Pittsburgh Glass Works, LLC., Pittsburgh, PA) to yield a hydrophobic coating around channels. Buffer solutions were delivered through 24-gauge tubing (Cole-Parmer, Vernon Hills, IL) attached to glass sealed syringes (Hamilton Company, Reno, NV). Syringes were controlled using syringe pumps (Pump 11 Pico

Plus Elite, Harvard Apparatus). —carrier oil - 6 μL min^{-1}; droplet generator - 2 μL min^{-1}; oil spacer - 14 μL min^{-1}; pico injector - 4 μL min^{-1}. The carrier oil phase was composed of fluorinated oil Novec 7500 with 2% (w/w) perfluoropolyether polyethylene glycol block co-polymer surfactant. The tubing delivering cells was treated overnight with 1% (w/v) Pluronic F127 (Sigma-Aldrich, St. Louis,MO). Pre-encapsulated, functionalized Dynabeads were delivered through a pico injector and merged using electrolyte channels filled with 3M sodium chloride. A full circuit AC electric field was achieved by connecting clamps to the needles supplying 3M NaCl solution. Metal alligator clamps were connected to an in-house DC-AC converter (12V DC input, 0-360V AC at 36 kHz as output) connected to a power supply. Droplets were collected using 30 gauge (Cole-Parmer, Vernon Hills, IL) into a 1.5 mL Eppendorf (EppendorfDNA LoBind, Fisher Scientific, Waltham, MA) and incubated overnight at 4°C.

CAR Wash Module: Operation of the magnetic washing module was visualized through a M80 Stereomicroscope connected to Phantom Miro Ex2 high Speed Camera (Vison Research, Inc.) or a DMi8 Microscope (Leica Microsystems) with a VEO 640L High Speed Camera (Vision Research, Inc.). Functionalized magnetic beads with desired product along with wash buffers were delivered through 30-gauge tubing controlled by an in-house built pressure system. Nitrogen (N_2) gas was used to pressurize the headspace of solution-containing vials. This pressure is applied from a manifold delivering gas to individually controlled, two-stage regulators to the vial through steel pins inserted through a septum. Solution is driven onto device via 20-cm-long, 30-gauge tubing. A LabVIEW (National Instruments, Austin, TX) virtual instrument paired with a data acquisition device and solenoid valve array controlled whether fluid inputs were on or off.

Segmented product was introduced at 50 kPa, spaced out with an oil flow (55 kPa), and merged via electrolyte channels with a co-laminar buffer stream (Low Salt Immuno Complex Wash Buffer – 55 kPa; High Salt Immuno Complex Wash Buffer – 65 kPa; LiCl Immuno Complex Wash Buffer – 65 kPa; TE Buffer – 40 kPa). Eight magnets were positioned on device to attract magnetic particles through each buffer streamline into the TE buffer. Oil was delivered on device at 55 kPa to coflow alongside the wash buffer stream to prevent Dyna beads from sticking to the PDMS wall. The initial droplet solution is maintained in the top streamline and sent to waste (20 kPa), while the washed beads were resegmented by oil (55 kPa) flowing into a flow-focusing junction. Resulting droplets were collected and coalesced through the addition of 1H, 1H, 2H, 2H-perfluoro-1-octanol (Sigma-Aldrich, St. Louis, MO). Note, 1% (w/w) F008 in Novec 7500 was used for all oil inputs into the CAR-Wash device.

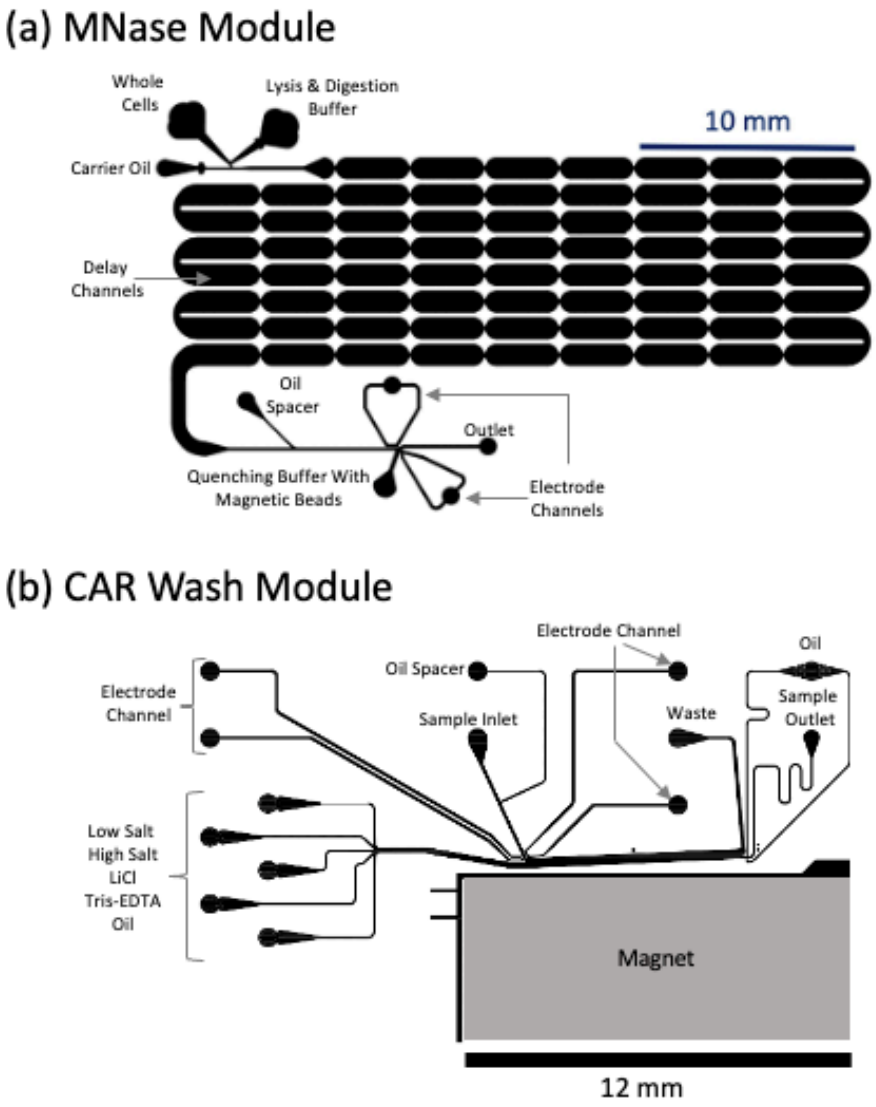

Figure: 2.1 Schematic of microfluidic devices utilized for droplet integrated chromatin immunoprecipitation. MNase module utilized syringe pumps to deliver reagents while the CAR Wash module uses a pressure system to deliver reagents.

2.2.6 Droplet Integrated ChIP

Droplets were generated on the MNase module containing whole HeLa cells in 30% OptiPrep – PBS (30 µL at a concentration of 7 million cells per 1 mL) with Lysis and Digestion Buffer and Micrococcal Nuclease (2000 GU/µL; New England Biolabs,Ipswich, MA) (30 µL of buffer cocktail). Droplets incubated for 3 minutes and 30 seconds. Once each droplet reached the end of module, it was injected with quenching buffer and functionalized magnetic beads. Droplets were collected and incubated overnight at 4°C.

The next day, droplets were delivered into the CAR-Wash device and merged with the colaminar buffer stream. Sample-laden beads were drawn through increasingly stringent wash buffers towards magnets installed on the device. Washed beads were then resegmented into new droplets, which were collected and chemically coalesced. The oil and aqueous, bead-containing layers were separated before continuing with processing alongside in tube samples.

2.2.7 Bulk ChIP Samples, Controls, and Input

Off-chip, bulk samples were prepared for comparison of bulk against segmented processing. In a standard 1.5-mL Eppendorf vial, 30 µL of whole HeLa cells in 30% OptiPrep – PBS were pipetted along with 30 µL of the lysis and digestion buffer cocktail. Samples incubated for 3 minutes and 30 seconds at room temperature. To halt the digestion process/reaction, 60 µL of 2X STOP was added to solution along with functionalized magnetic beads. Bulk samples incubated alongside droplet samples overnight at 4°C on a rocker.

The following day samples were washed using a magnetic rack, with 1 mL of Low Salt Immune Complex Wash Buffer (pH 8.1), High Salt Immuno Complex Wash Buffer (pH 8.1),

LiCl Immune Complex Wash Buffer (pH 8.1), and TE Buffer (pH 8.1), each incubating for 5 minutes on a rotator at 4°C. After wash steps, samples were resuspended in 100 µL 2X EB Buffer from Mayo EDL (pH 8.0), and 2 µL of RNase A (10 mg/mL, Sigma-Aldrich, St. Louis, MO) was added. Samples incubated for 1 hour at 65°C. Following RNA degradation, 2 µL of Proteinase K (10 mg/mL, ThermoFisher Scientific, Grand Island, NY) was added to each sample and samples incubated at 65°C for 2 hours.

Bulk samples, controls, and input samples were purified using the QIAquick PCR Purification Kit (Qiagen, Hilden, Germany), using the standard manufacturing instructions - immunoprecipitated samples were eluted in 15 µL of ED buffer and input samples were eluted in 50 µL of EB buffer. All samples were then quantified using Qubit double stranded DNA High Sensitivity Assay (Thermo Fisher Scientific, Grand Island, NY).

2.2.8 Data Analysis – Bioanalyzer and qPCR

To assess immunoprecipitation efficiency, samples were initially characterized through Bioanalyzer (Agilent Technologies, Santa Clara, CA) to assess fragmentation patterns. All samples were diluted to a concentration of 0.5 ng/uL and submitted to the Advanced Genomic Core. Along with fragmentation analysis, quantitative polymerase chain reaction (qPCR) on two loci regions for each sample. Ideally, one loci region represents where the target is located (region of enrichment) and a second region represents where the target isn't present (region of depletion). See Table 2.1 for list of targets, their regions of depletion and enrichment, along with sequences of primer pairs.

Using a 384-well plate (Applied Biosystems Catalog No. 4309848, Fisher Scientific),10 µL of Power Up™ SYBR™ Green master mix (Applied Biosystems Catalog No. A25776, Fisher

Scientific) was added along with 2 μL of forwards and reverse primers (Integrated DNA technologies, Coral, IA) (5 μM stock concentration), 2 μL of template DNA (minimum 10 ng of DNA needed per reaction), and nuclease-free water (Invitrogen™ UltraPure™ DNase/RNase-Free Distilled Water, Catalog No. 10-977-015, Fisher Scientific) to bring the volume up to 20 μL. Once the plate was set up according to manufacturer's instructions, it was run on a 7900HT Fast Real-Time PCR System (Applied Biosystems) with standard parameters (Hold Stage: 50°C for 2 minutes, 95°C for 10 minutes, PCR Stage, 40 Cycles: 95°C for 15 seconds, 60°C for 1 minute, 95°C for 15 seconds, Melt Curve Stage: 95°C for 15 seconds, 60°C for 1 minute, 95°C for 15 seconds) set by the Advanced Genomics Core (University of Michigan). The fold change for the region of enrichment was calculated utilizing equation 2.1 to assess the immunoprecipitation efficiency of the targeted histone tail modification.

$$\text{Log}_2\ \Delta\Delta\ \text{Ct} = \Delta\text{Ct}_{\text{Sample}} - \Delta\text{Ct}_{\text{Calibrator}}$$

$$\text{Log}_2\ \Delta\Delta\ \text{Ct} = (\text{Ct}_{(\text{gene of interest})} - \text{Ct}_{(\text{reference gene})}) - \text{Ct}\ (\text{Ct}_{(\text{gene of interest})} - \text{Ct}_{(\text{reference gene})})$$

(2.1)

Table 2.1 Targets of interest (histone tail modifications and transcription factor) and their associated genes of enrichment as well as depletion.

Target	Enrichment	Depletion
H3K4me3	BRG1-TSS, Actin-TSS	MYT1-TSS
H3K4me	Ch1.Intergentic, DZIP	MYT1-TSS
H3K27ac	BRG1, Actin-TSS	MYT1-TSS
H3K27me3	MYT1-TSS	BRG1
H3K36me3	Actin-TSS	MYT1-TSS
CTCF	Ch-hCTCF-His	MYT1-TSS

Table 2.2 Forward and reverse primer sequences for genes utilized to depict enrichment of droplet integrated ChIP

Gene	Forward	Reverse
BRG1-TSS	TTG GCG AAG CTG CGA TCG GG	CCC GAT CGC AGC TTC GCC AA
MYT1-TSS	CCT GCC GTG TGC TGT TTT T	AAA AAC AGC ACA CGG CAG G
Actin-TSS	CCT CAT GGC CTT GTC ACA C	GCC CTT TCT CAC TGG TTC TCT
Ch1.Intergentic	ATGGCCATCCCCTTATGAGC	GGGCTAGGGCATTTTTAATCTTAG
DZIP	CTCTGCATAACCACTAGGTGGCA	TTTTTAAACAAGTGCAGTCGTGTGG
Ch-hCTCF-His	TTTTCTAGCGCCTCTGGTGG	ATCCAGCTGTGAGAACGGAC
C19	AGC TTG TCT TTC CCA AGT TTA CTC	GAG TAA ACT TGG GAA AGA CAA GC

2.3 Results and Discussion

2.3.1 MNase Module Alterations for ChIP

As with all chromatin profiling assays, the introductory portion of the protocol regards gaining access to the genome. Traditionally, this consists of breaking down the cellular and nuclear membranes through separate steps using detergents and salts. Digesting the chromatin then occurs through enzymatic or mechanical means. Previous work in the Bailey lab has married these individual incubations into a single droplet microfluidic device. However, to meet the necessities for ChIP-grade fragmentation, design alternations were needed at the droplet generation site, pico injector, and delivery of quenching buffer.

A persistent challenge in designing microfluidic modules is minimizing microchannel clogging from fibers and debris. The droplet generation site within the original MNase module follows the design of a standard T-junction, two microchannels perpendicular to each other. Droplets are generated when the oil phase pinches off a fraction of the aqueous phase. The T channel has a 90° angle between the two microchannels, making it prone to clogs by elongated fibers. To reduce this probability the T- channel was redesigned to be a Y-junction (Figure 2.2b). Instead of a 90°angle, the aqueous channel was altered to a 120° angle. This obtuse angel allows for elongated fibers to pass into the oil stream and prevent blockage of the droplet generation.

Similar to the droplet generator, the pico injector at the end of the original MNase module injects each droplet at a 90° angle. This feature can be repurposed to not only deliver quenching buffer but also to deliver functionalized magnetic beads. Considering that at this point the genome has been liberated, antibodies attached to magnetic beads can be utilized to identify the target of interest. However, magnetic beads are prone to clumping when they aren't evenly distributed across the solution. Additionally, fibers and debris can reside in the bead stock and

pass into the pico injector. To dissuade these issues, the pico injector was reoriented from 90° to 225° (Figure 2.2c). At this angle, any potential fibers would be eased into the oil stream. Secondly, to encourage an even distribution of the magnetic beads quenching solution would be segmented into droplets prior to introduction into the MNase module (Figure 2.2d).

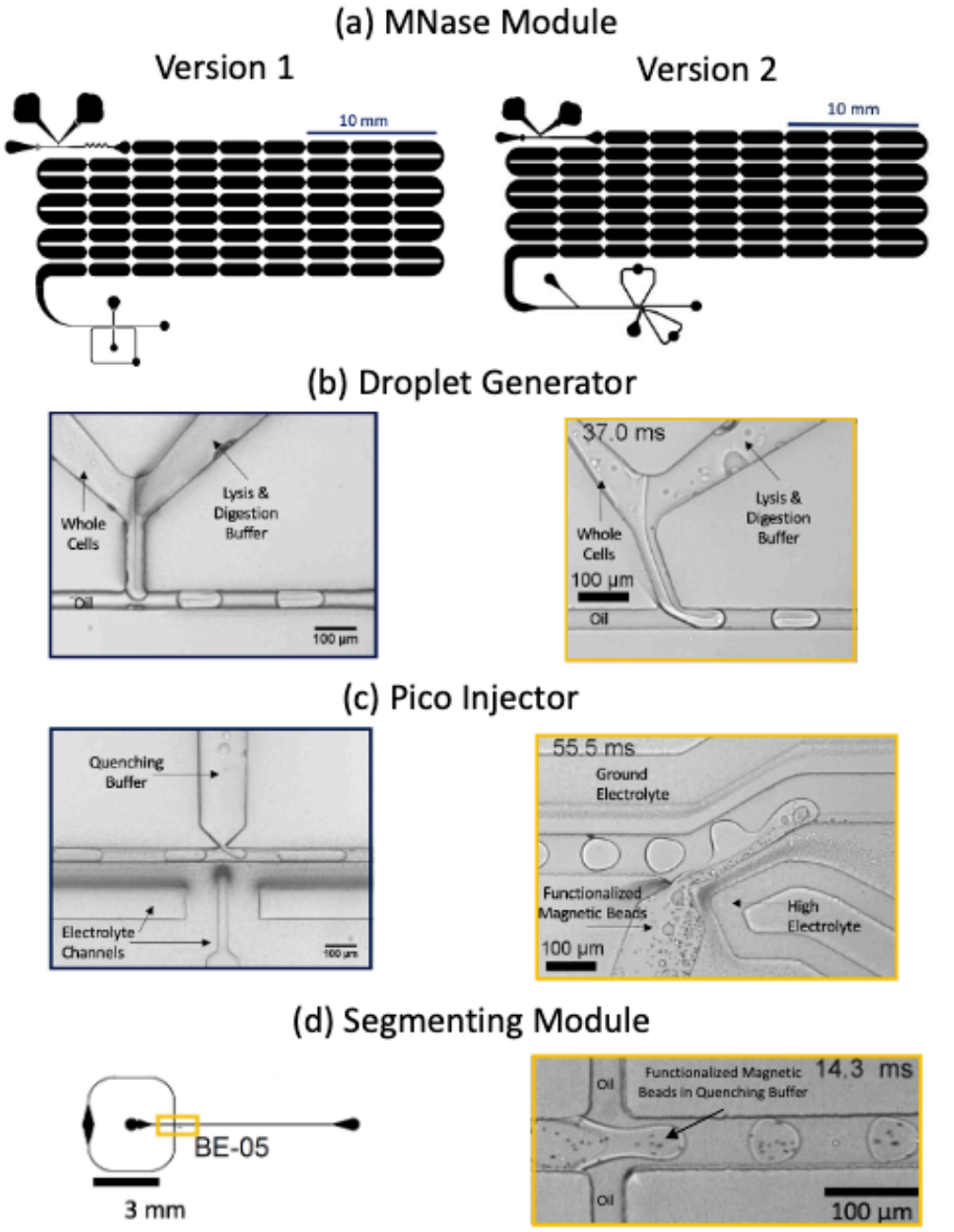

Figure 2.2 In order to the adapt the MNase module to address the initial portion of ChIP schematic changes needed to be made at the (b) droplet generator (c)pico injector along with (d) segmenting of magnetic beads before delivery through pico injector.

2.3.2 Bulk ChIP Assay Development and Optimization

The bulk format of the ChIP assay was developed to optimize and test out different variables prior to utilizing microfluidic processing. These samples also aided in contrasting bulk versus segmented formats. The bulk assay performed all the consolidated steps of the droplet integrated version, albeit in a single tube. The protocol began by harvesting the desired amount of cells, adding in lysis and digestion buffer to incubate for 3.5 minutes at room temperature to generate nucleosomal length DNA. Quenching buffer and functionalized magnetic beads were added to prevent over digestion. After resting for 5 minutes at room temperature, samples incubated overnight at 4^{o}C. The following day, each sample was washed with low salt, high salt, LiCl, and TE wash buffers.

To assess the performance of the bulk assay, as well as droplet integrated ChIP, DNA retention was quantified using a fluorimeter. qPCR was utilized to assess the specificity of the immunoprecipitation. qPCR works by looking at the abundance of two specific gene regions: ideally, one where the target is abundantly present (region of enrichment) and one where it is lacking (region of depletion). The region of abundance should have a ΔΔCt value above 2.2, depicting a 10-fold enrichment and visually demonstrating the presence of the target of interest through an antibody pull down. The region of depletion should have negligible signal, suggesting minimal nonspecific binding.

Well known histone tail modifications were chosen as targets of interest – H3K4me3, H3K27me3 and H3K27ac. Histone 3 lysine 4 trimethylation is associated with active transcription[17], and therefore, its region of enrichment is the Brg1 transcription start site and its region of depletion is MYT1. In contrast, H3K27me3 is a repressive mark connected to heterochromatin formation[20]. As such, the region of enrichment would be MYT1 and region of

depletion Brg1. Lastly, H3K27ac is an active mark but less abundant throughout the genome, making it an arduous target to profile. Successful profiling of this mark will depict the capabilities of the droplet integrated ChIP system.

In order to improve the performance of the droplet integrated ChIP system, bulk experiments were carried out by incorporating and isolating variables. First, two individual procedural steps were incorporated to increase the pull-down efficiency and decrease carry over debris. Figure 2.3a shows the enrichment profiles for H3K4me3 when a centrifuge step was included after the cell and chromatin lysis. There is noticeably higher enrichment at the Brg1 gene (region of enrichment) when a centrifuge step is incorporated. Similarly, when incorporating a preclear step with non-functionalized magnetic beads (Figure 2.3b), there is equal enrichment with and without the clearing of debris with beads. Secondly, pull down incubation time was assessed for a 2 hour, room temperature incubation compared to an overnight, 4°C (Figure 2.3c). Enrichment at the Brg1 region between these two samples targeting H3K4me3 was similar.

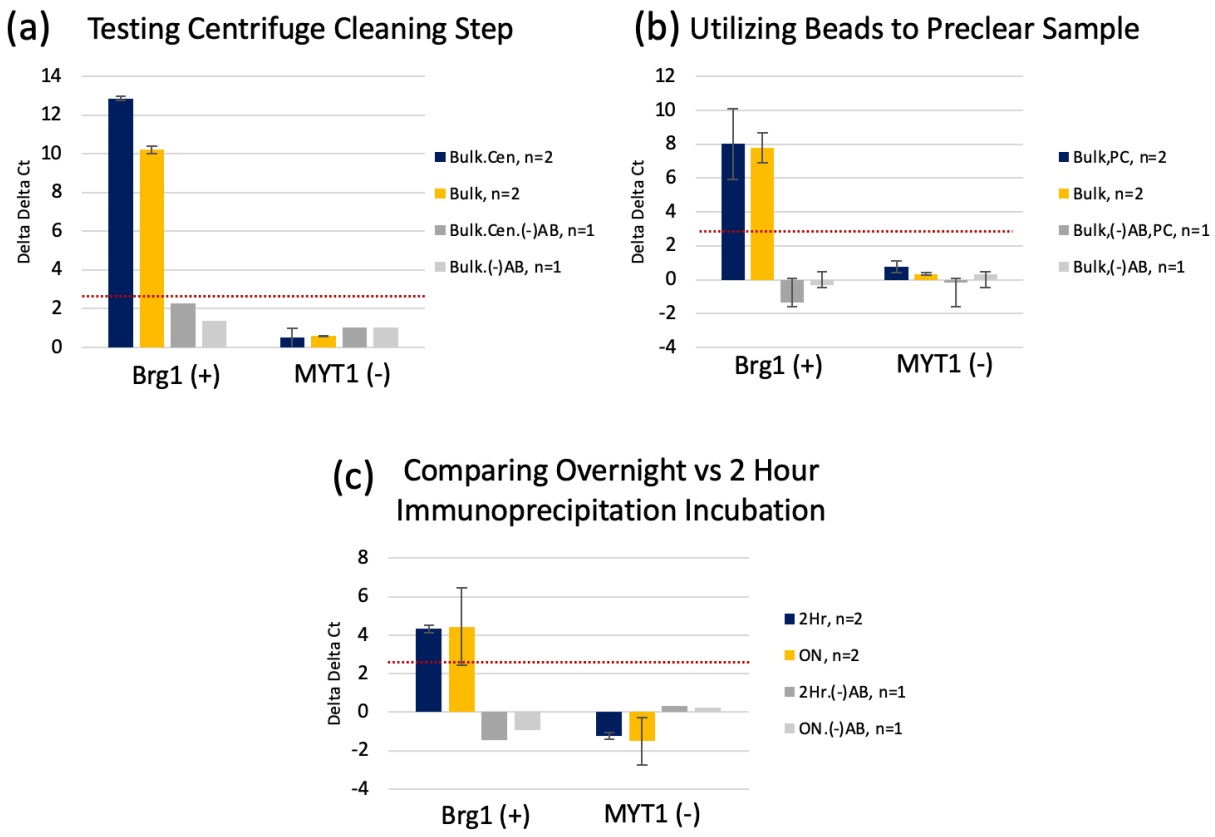

Figure 2.3 qPCR enrichment profiles testing different variables to increase signal for bulk ChIP protocol - (a) incorporating a centrifuge step to clean up debris (b) using poly styrene beads to clean debris in sample (c)incubating immunoprecipitation for 2 hours at room temperature compared to overnight at 4°C.

2.3.3 Droplet Integrated Chromatin Immunoprecipitation (ChIP)

Having optimized the bulk ChIP assay, we transitioned to developing the droplet integrated ChIP assay. In order to demonstrate its utility, 3 histone tail modifications were profiled (Figure 2.4). First, H3K4me3 showed significant enrichment in the Brg1 gene region (region of enrichment) for the droplet sample as well as the bulk assay (Figure 2.4a). There is little to no enrichment with the negative controls (bare and IgG-functionalized beads) indicating the pull down is specific to the presence of the antibody on the magnetic beads. There is also miniscule signal in the MYT1 gene region (region of depletion), indicating little to no nonspecific binding. H3K27me3, the complimentary repressive target, was also profiled with the droplet ChIP system (Figure 2.4b). For the droplet and bulk samples there is significant enrichment in the MYT1 gene region (region of enrichment) compared to the negative controls and minimal enrichment in the Brg1 gene (region of depletion). The last target, H3K27ac, showed compelling results when comparing droplet to bulk formats (Figure 2.4c). As previously stated, H3K27ac is not as abundant throughout the genome and can be challenging to pull down. When observing the response in the Brg1 region (region of enrichment), there is significant enrichment for the droplet samples compared to the bulk assay. While it is possible for the bulk sample to have failed, it's also possible that the segmented format increased the probability of target identification. Droplets have intermolecular forces that play into discovery and interaction/binding of the target by the antibody. Conversely, there is significantly higher amount of surface area in the bulk sample that decreases the probability of interaction.

Lastly, to expand the utility and functionality of the droplet ChIP system the same histone tail modifications were profiled in a model cell line to study a rare lymphoplasmacytic lymphoma. The cell line MWCL-1 was specifically developed to study Waldenström

macroglobulinemia (WM)—a lymphoplasmacytic lymphoma subtype that produces excess immunoglobulin (IgM) protein—as well as tumor development in bone marrow and lymphatic tissue[33]. When profiling H3K4me3 (Figure 2.5a), it's noted that droplet integrated ChIP processing produces enrichment not as a high as the bulk samples. Compared to profiling H3K27ac, enrichment between the droplet and bulk samples is comparable.

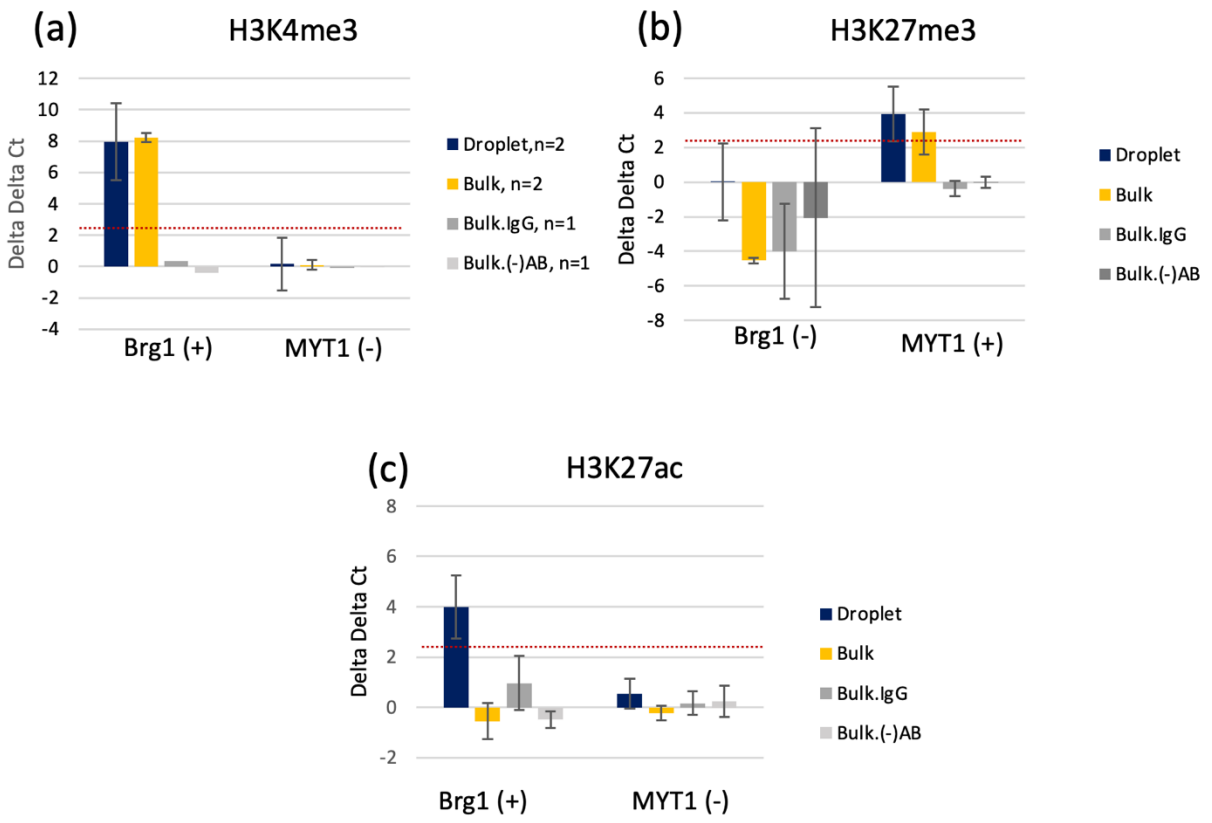

Figure 2.4 Droplet integrated ChIP system profiled (a)H3K4me3, (b)H3K27me3, and (c)H3K27ac in HeLa cells with 250K cells per sample. Enrichment of droplet samples is depicted in blue, bulk samples in yellow, and bulk negative controls in grey (IgG & bare beads). All targeted samples showcase adequate enrichment signal, above the threshold of 2.2

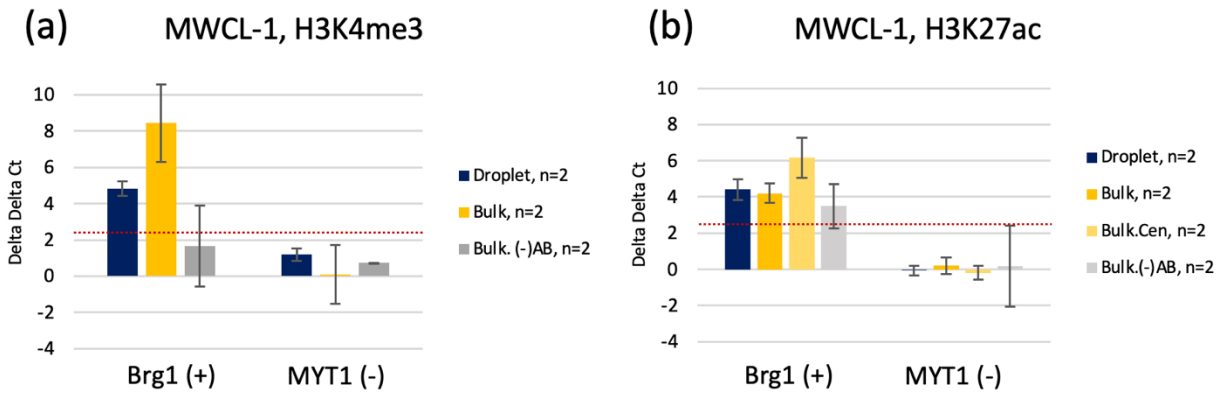

Figure 2.5 To demonstrate the adaptability of the developed droplet integrated ChIP system, H3K4me3 and H3K27ac were profiled in MWCL-1 cells.

2.3.4 Development of a Droplet Microfluidic Module for Reverse Crosslinking

Conventional ChIP incorporates formaldehyde crosslinking to reinforce protein-DNA interactions and increase the immunoprecipitation retention throughout the duration of the procedure. Subsequent downstream steps incorporate overnight reverse crosslinking at 65ºC with RNase A to degrade RNA and Proteinase K for protein digestion. This allows the liberation of the DNA fragments associated with the target of interest. Following the CAR-Wash module, a cylindrical heater was developed and incorporated to automate the reverse crosslinking and chromatin liberation section. Addition of this third module would complete the goal of automating the entirety of the ChIP protocol through different microfluidic modules.

To begin incorporating the reverse crosslinking steps to a droplet microfluidic platform, the normally 4–12 hour treatment needed to be shortened to potentially under one hour. As separate incubations, the RNase A incubation could be decreased to 15 minutes with a 2-hour Proteinase K incubation and still retain sufficient DNA. Next, it was noted that the Proteinase K treatment could be brought down to 30 minutes, after a 1-hour RNase A incubation, with comparable DNA yields (Figure 2.7). Compression of the individual bulk incubations suggests the potential to transition into droplets to effectively continue decreasing the incubation time.

To expedite the reverse crosslinking treatment, RNase A and Proteinase K were added simultaneously for a duration of 2 hours at 65ºC. Routinely, these reagents are separately added due to the digestion of RNase A by Proteinase K. The bulk simultaneous addition of RNase A and Proteinase K yielded 93% of DNA (Table 2.3); however, the simultaneous addition into droplets only yielded 50% of DNA (Table 2.3). The encapsulation of RNase A and Proteinase K proves unfavorable, possibly due to the enclosed volume increasing the probability for Proteinase K to digest RNase A over the nucleosomes. In parallel, droplet stability at 65ºC was

confirmed and prompted us to incorporate a cylindrical heater (Figure 2.6) to streamline the reverse crosslinking procedure within droplets. This is a modified isothermal design from a cylindrical heater for real-time PCR[34]. Initial experiments consisted of cell lysis and digestion through our enzymatic nucleosome prep module with droplets proceeding to the cylindrical heater at 65^{o}C for approximately one hour. Processed droplets were collected and purified, and DNA was quantified through Qubit Fluorometer. Table 2.4 depicts 70% (n=1) retention of nucleosomal DNA without the spacer, however with the space recovery increases to 82% (n=1).

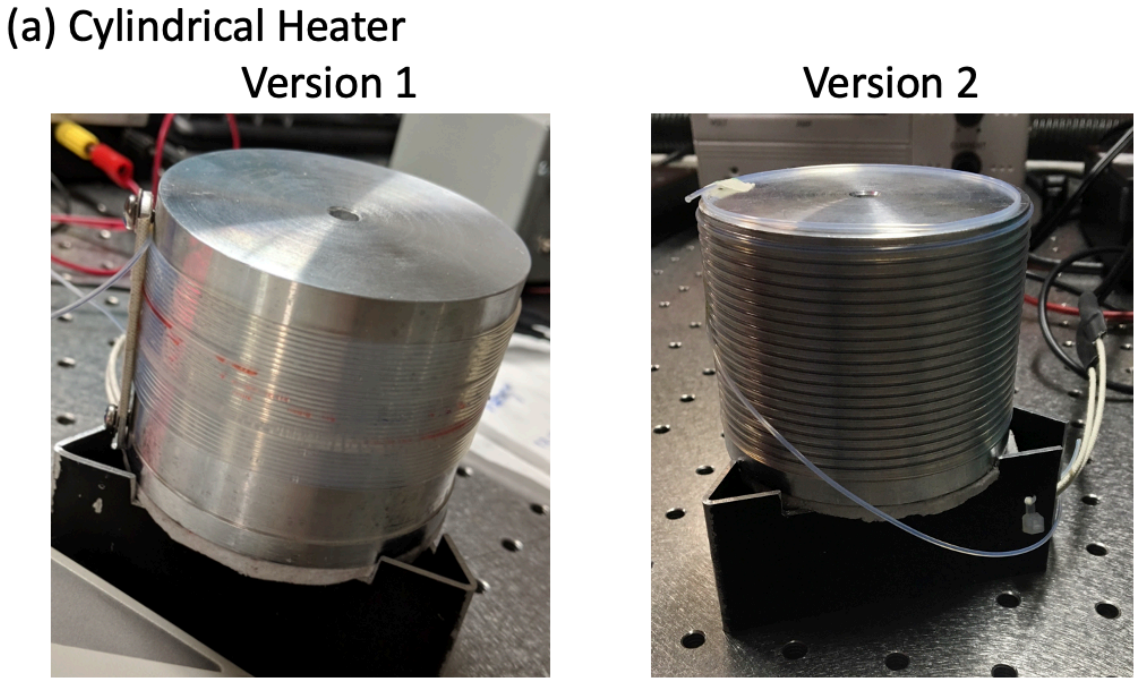

Figure 2.6 Cylindrical heater, made by the chemistry department electrical shop to adapt the latter portion of ChIP. Through this cylindrical heater samples injected with Proteinase K and RNase A incubate in droplets to digest RNA and proteins for chromatin liberation. The second version incorporated grooves to hold tubing in place.

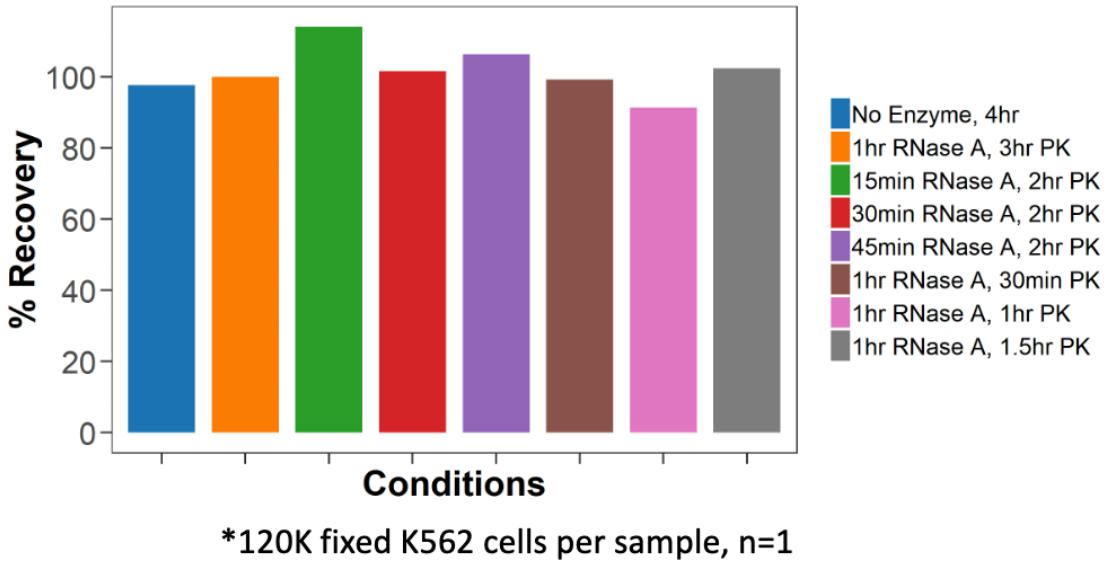

Figure 2.7 Bar chart titrating separate RNase A and Proteinase K incubation periods. As detached incubations, the RNase A treatment can go as low as 15 minutes with a 2-hour proteinase K treatment and still yield sufficient DNA. While the Proteinase K treatment can decrease to 30 minutes with a 1 hour RNase A treatment produces comparable amounts of DNA.

Table 2.3 Testing the simultaneous addition of RNase and Proteinase K in bulk and droplet experiments at 65°C. Bulk samples incubated on a heat block while droplet samples incubated using the newly developed cylindrical heater.

Format	Treatment *120K fixed K562 cells per sample, n=1	DNA Retention
Bulk	1hr RNase A at 65°C, 3hr Proteinase K at 65°C	760 ng
Bulk	Simultaneous Addition of Proteinase K and RNase A at 65°C for 2 hours	735 ng
Droplet	Simultaneous Addition of Proteinase K and RNase A at 65°C for 3hr, 10 wraps on cylindrical heater	403 ng

Table 2.4 Developing the simultaneous incubation of RNase A and Proteinase K treatment in droplets with additional with and without spacer flow.

Format	Treatment *120K fixed Jurkat cells per sample, n=1	Treatment Duration *10 wraps on cylindrical heater	DNA Retention
Bulk	1hr RNase A at 65°C, 3hr Proteinase K at 65°C	N/A	437 ng
Droplet	Simultaneous Addition of Proteinase K and RNase A at 65°C for 3hr, 10 wraps on cylindrical heater	1 hour with spacer	361 ng (82%)
Droplet		1 hour without spacer	315 ng (72%)

2.4 Conclusion

In conclusion, this chapter discusses the integration of two microfluidic droplet modules that translate ~70% of the ChIP protocol. Additionally, it touches on constructing and optimizing a third module for RNA and protein digestion to liberate chromatin fragments. The proof-of-concept data, generated from DNA enrichment profiles, demonstrates the successful ability to profile an active (H3K4me3) and repressive (H3K27me3) target. Additionally, the system's profiling capabilities were expanded by profiling targets in mammalian cultures and a model cell line developed for Waldenström macroglobulinemia (WM) research. Overall, the work in this chapter addresses the challenges that previous microfluidic ChIP modules face. It progresses towards adapting the entirety of the protocol instead of focusing on a specific portion. This multimodule bioassay has potential application to make profiling epigenetic modifications more accessible in clinical settings.

Acknowledgements

We gratefully acknowledge financial support from the National Institutes of Health (NIH CA 191186). G.E.D. was also supported by the Rackham Merit Fellowship. S. Doonan, C. Cook, Y. Xu, and V. Sahore (University of Michigan) participated in experiment design, microfluidic device design and fabrication, and data collection. J.-H. Lee and T. Ordog (The Mayo Clinic) provided indicated samples and reagents, participated in experiment design, and assisted in data analysis.

References

(1) Chen, T.; Dent, S. Y. R. Chromatin modifiers and remodellers: regulators of cellular differentiation. *Nat. Rev. Genet.,* **2014**, *15* (2), 93– 106.

(2) Goldberg, A. D.; Allis, C. D.; Bernstein, E. Epigenetics: A Landscape Takes Shape. *Cell,* **2007**, *128* (4), 635– 638.

(3) Plongthongkum, N.; Diep, D. H.; Zhang, K. Advances in the profiling of DNA modifications: cytosine methylation and beyond. *Nat. Rev. Genet.,* **2014**, 15(10), 647-61.

(4) Zhao, Z.; Shilatifard, A. Epigenetic modifications of histones in cancer. *Genome Biol.,* **2019**, *20* (1), 245.

(5) Jiang, C., Pugh, B. Nucleosome positioning and gene regulation: advances through genomics. *Nat. Rev. Genet.,* **2009**, **10**, 161–172.

(6) Klemm, S.L., Shipony, Z. & Greenleaf, W.J. Chromatin accessibility and the regulatory epigenome. *Nat. Rev. Genet.,* **2019**, 20, 207–220.

(7) Holoch, D.; Moazed, D. RNA-mediated epigenetic regulation of gene expression. *Nat. Rev. Genet.,* **2015**, 16 (2), 71– 84.

(8) Woodcock, C.L. Chromatin Architecture. *Curr. Opin. Struct. Biol.*, **2006**, 16, 213–220.

(9) McGinty, R. K.; Tan, S. Nucleosome structure and function. *Chem. Rev.,* **2015**, *115* (6), 2255– 73.

(10) Luhar, K.; Mäder, A.W.; Richmond, R.K.; Sargent, D.F.; Richmond, T.J. Crystal structure of the nucleosome core particle at 2.8 A resolution. *Nature*, **1997**, 389(6648), 251-60.

(11) Kouzarides, T. Chromatin modifications and their function. *Cell*, **2007**, 128, 693–705.

(12) Wan, J.; Liu, H.; Chu, J.; Zhang, H. Functions and mechanisms of lysine crotonylation. *J. Cell Mol. Med.,* **2019**, 23(11), 7163-7169.

(13) Rabut, G.; Peter, M. Function and regulation of protein neddylation, *EMBO Reports,* **2008**, 9, 969-976.

(14) Chen, Y.; Sprung, R.; Tang, Y.; Ball, H.; Sangras, B.; Kim, S.C.; Falck, J.R.; Peng, J.; Gu, W.; Zhao, Y. Lysine propionylation and butyrylation are novel post-translational modifications in histones. *Mol Cell Proteomics*, **2007**, 6(5), 812-9.

(15) Jenuwein, T.;Allis, C.D. Translating the Histone Code. *Science,* **2001**, 293 (5532), 1070-1080.

(16) Martin, C.; Zhang, Y. The diverse functions of histone lysine methylation. *Nat. Rev. Mol. Cell Biol.,* **2005**, 6(11), 838-49.

(17) Santos-Rosa, H.; Schneider, R.; Bannister, A.J.; Sherriff, J.; Bernstein, B.E.; Emre, N.C.T.; Schreiber, S.L.; Mellor, J.; Kouzarides, T. Active genes are tri-methylated at K4 of histone H3. *Nature*. **2002**, 419, 407–11.

(18) Wagner, E.J.; Carpenter, P.B. Understanding the language of Lys36 methylation at histone H3. *Nat. Rev. Mol. Cell Biol*., **2012**, 13, 115–26.

(19) Lehnertz, B.; Ueda, Y.; Derijck, A.A.H.A.; Braunschweig, U.; Perez-Burgos, L.; Kubicek, S.; Chen, T.P.; Li, E.; Jenuwein, T.; Peters, A.H.F.M. Suv39h-mediated histone H3 lysine 9 methylation directs DNA methylation to major satellite repeats at pericentric heterochromatin. *Curr. Biol*., **2003**, 13, 1192–200.

(20) Cao, R.; Wang, L.J.; Wang, H.B.; Xia, L.; Erdjument-Bromage, H.; Tempst, P.; Jones, R.S.; Zhang, Y. Role of histone H3 lysine 27 methylation in polycomb-group silencing. *Science*, **2002**, 298, 1039–43.

(21) Shi, Y.; Lan, F.; Matson, C.; Mulligan, P.; Whetstine, J.R.; Cole, P.A.; Casero, R.A.; Shi, Y. Histone demethylation mediated by the nuclear amine oxidase homolog LSD1. *Cell*, **2004**, 119, 941–53.

(22) Li, Y.; Seto, E.; HDACs and HDAC inhibitors in cancer development and therapy. *Cold Spring Harb. Perspect. Med.*, **2016**, 6, a026831.

(23) Josling, G.A.; Selvarajah, S.A.; Petter, M.; Duffy, M.F. The role of bromodomain proteins in regulating gene expression. *Genes (Basel)*, **2012**, 3, 320–43.

(24) Collas, P. The current state of chromatin immunoprecipitation. *Mol. Biotechnol.*, **2010**, 45(1), 87-100.

(25) Carey, M.F.; Peterson, C.L.; Smale, S.T. Chromatin Immunoprecipitation (ChIP) *Cold Spring Harb. Protoc.,* **2009**.

(26) Brind'Amour, J.; Liu, S.; Hudson, M.; *et al*. An ultra-low-input native ChIP-seq protocol for genome-wide profiling of rare cell populations. *Nat. Commun.,* **2015**, 6, 6033.

(27) Rhee, H.S.; Pugh, B.F. Comprehensive genome-wide protein-DNA interactions detected at single-nucleotide resolution *Cell*, **2011**, 147(6), 1408-19.

(28) Gilfillan, G.D.; Hughes, T.; Sheng, Y. *et al*. Limitations and possibilities of low cell number ChIP-seq. *BMC Genomics,* **2012**, 13, 645.

(29) Park, P. ChIP–seq: advantages and challenges of a maturing technology. *Nat. Rev. Genet.,* **2009**, 10, 669–680.

(30) Wu, A.R.; Kawahara, T.L.; Rapicavoli, N.A.; van Riggelen, J.; Shroff, E.H.; Xu, L.; Felsher, D.W.; Chang, H.Y.; Quake, S.R. High throughput automated chromatin

immunoprecipitation as a platform for drug screening and antibody validation. *Lab Chip*, **2012**,12(12), 2190-8.

(31) Xu, Y.; Doonan, S.R.; Ordog, T.; Bailey, R.C. A droplet microfluidic platform for efficient enzymatic chromatin digestion enables robust determination of nucleosome positioning *Lab Chip*, **2018**,18, 2583-2592.

(32) Doonan, S. R.; Lin, M.; Bailey, R.C. Droplet CAR-Wash: continuous picoliter-scale immunocapture and washing *Lab Chip*, **2019**, 19, 1589.

(33) Hodge, L.S.; Novak, A.J.; Grote, D.M.; Braggio, E.; et al. Establishment and characterization of a novel Waldenstrom macroglobulinemia cell line, MWCL-1. *Blood*, **2011**, 117(19), e190-7.

(34) Hatch, A.C.; Ray, T.; Lintecum, K.; Youngbull, C. Continuous flow real-time PCR device using multi-channel fluorescence excitation and detection. *Lab Chip*, **2014**, 14, 562-568.

Chapter 3 Drip, Drop, CUT&RUN – Towards Automation of Cleavage Under Target and Release Under Nuclease Utilizing Droplet Microfluidics

Gloria Diaz, Ryan C. Bailey

Abstract

Enzymatic tethering methods are the latest technique incorporated into epigenetic and chromatin profiling assays. In 2017, the Henikoff lab introduced Cleavage Under Target and Release Under Nuclease (CUT & RUN), an enzyme tethering assay inherently better than previous assays because it has a lower background, allowing for a better signal-noise ratio. These benefits are achieved by directly fragmenting the genomic region associated with the target of interest rather than solubilizing an entire cell and genome. By expanding the MNase module's potential, we can utilize it to assemble the multi-unit complex that drives the selective digestion processes. The goal is to transition this multi-step assembly process to a single droplet incubation by adding the component simultaneously in a single buffer. These alterations removed repetitive and monotonous wash steps and decreased the assay time by half the required bench time while allowing the MNase digestion to occur at low temperatures. Significant enrichment of targeted gene regions was observed in droplet- and bulk-processed samples through quantitative polymerase chain reaction analysis (relative to negative controls), demonstrating the validity of the droplet adapted CUT&RUN assay

3.1 Enzymatic Tethering Assays

A modern staple of molecular biology is the genomic profiling of protein-binding sites. To do such enzymatic tethering assays (ETA) are the in-vogue technique. These assays genetically engineer fusion proteins with an enzyme and bind the unit to chromatin proteins to implement a modification on the surrounding DNA landscape[1]. The most notable benefit to this category of assays is their performance *in vivo*, meaning no formaldehyde crosslinking is required[2]. Additionally, they circumvent concerns regarding chromatin solubility because it is not necessary to digest down an entire genome. Early iterations required direct genetic fusion of an enzyme to the target of interest.[3] However, these assays have been redesigned so the enzyme attaches through immunological targeting[4-6], and they have become readily adaptable to different targets of interest.

The framework for enzymatic tethering assays was initiated as an orthogonal technique to confirm ChIP-based results and as an alternative route to chromatin profiling insight. The first notable ETA, DNA adenine methyltransferase identification (DamID), functioned by genetically fusing DNA adenine methyltransferase (Dam) to a target of interest[3]. The tethered Dam enzyme then methylated adenines in the surrounding DNA regions[7], generating a digestion site for the restriction enzyme DpnI. DpnI specifically cuts at methylated GATC regions to generate fragments where the target of interest sits on chromatin.

Following the template for this initial ETA, chromatin endogenous cleavage (ChEC)[4] was designed to improve the special resolution of DamID. Similarly, a fusion protein construct is expressed, however, utilizing micrococcal nuclease (MNase) instead of DpnI. MNase is an endo-exonuclease that digests double-stranded DNA in the presence of calcium ions[9]. Initially, this technique was coupled with southern blotting[4] and later joined with microarray[10] and sequencing

analysis[11]. To transition away from genetically expressed fusion protein constructs, chromatin immunocleavage (ChIC) incorporated an antibody incubation for directing MNase tethering to a target of interest[4]. Considering this assay was simultaneously introduced with ChEC, its initial read out was southern blotting. In 2017, cleavage under target and release under nuclease (CUT&RUN) improved ChIC by incorporating a sequencing read out and procedural alterations to quantify binding events. It garnered popularity through its adaptability to profile a diverse range of targets in budding yeast and human cells[5].

CUT&RUN is a highly impactful ETA due to its many benefits that outperform ChIP-based protocols as well as preceding tethering assays[5]. It works by permeabilizing cells and binding them to magnetic beads for facile sample manipulation. An antibody targeting the protein of interest is then added and gains access to the genome through the permeabilized membrane. Once it has identified the target of interest, the antibody directs chromatin digestion by tethering to pA-MNase which is activated through the addition of divalent ions. Initially published by Peter Skene and Steven Henikoff, this assay has a high signal-to-noise ratio and low background through a temperature sensitive digestion that limits the nonspecific activity of pA-MNase.[5] Additionally, it can profile histone tail modifications as well as chromatin proteins within low inputs. In the published work, CUT&RUN was able to profile transcription factor CTCF utilizing the small amount of 600,000 cells. Not only does it have a high resolution for peak localization, moreover it can quantify binding events by spiking in a known amount of heterologous DNA. Lastly, this assay transcends its initial utility by opening a window into three-dimensional architecture detection of the loci associated with the target of interest. By manipulating the temperature sensitive digestion, MNase has the potential to digest nearby chromatin regions, yielding insight into the surrounding, distal genomic landscape.

This chapter describes our attempt to condense the bulk assay protocol for CUT&RUN and validate the droplet microfluidic protocol. The condensed protocol joins separate incubations to assemble the immunoprecipitation unit that allows for directed chromatin digestion. We also address unexpected variables when transitioning the procedure to a microfluidic format, such as nonspecific binding and the formation of large aggregates. Lastly, we demonstrate two alternative formats for a droplet integrated CUT&RUN protocol by validating the target pull down through quantitative polymerase chain reaction (qPCR).

Table 3.1 Enzymatic tethering assays listed in chronological order of development. Advantages and disadvantages showcase how newly developed assays worked to improve on the limitations of the previous assays.

Assay	Advantages	Disadvantages	Citation
DamID DNA Adenine Methyltransferase Identification	- Not antibody dependent	- Requires fusion protein expression - Low special resolution - 'GATC' sequence needed for chromatin digestion	*Mol Biol Cell* 1997; 8: 2017 - 2038
ChEC Chromatin Endogenous Cleavage	- Not antibody dependent - High resolution through targeted digestion	- Requires fusion protein expression	*Mol Cell* 2004; 16: 147–157
ChIC Chromatin Immunocleavage	- High resolution through targeted digestion	- High quality antibody is needed	*Mol Cell* 2004; 16: 147–157
CUT&RUN Cleavage Under Target & Release Under Nuclease	- High resolution through targeted digestion - Compatible with sequencing	- High quality antibody is needed - Temperature sensitive chromatin digestion	eLife 2017; 6: e21856
CUT&Tag Cleavage Under Target & Tagmentation	- High resolution through targeted digestion - Compatible with sequencing - Library preparation incorporated into assay	- High quality antibody is needed	*Nat Commun 2019; 10: 1930*

3.2 Materials and Methods

3.2.1 Buffer Recipes

Bead Activation Buffer** (pH 7.9) contains 20 mM HEPES, 10 mM KCl, 1 mM $CaCl_2$, 1 mM $MnCl_2$. **BAW Buffer** (pH 8) contains 20 mM HEPES, 10 mM KCl, 1 mM $CaCl_2$, 1 mM $MnCl_2$, 150 mM NaCl, 0.5 mM Spermidine, *Roche cOmpleteTM EDTA-free Protease Inhibitor. **Digitonin Buffer**** (pH 7.5) contains 20 mM HEPES, 150 mM NaCl, 0.5 mM Spermidine, 0.01% (w/v) digitonin, *Roche cOmpleteTM EDTA-free Protease Inhibitor. **Assembly Buffer** (pH 7.5) contains 20 mM HEPES, 150 mM NaCl, 0.5 mM Spermidine, 0.01% (w/v) digitonin, 6 mM EDTA, *Roche cOmpleteTM EDTA-free Protease Inhibitor. **STOP Buffer**** contains 350 mM NaCl, 20 mM EDTA, 4 mM EGTA, 50 μg/mL RNase A, 50 μg/mL Glycogen.

*1 EDTA-free Protease Inhibitor tablet per 10 mL of solution

** Buffer recipes from EpiCypher CUTANA CUT&RUN Protocol[12]

3.2.2 Microfluidics Device Preparation

Devices were fabricated using standard soft lithography in poly-(dimethylsiloxane) (PDMS) (RTV615, Momentive Performance Materials, Inc.). Devices were designed using AutoCAD software (Autodesk, Inc.) and sourced as transparent photolithography masks (CAD/Art Services, Inc.). SU8 2025 and 2050 negative epoxy photoresist (MicroChem Corp.) were spin coated onto silicon wafers (University Wafer, Boston MA) and features were crosslinked by standard photolithography. For the initial layer, SU8 2025 was spin coated at 2000 rpm for 30 seconds for a thickness of 40 um. After wafer baking (Cimarec, Thermo Scientific) and exposure to UV light (MJB3 Mask Aligner, SUSS MicroTec) the initial layer was

developed using propylene glycol monomethyl ether acetate (PGMEA) (Sigma-Aldrich, St. Louis, MO). For the second layer, SU8 2050 was spin coated at 1150 rpm for 30 seconds for a thickness of 160 um. Following baking, exposure and development, master was surface treated with tridecafluoro-1,1,2,2-tetrahydrooctyl trichlorosilane (Gelest, Inc., Morrisville, PA).

A 10:1 base to curing agent ratio was mixed, followed by the addition of PDMS-PEG copolymer at 0.25% (w/w) and degassed under vacuum. The PDMS mixture was poured over the master in a Petri dish and allowed to cure for 1 hour at 70°C (HeraTherm Oven, Thermo Scientific). PDMS stamps were cut, and hole punched with blunt end needles (24-gauge inlets, 30-gauge outlet and electrolyte channels). Stamps were sonicated in water, dried with compressed air, and bonded to glass cover slides (1 mm thickness, 75 mmx 50 mm, Thermo Fisher Scientific) via oxygen plasma activation (Plasma cleaner PDC-32G, Harrick Plasma, Inc). Devices were then baked overnight and treated with Aquapel (Pittsburgh Glass Works, Pittsburgh, PA) before use.

3.2.3 Cell Culturing

HeLa cells were cultured in DMEM medium (Gibco DMEM High Glucose, Catalog No. 11965092, Fisher Scientific) supplemented with 10% v/v fetal bovine serum at 37°C with 5% CO_2. Each cell flask was treated with 0.5% trypsin-EDTA (Gibco 0.05% Trypsin-EDTA, Catalog No. 25300-054, Fisher Scientific) for 5 minutes at 37°C to separate the cells from the flask. To quench the trypsin solution, DMEM medium was used (1:1), cells were mixed using a pipette and pelleted at 600 x g for 5 min at 4°C. Cells were watched twice with cold PBS (Lonza™ BioWhittaker™ Phosphate Buffered Solution, Catalog No. BW17516F12, Fisher Scientific) to, resuspended in 30% OptiPrep-PBS (OptiPrep™ Density Gradient Medium,

Catalog No. D1556-250ML, Millipore Sigma) to a concentration of 3 million cells per mL, divided into aliquots of 30 μL, and kept on ice until needed.

3.2.4 Magnetic Bead Preparation

From bead stock (BioMag ® Plus Concanavalin A, Catalog No. BP531, Bangs Laboratories, Inc) 11 μL of bead solution (per reaction) was transferred to an Eppendorf (Eppendorf DNA LoBind, Fisher Scientific, Waltham, MA) for batch preparation. Using a magnetic rack, beads were washed twice with 100 μL (per reaction) of bead activation buffer and resuspended in 40 μL (per reaction) of BAW buffer. The bead batch was divided into aliquots of 35 μL and kept on ice till use.

3.2.5 Syringe Preparation

Buffer solutions were delivered through 24-gauge tubing (Cole-Parmer, Vernon Hills, IL) connected to glass tight syringes (Hamilton Company, Reno, NV). Syringes were controlled using syringe pumps (Pump 11 Pico Plus Elite, Harvard Apparatus) – carrier oil 6 μL min^{-1}, droplet generator 2 μL min^{-1}, oil spacer 14 μL min^{-1}, pico injector 4 μL min^{-1}. Carrier oil phase was composed of fluorinated oil Novec 7500 (3M, St. Paul, MN) with 2% (w/w) perfluoropolyether polyethylene glycol block co-polymer surfactant (RAN Biotechnologies, Inc. Beverly, MA). The tubing delivering cells was treated overnight with 1% (w/v) Pluronic F127 (Sigma-Aldrich, St. Louis, MO).

3.2.6 Microfluidic Device Operation

Within 6 hours of experiment, microfluidic devices were treated using Aquapel (Pittsburgh Glass Works, LLC., Pittsburgh, PA) to produce a hydrophobic coating. Prior to

device assembly, tubing was cleaned with isopropanol. A full circuit AC electric field was achieved by connecting metal alligator clamps from an in-house DC-AC converter (12V DC input, 0-360V AC at 36 kHz as output) connected to a power supply to needles supplying 3M NaCl solution into electrolyte-filled microchannels on device. Aqueous solution containing cells, magnetic beads, and additional reaction components were emulsified at Y-junction. After incubating for 3.5 minutes in delay channels, each droplet was injected with pA-MNase (Catalog No. 15-1016: EpiCypher, Inc, Durham, North Carolina) cocktail before being collected using 30 gauge (Cole-Parmer, Vernon Hills, IL) into a 1.5 mL Eppendorf and incubated overnight at 4^{o}C on a rocker. After delivery of cell solution, the device continued to run for 6 additional minutes to push remaining droplet product out. Following immunoprecipitation, droplets samples were coalesced by adding 50 μL of 1H, 1H, 2H, 2H – perfluoro-1-octanol (Sigma-Aldrich, St. Louis, MO), gently hand mixing, and spinning down at 5,000 rpm for 1 minute. The aqueous layer was pipetted out and washed twice with 150 μL digitonin buffer for digestion and extraction

3.2.7 Bulk Sample preparation

Bulk sample controls were prepared in parallel. Using a 1.5 ml Eppendorf vial, 30 μL of whole HeLa cells were incubated with 30 μL of magnetic beads with BAW buffer for 3 minutes at room temperature. Following cell permeability and bead attachment, 60 μL of pA-MNase cocktail was added, gently mixed, and incubated overnight at 4^{o}C. Following overnight incubation, samples were washed with digitonin buffer for digestion and extraction.

3.2.8 Extraction and Purification

(This section has been adapted from the EpiCypher CUTANA protocol) Both bulk and segmented samples were resuspended in 50 μL of digitonin buffer, 1.5 μL of 100 mM $CaCl_2$ was

pipetted into each reaction and incubated on a cold block for 1 hour at 4°C. Following digestion, 30 µL of STOP buffer was added and vortexed. Samples were then incubated at 37°C for 10 minuets. Solution was pipetted out and purified using the QIAquick PCR Purification Kit (Qiagen, Hilden, Germany), using the standard manufacturing instructions. All samples were eluted in 15 µL, 2 µL of which were used to quantify samples using Qubit double stranded DNA High Sensitivity Assay (Thermo Fisher Scientific, Grand Island, NY).

3.2.9 PCR Amplification

For each reaction, 10 µL of PowerUP™ SYBER™ Green master mix (Applied Biosystems Catalog No. A25776, Fisher Scientific) was used with 2 µL of forward and reverse primer (Integrated DNA technologies, Coral, IA) (working stocks for forward and reverse primer - 5 µM). 2 µL of template DNA was mixed into each reaction and the volume was brough to 20 µL using ultra distilled water (Invitrogen™ UltraPure™ DNase/RNase-Free Distilled Water, Catalog No. 10-977-015, Fisher Scientific). A standard 384-well plate Applied Biosystems Catalog No. 4309848, Fisher Scientific) was run on a 7900HT Fast Real-Time PCR System (Applied Biosystems) with the parameters outlined in Table 3.2. Fold change was calculated using Equation 3.1 to assess the pull-down efficiency of the target of interest.

Table 3.2 Standard qPCR parameters established by the North Campus Research Complex Advance Genomics Core where qPCR plates were run on a 7900HT Fast Real-Time PCR System.

Hold Stage	PCR Stages *40 cycles	Melt Curve
5°C x 2 minutes 95°C x 10 minutes	95°C x 15 seconds 60°C x 1 minute	95°C x 15 seconds 60°C x 1 minute 95°C x 15 seconds

$$\text{Log}_2\ \Delta\Delta\ \text{Ct} = \Delta\text{Ct}_{\text{Sample}} - \Delta\text{Ct}_{\text{Calibrator}}$$

$$\text{Log}_2\ \Delta\Delta\ \text{Ct} = (\text{Ct}_{(\text{gene of interest})} - \text{Ct}_{(\text{reference gene})}) - \text{Ct}\ (\text{Ct}_{(\text{gene of interest})} - \text{Ct}_{(\text{reference gene})})$$

(3.1)

3.3 Results and Discussion

3.3.1 Condensing the Bulk CUT&RUN Assay

Procedural portions need to be condensed for droplet adaptability to translate a benchtop molecular assay to a microfluidic format. Joining protocol sections allows the streamlining of monotonous steps and reduces buffer exchanges as well as the number of buffers utilized. Prior to utilizing a microfluidic chip, assay alterations must be tested in bulk and demonstrate the appropriate qPCR enrichment. The initial focus was on combining the separate incubations of the antibody immunoprecipitation and attachment of the fusion enzyme, pA-MNase. In the conventional benchtop protocol, these incubations occur in similar buffer formulations, antibody and dig-wash buffer. The only difference being that the antibody buffer contains EDTA to chelate any optional divalent ion carryover. To assess the ability to join these incubations, both H3K27me3 antibody and pA-MNase were added simultaneously in the different buffer formulations, and enrichment was detected through qPCR (Figure 3.1). Looking at enrichment profiles for H3K27me3 in antibody buffer (blue) and dig-wash buffer (yellow) the region of interest, MYT1, yields comparable signal between both buffers. Additionally, no enrichment within the negative IgG controls suggests that an antibody is needed to direct the pA-MNase digestion in both buffer formulations.

3.3.2 Practical Challenges When Adapting to Microfluidic Format

With the joining of these two incubations, it was time to transition these alterations to a microfluidic format. This was done by utilizing the previously published MNase microfluidic modules[13]. However, initial runs of the droplet adapted protocol demonstrated design challenges. Droplets were generated with permeabilized cells attached to magnetic beads (cell-magnetic

beads) along with antibodies and pA-MNase. Upon introduction of the cell-magnetic beads into the device, the unit nonspecifically bound to the PDMS channels. Additionally, within the tubing, the cell-magnetic beads began clumping, forming larger aggregates that adhered to the channel walls and clogged the droplet generator (Figure 3.2a). As the fragments enlarged, the clumps that made it into droplets began affecting droplet uniformity. Different surface modifications and combinations of treatments were tested to reduce the nonspecific binding. Initially, a 15-minute pluronic FC-40 treatment was used, however, it was not promising as there was significant wetting of the channel walls and droplet formation was inconsistent (Figure 3.2b). The second treatment tested was a combination of aquapel for 3-5 minutes followed by a 15-minute pluronic treatment. After 15 minutes, a white coating appeared on the fluidic walls (Figure 3.2c). After visualization of the channels on a Leica microscope, it was noted that there was also significant swelling of the channel walls. The last surface modification tested was the addition of a smart PEG copolymer[14]. This addition is mixed into uncured PDMS at the desired weight by weight percentage. 1%, 0.5%, and 0.25% were tested, and 0.25% was enough to reduce the nonspecific binding and not alter the fabrication protocol.

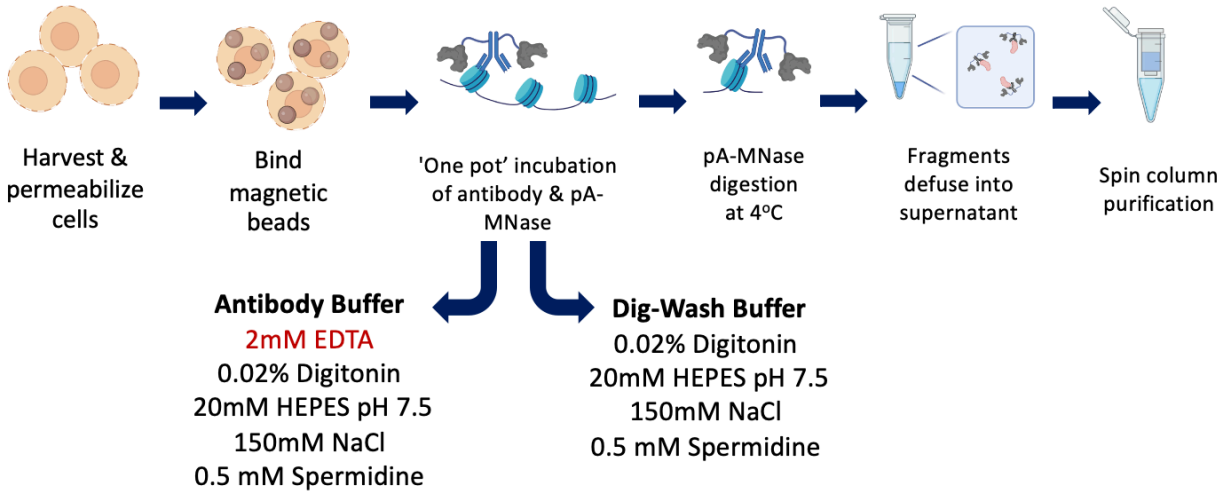

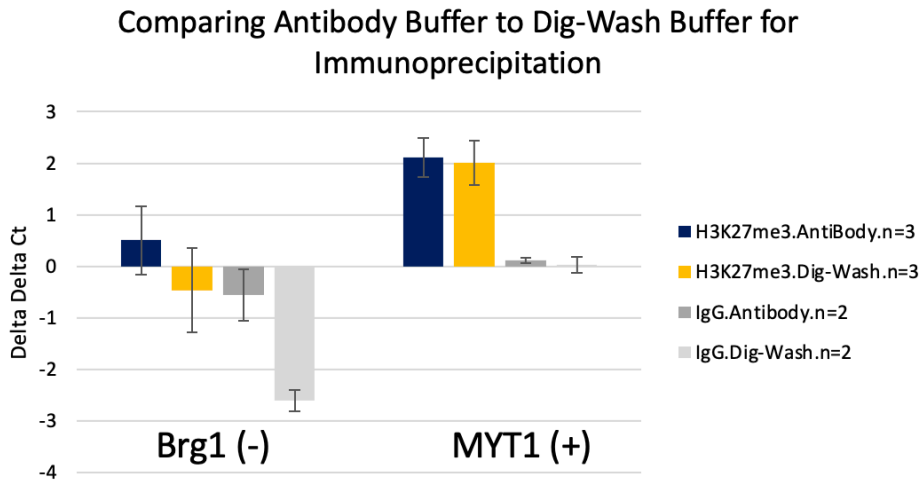

Figure 3.1 Bulk experiment procedure to condense assembly of immunoprecipitation unit into a single incubation. Testing buffer recipes (antibody and dig-wash) for simultaneous incubation. Pull down efficiency for H3K27me3 in HeLa cells is depicted by qPCR enrichment profiles.

3.3.3 Profiling Histone Tail Modifications

With the reduction of nonspecific binding, adaptation of the CUT&RUN protocol to a droplet format could progress. The smart copolymer additive was incorporated, and droplets were generated with permeabilized cells bound to magnetic beads along with a cocktail containing the antibody for the target of interest and the fusion enzyme, pA-MNase. With the cells already permeabilized, the antibody and pA-MNase benefit from active mixing induced by intermolecular forces within droplets. This segmented format also reduces the distance the biological components must diffuse to discover their binding partner. By extension this allows an efficient assembly of the immunoprecipitation unit before chromatin tagmentation. Once droplets reached the end of the module, they were injected with calcium ions to initiate chromatin digestion at 0^{o}C. The enrichment data for H3K27me3 within HeLa cells (Figure 3.3) depicts enrichment for both the bulk (blue) and droplet adapted protocol (yellow) in the region of enrichment, MYT1, and no signal in the region of depletion, Brg1. Because this is a targeted tagmentation, the amount of chromatin retained is lower compared to ChIP-based assays. This is significant signal to consider when comparing the ΔΔ Ct value to the negative IgG control. Taking into consideration the relative error of the bulk versus droplet samples, error is significantly decreased in samples that are microfluidically processed compared to the bulk. Suggesting that the microfluidic adaptations increase the uniformity of sample processing.

We have also been able to successfully translate modifications from work on adapting a secondary ETA to a microfluidic format to our work towards droplet integrated CUT&RUN. In this new version, droplets were generated with whole cells, magnetic beads, and buffer conditions gentle enough to permeabilize the cellular membrane and attach the magnetic beads. The droplets then incubated through the delay channels and, at the end, were injected with the

pA-MNase and the antibody probing the target of interest. Figure 3.4 depicts the protocol as well as the enrichment profiles. The region of enrichment, MYT1, had significant signal for both the bulk and droplet samples as well as minimal enrichment within the region of depletion, Brg1. The negative IgG control also has minor enrichment suggesting the need for a primary antibody to direct the assembly of the immunoprecipitation unit.

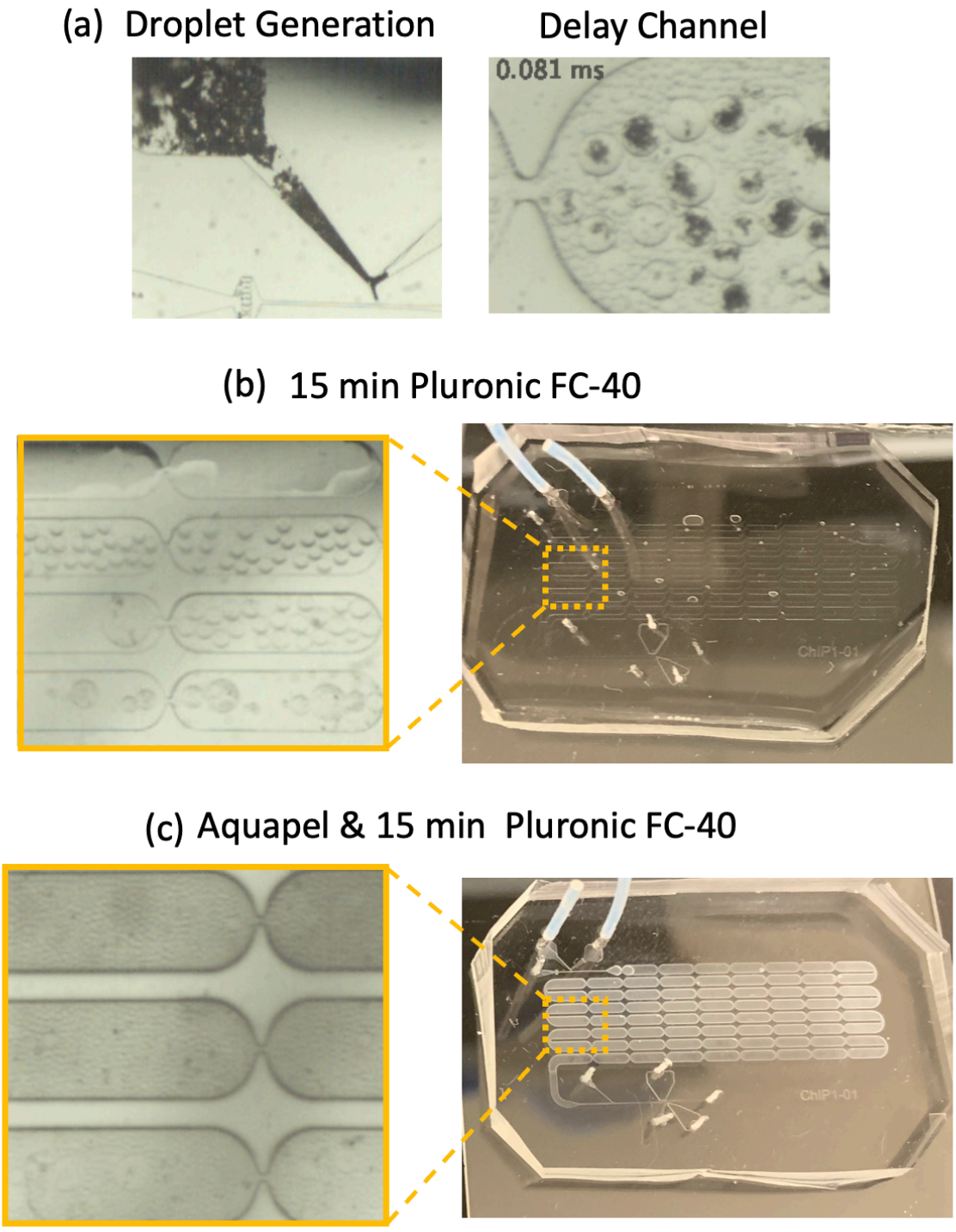

Figure 3.2 Unforeseen challenges, (a) permeabilized cells bound to magnetic beads clump and clog droplet generation channels. Additionally, droplet uniformity was affected by aggregates. Aggregates bind nonspecifically to channels, exacerbating clogging. Different treatments were tested to decrease the nonspecific binding, (b) 15 minutes Pluronic FC-40 and (c) Aquapel with 15 minutes Pluronic FC-40.

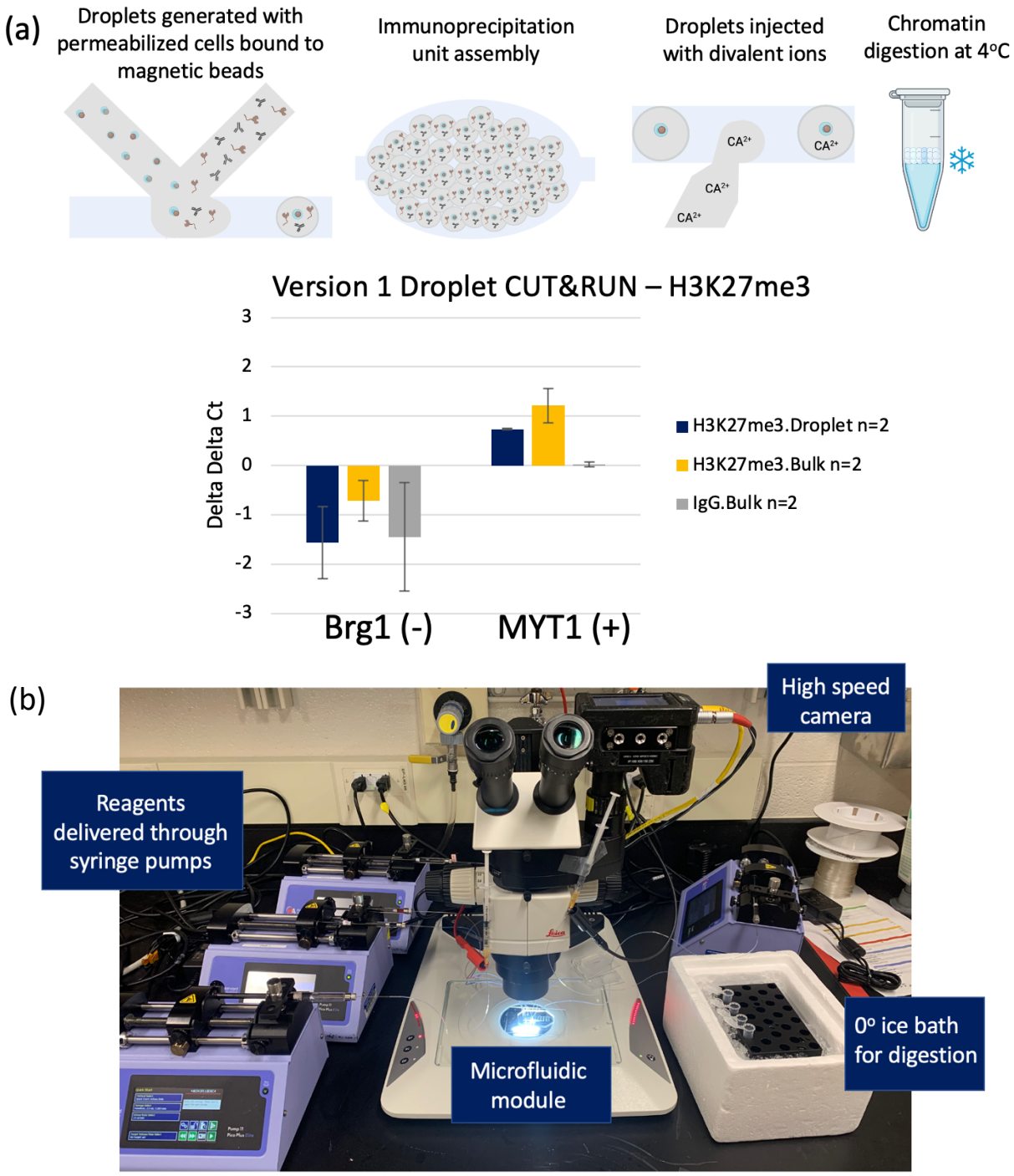

Figure 3.3 (a) Initial version of droplet integrated CUT&RUN. Droplets were generated with permeabilized cells bound to magnetic beads, antibody, and pG-MNase. Once droplets reach the end of the module, calcium ions are injected initiating directed digestion. Enrichment of the MYT1 gene region can be seen for bulk and droplet processed samples, with no enrichment seen in the IgG negative control. (b) Picture of camera and microfluidic set up. Reagents delivered using syringes, microfluidic chip visualized on a microscope, and samples collected in Eppendorf on ice

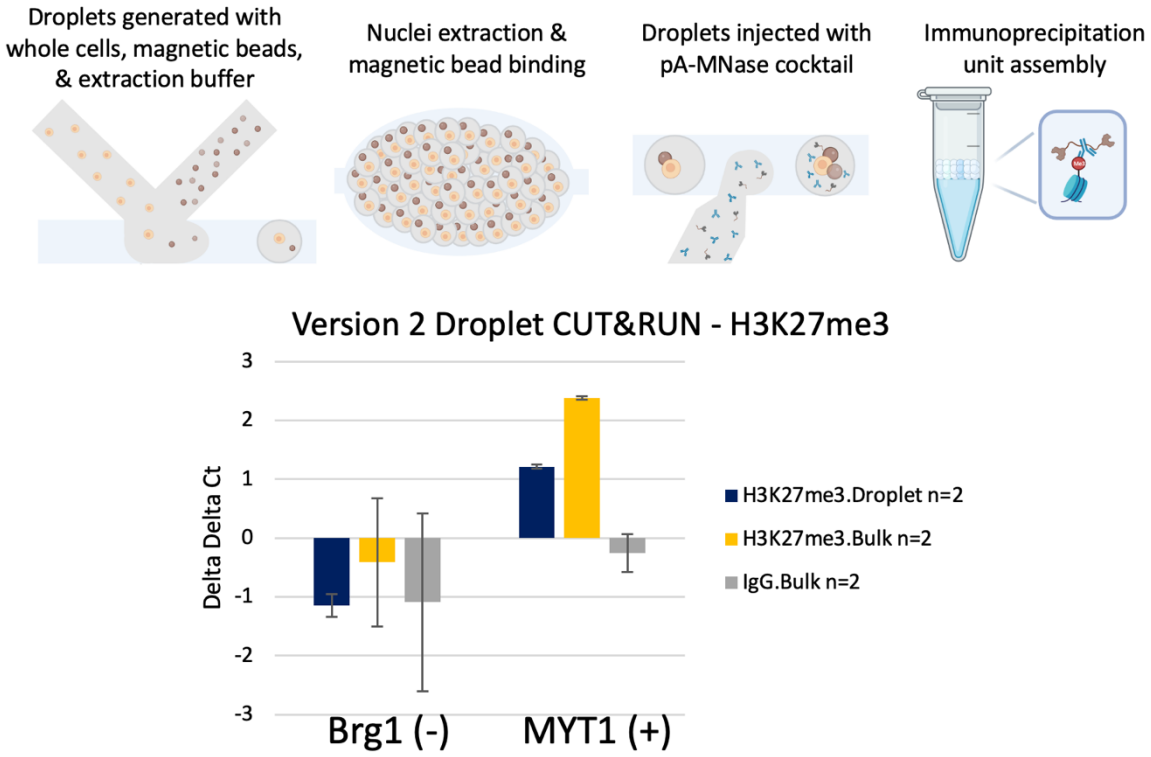

Figure 3.4: Second version of droplet integrated CUT&RUN. Droplet generation consisted of whole cells, magnetic beads, and a buffer formulation for permeabilizing cells and binding magnetic beads as droplets incubated through delay channels. At the end of the module, droplets were injected with an antibody to probe for the target of interest and pAG-MNase. Sample then incubated in droplets for the simultaneous assembly of the immunoprecipitation unit. qPCR analysis reveals enrichment of droplet and bulk processed samples.

3.4 Conclusion

This chapter establishes promising foundational progress toward automating enzymatic tethering assays, particularly CUT&RUN. This assay exploits microfluidic adaptation by condensing laborious procedural sections to streamline the protocol and expand its utility. The presented data displays the development of a shortened microfluidic protocol for CUT&RUN that is capable of profiling H3K27me3, validated through qPCR enrichment profiles where enrichment of a gene regions associated with the mark of interest was statistically different from the negative controls. It provides insight into design challenges such as nonspecific interactions to the microchannels and magnetic beads to cell clumping. Droplet implementation of CUT&RUN reduces the amount of incubations by 50% in the first half of the protocol. This droplet automated version is achieved in as little as 12 hours, a 4-fold decrease from the originally published protocol. The development of this droplet microfluidic bioassay yields the infrastructure to adapt additional profiling assays and breaks ground for alterations that improve assay functionality.

Acknowledgements

We gratefully acknowledge the funding support from the National Science Foundation (NSF – Understanding the Rules of Life Epigenetics: 1921677). G.E.D. was also supported by the Rackham Merit Fellowship. We also thank the Duo lab (previously University of Michigan, Department of Pathology, now University of Southern California, Department of Biochemistry) for providing the fusion enzyme pA-MNase. G. Diaz (University of Michigan) participated in the experiment design microfluidic device fabrication, and data collection.

References

(1) Policastro, R.A.; Zentner, G.E. Enzymatic methods for genome-wide profiling of protein binding sites. *Brief Funct. Genomics*, **2018**, 17(2), 138-145.

(2) Meyer, C.A.; Liu, X.S. Identifying and mitigating bias in next-generation sequencing methods for chromatin biology. *Nature Reviews Genetics*, **2014**, 15 (11), 709–21.

(3) van Steensel, B.; Henikoff, S. Identification of in vivo DNA targets of chromatin proteins using tethered Dam methyltransferase. *Nat. Biotechnol.,* **2000**, 18, 424–8.

(4) Schmid, M.; Durussel, T.; Laemmli, UK. ChIC and ChEC: genomic mapping of chromatin proteins. *Mol. Cell.,* **2004**, 16, 147–57.

(5) Skene PJ, Henikoff S. An efficient targeted nuclease strategy for high-resolution mapping of DNA binding sites. *eLife,* **2017**, 6, e21856.

(6) Kaya-Okur, H.S.; Wu, S.J.; Codomo, C.A. *et al*. CUT&Tag for efficient epigenomic profiling of small samples and single cells. *Nat. Commun.,* **2019**, 10, 1930.

(7) Marinus, M.G.; Morris, N.R. Isolation of deoxyribonucleic acid methylase mutants of Escherichia coli K-12". *Journal of Bacteriology*, **1973**, 114 (3), 1143–50.

(8) Geier, G.E.; Modrich, P. Recognition sequence of the dam methylase of Escherichia coli K12 and mode of cleavage of Dpn I endonuclease". *The Journal of Biological Chemistry*. **1979**, 254 (4), 1408–13.

(9) Heins, J.N.; Suriano, J.R.; Taniuchi, H.; Anfinsen, C.B. Characterization of a nuclease produced by Staphylococcus aureus. *The Journal of Biological Chemistry*. **1967**, 242 (5), 1016–20.

(10) Schmid, M.; Arib, G.; Laemmli, C.; et al. Nup-PI: the nucleopore-promoter interaction of genes in yeast. *Mol. Cell,* **2006**, 21, 379–91.

(11) Zentner, G.E.; Kasinathan, S.; Xin, B.; et al. ChEC-seq kinetics discriminates transcription factor binding sites by DNA sequence and shape in vivo. *Nat. Commun.,* **2015**, 6, 8733.

(12) EpiCypher® CUTANA™ CUT&RUN Protocol – Methods Overview, *EpiCypher*.

(13) Xu, Y.; Doonan, S.R.; Ordog, T.; Bailey, R.C. A droplet microfluidic platform for efficient enzymatic chromatin digestion enables robust determination of nucleosome positioning. *Lab Chip*, **2018**,18, 2583-2592.

(14) Gökaltun, A.; Kang, Y.B.A.; Yarmush, M.L.; Usta, O.B.; Asatekin, A.; Simple Surface Modification of Poly(dimethylsiloxane) via Surface Segregating Smart Polymers for Biomicrofluidics. *Sci. Rep.*, **2019**, 9(1), 7377.

Chapter 4 DropCUTT – Leveraging the Capabilities of Droplets to Automate Enzymatic Tethering Assays

Gloria Diaz, Ajay Larkin, Claire Cook, Kaushik Ragunathan, and Ryan C. Bailey

Abstract

Phenotypic attributes experienced by cells differ due to the epigenome, a vast genome body of proteins, chemical structures, and nucleic acids that regulate gene expression. Monitoring naturally occurring modifications to the epigenome can aid in understanding disease development and be used for patient diagnostics in clinical settings. Cleavage under target and tagmentation (CUT&Tag) is an enzymatic tethering assay that identifies genomic sequences associated with epigenetic modification targets of interest, such as chromatin proteins and histone tail modifications. While CUT&Tag is a low-cost, high-resolution method amenable to clinical and medical research, increasing the processing throughput would expand the utility of the assay. This report presents DropCUTT, a semiautomated droplet microfluidic platform for CUT&Tag, capable of simultaneously extracting nuclei from whole cells, attaching concanavalin A magnetic beads, and assembling a multi-unit immunoprecipitation construct in droplets. This modified assay expands our droplet microfluidic toolbox by reconfiguring our previously published MNase module to condense assay incubation steps, decreasing the number of pipetting steps, and minimizing user variation. This semiautomated procedure supports a range of whole-cell inputs (10K-250K cells per sample) while yielding quality, tagmented DNA fragments.

4.1 Introduction

Chromatin, DNA packaged into a complex with histones and transcription factors, exists in accessible (euchromatin) and non-accessible (heterochromatin) regions[1]. Identifying accessible chromatin regions within the genome is of high importance. The accessible regions outline the possible transcriptionally active portions of the genome that yield insight into regulatory status[2,3]. Accessible chromatin regions with high activity of transcription factor bound proteins have increased mutation rates because of impaired regulatory regions[4].

Initial techniques used to study accessible chromatin regions include DNase-seq, which utilizes the enzyme deoxyribonuclease (DNase) to catalyze the hydrolytic cleavage of phosphodiester bonds in open genomic regions[5]. The cleaved segments are then isolated and prepared for sequencing[6]. The successor to DNase-seq is Formaldehyde Assisted Isolation of Regulatory Elements (FAIRE-Seq)[7]. Both techniques focus on the exposure of open chromatin; however, FAIRE-Seq uses formaldehyde to reinforce DNA to protein interactions and sonication to fragment delicately open genomic regions. While these techniques pioneered assay development into accessible chromatin profiling, there were certain limitations to overcome such as the need to fixate samples and the low resolution when identifying open chromatin at highly expressed gene promoters.

The incorporation of the transposase Tn5 into profiling assays yielded Assay for Transposase Accessible Chromatin with sequencing (ATAC-seq)[8]. The Tn5 transposition mechanism is an efficient and influential tool that has been incorporated into chromatin and epigenetic profiling assays. Barbara McClintock identified the first transposon in maize[9], but currently, the most popular transposase is Tn5. Transposases utilized in *in vitro* genomic research have been modified from the wild type to be hyperactive and only have the necessary

elements- (1) terminal sequences on the transposon, (2) transposase (Tnp), (3) divalent ion activator (Mg 2+), and (4) the target DNA[10,11]. Tn5 works by activating a dimerized synaptic complex that has been conjugated with partial P5 and P7 sequencing adaptors. This active complex identifies the target DNA, uses the Tnp catalytic sites to activate a water molecule, which initiates nucleophilic attacks on both strands of the target DNA. The mechanism finishes by inserting a P5 and P7 partial adaptor onto the target DNA. Following this, barcoded indexes can be added, target DNA is amplified, and library preparation is complete[12,13]. The lead by excision and follow by integration functionality, or 'cut and paste', is a highly productive mechanism since it incorporates and shortens benchwork when constructing next-generation sequencing libraries. Integration of Tn5 increased experimental throughput by not only cleaving open chromatin but also ligating on partial sequencing adaptors. This assay yielded higher sensitivity and accurate measurements[8].

To further the potential and utility of this technology, Cleavage Under Target and Tagmentation (CUT&Tag) was developed to increase specificity through determination of loci interacting with a specific epigenetic modification target of interest[14]. In contrast to predecessor protocols that produce an overall mapping of accessible region, CUT&Tag focuses on identifying the positions of chromatin proteins, transcription factors, and histone tail modifications by utilizing a genetically engineered fusion protein transposase, pA-Tn5. CUT&Tag extracts nuclei from harvested cells and binds them to magnetic beads. An antibody is added, gains accessibility to the genome, and identifies the target of interest. The antibody directs the tethering of the pA-Tn5 and tagmentation is initiated with addition of a divalent ion[15]. CUT&Tag has a remarkable signal to noise ratio as there is no need to break down a cell entity or digest an entire genome[14]. Low-cost high-resolution methods like CUT&Tag are the

techniques needed in clinical and medical research. However, they would benefit from automation to achieve higher throughput processing.

In this chapter, we describe the development of DropCUTT: a droplet microfluidic platform for CUT&Tag that automates this epigenetic profiling assay. Through the precise control and manipulation of fluids, our platform takes whole cells, extracts the nuclei, binds magnetic beads to nuclei, and proceeds with segmented chromatin processing for next-generation sequencing (NGS). This chapter discusses condensing three separate incubations within the CUT&Tag assay into a single incubation that assembles the complete immunoprecipitation unit. The transition of the redesigned assay to a microfluidic chip is also discussed. The assay was validated by profiling H3K27me3 in different cell populations as well as additional targets. We demonstrate its use by profiling histone tail modifications in wild type and mutant glioma cell lines. This research focuses on expanding the Bailey lab's droplet microfluidic toolbox into enzymatic tethering assays, while simultaneously broadening the utility of this influential assay for biomarker monitoring.

4.3 Materials and Methods

4.3.1 Buffer Recipes

Bead Activation Buffer (pH 7.9) contains 20 mM HEPES, 10 mM KCl, 1 mM $CaCl_2$, and 1 mM $MnCl_2$. **EBA Buffer** (pH 8) contains 20 mM HEPES, 10 mM KCl, 1 mM $CaCl_2$, 1 mM $MnCl_2$, 0.5 mM Spermidine, 0.1% Triton X-100, 20% Glycerol, and Roche cOmpleteTM EDTA-free Protease Inhibitor*. **Cocktail Buffer** (pH 7.5) contains 20 mM HEPES, 1mM NaCl, 0.5 mM Spermidine, 0.01% Digitonin, 6 mM EDTA, and Roche cOmpleteTM EDTA-free Protease Inhibitor*. **Wash Buffer** (pH 7.5) contains 20 mM HEPES, 300 mM NaCl, 0.5 mM Spermidine, 0.01% Digitonin, and Roche cOmpleteTM EDTA-free Protease Inhibitor*. **Tagmentation Buffer** (pH 7.5) contains 20 mM HEPES, 300 mM NaCl, 0.5 mM Spermidine, 10 mM $MgCl_2$, and Roche cOmpleteTM EDTA-free Protease Inhibitor*. **TAPS Buffer** (pH 8.5) contains 10 mM TAPS, and 0.2 mM EDTA. **Release Buffer** (pH 8.5) contains 10 mM TAPS with 0.1% SDS. **Quenching Buffer** contains 0.67% Triton-X 100 in molecular grade H_2O.

*1 tablet of Roche cOmpleteTM EDTA-free Protease Inhibitor (Roche, Basel, Switzerland) per 10 mL of solution.

** Buffer adapted from the EpiCypher® CUTANA™ Direct -to-PCR CUT&Tag Protocol[16]

4.3.2 Microfluidic Device Fabrication

Devices were fabricated using standard soft lithography in poly-(dimethylsiloxane) (PDMS) (RTV615, Momentive Performance Materials, Inc.). Devices were designed using AutoCAD software (Autodesk, Inc.) and sourced as transparent photolithography masks (CAD/Art Services, Inc.). SU8 2025 and 2050 negative epoxy photoresist (MicroChem Corp.) were spin coated onto silicon wafers (University Wafer, Boston MA) and features were

crosslinked by standard photolithography. For the initial layer, SU8 2025 was spin coated at 2000 rpm for 30 seconds for a thickness of 40 μm. After wafer baking (Cimarec, Thermo Scientific) and exposure to UV light (MJB3 Mask Aligner, SUSS MicroTec), the initial layer was developed using propylene glycol monomethyl ether acetate (PGMEA) (Sigma-Aldrich, St. Louis, MO). For the second layer, SU8 2050 was spin coated at 1150 rpm for 30 seconds for a thickness of 160 μm. Following baking, exposure and development, the master was surface treated with tridecafluoro-1,1,2,2-tetrahydrooctyl trichlorosilane (Gelest, Inc., Morrisville, PA).

A 10:1 base to curing agent ratio was mixed, along with PDMS-PEG at a 0.25% (w/w). Mix was degassed under vacuum. The PDMS mixture was poured over the master in a Petri dish and allowed to cure for 1 hour at 70°C (Hera Therm Oven, Thermo Scientific). PDMS stamps were cut, and hole punched with blunt end needles (24-gauge inlets, 30-gauge outlet and electrolyte channels). Stamps were sonicated in water, dried with compressed air, and bonded to glass cover slides (1 mm thickness, 75 mmx 50 mm, Thermo Fisher Scientific) *via* oxygen plasma activation (PDC-32G, Harrick Plasma, Inc.). Devices were then baked overnight and treated with Aquapel (Pittsburgh Glass Works, Pittsburgh, PA) before use.

4.3.3 Cell Culturing

K562 cell were cultured in RPMI medium (Gibco RPMI 1640 Medium, Catalog No. A1049101, Fisher Scientific) supplemented with 10% fetal bovine serum (Catalog No. F4135-500ML, Sigma Aldrich) at 37°C with 5% CO_2. To assure cellular debris was sufficiently removed, cell samples were washed twice with cold PBS (Lonza™ BioWhittaker™ Phosphate Buffered Solution, Catalog No. BW17516F12, Fisher Scientific) by vigorously mixing using a pipette and pelleting at 600 x g for 5 minutes at room temperature. Cells were resuspended to the

desired concentration in 30% OptiPrep-PBS (OptiPrep™ Density Gradient Medium, Catalog No. D1556-250ML, Millipore Sigma) and kept on ice until needed.

NPA & NPAI cells were cultures in (neurosphere media) DMEM/F12 medium (Gibco DMEM/F-12 Medium, Catalog No. 11320033, Fisher Scientific) supplemented with 1X antibiotic-antimycotic (Gibco Antibiotic Antimycotic, Catalog No. 15240062, Invitrogen), 1X N2 supplement (Gibco N2 Supplement, Catalog No. 17502048, Invitrogen), 1X B27 supplement with vitamin A (Gibco B27 Supplement, Catalog No. 17504044, Invitrogen), 1X normocin (Catalog No. ant-nr-1, InvivoGen), EGF (Catalog No. AF-100-15, PeproTech, Inc.), and FGF (Catalog No. 100-18B, PeproTech, Inc.) at 37°C with 5% CO_2. To ensure homogenous resuspension, each flask was pelleted at 100 x g for 3 minutes and treated with Accutase (Catalog No. SCR005, Sigma Aldrich) for 1-2 minutes at 37°C. To quench the detachment solution, 4 mL of neurosphere media was added, mixed, and pelleted with previously stated conditions. Cells were resuspended to the desired concentration in 30% OptiPrep-PBS and kept on ice until needed.

4.3.4 Magnetic Bead Preparation

Bead stock (BioMag ® Plus Concanavalin A, Catalog No. BP531, Bangs Laboratories, Inc) was vortexed to ensure a homogenous mixture and 11 µL of stock (per reaction) was pipetted into an Eppendorf vial(Eppendorf DNA LoBind, Fisher Scientific, Waltham, MA). Beads were washed twice with 100 µL of bead activation buffer (per reaction) utilizing a magnetic rack. Lastly, beads were resuspended in 40 µL of EBA buffer (per reaction) and aliquoted into 35 µL. Aliquots were kept on ice and mixed by pipette before use.

4.3.5 Syringe Set Up

Glass tight syringes (Hamilton Company, Reno, NV) were pre-filled with filtered (0.2 μm PTFE membrane, VWR International, Inc) food dye. 24-gauge tubing (Cole-Parmer, Vernon Hills, IL) was connected to each syringe and food dye was pushed through to appropriate volume. Tubing delivering cells was treated overnight with 1% (w/v) Pluronic F127 (Sigma-Aldrich, St. Louis, MO). Glass syringes were filled with the following:

Syringe 1- red dye, 30 μL of suspended cells in 30% OptiPrep-PBS

Syringe 2- blue dye, 35 μL of magnetic beads in EBA buffer.

Syringe 3- green dye, 65 μL of pA-Tn5 cocktail.

pA-Tn5 cocktail was prepared by adding 2.5 μL of pAG-Tn5 (Catalog No. 15-1017: EpiCypher, Inc, Durham, North Carolina), 0.5 μL of secondary antibody (Catalog No. 13-0047, EpiCypher, Inc, Durham, North Carolina), 1 μL of primary antibody (H3K27me3 - Catalog No. 9733T, Cell Signal Technology, H3K4me3 - Catalog No. 9751T, Cell Signal Technology, H3K36me3 - Catalog No. 61102, Active Motif, CTCT - Catalog No. 3418T, Cell Signal Technology) to 65 μL of cocktail buffer. Syringes were controlled using syringe pumps (Pump 11 Pico Plus Elite, Harvard Apparatus) – carrier oil 6 μL min^{-1}, droplet generator 2 μL min^{-1}, oil spacer 14 μL min^{-1}, pico injector 4 μL min^{-1}. Carrier oil phase was composed of fluorinated oil Novec 7500 (3M, St. Paul, MN) with 2% (w/w) perfluoropolyether polyethylene glycol block co-polymer surfactant (RAN Biotechnologies, Inc. Beverly, MA).

4.3.6 Microfluidic Device Operations

The day of experiment, microfluidic devices were treated with Aquapel (Pittsburgh Glass Works, LLC., Pittsburgh, PA) for 5 minutes to produce a hydrophobic coating. Electrolyte

microchannels were filled with 3 M sodium chloride and the syringes delivering the solution were connected to metal alligator clamps connected to an in-house DC-AC converter (12V DC input, 0-360V AC at 36 kHz as output) connected to a power supply. Carrier oil was run for 30 seconds before starting droplet generation. Droplets were generated using syringes and were injected with the pA-Tn5 cocktail after incubation in the delay channel. Following delivery of cell solution, droplets from food dye continued to be generated for an additional 6 minutes to push product material out. Droplets were then collected using 30-gauge tubing into LoBind Eppendorf tubes and left to incubate overnight at 4°C on a rocker. Once cell solution had been delivered, sample continued to run for an additional 3 minutes to collect remaining droplets. The following day, droplet samples were coalesced by adding 50 µL of octanol (Sigma-Aldrich, St. Louis, MO), gently hand mixed, and spun down at 5,000 rpm for 1 minute. Using a pipette, the aqueous layer was removed and washed twice with 200 µL of wash buffer using a magnetic rack.

4.3.7 Bulk Protocol

In a standard Eppendorf tube, 30 µL of cells were incubated with 30 µL of magnetic beads in EBA buffer for 3 minutes at room temperature. Following nuclei extraction and magnetic bead attachment, 60 µL of pA-Tn5 cocktail was added, mixed by hand, and incubated overnight at 4°C. The next day, samples were washed twice with 200 µL of wash buffer.

4.3.8 Tagmentation & Release

* Adapted from the EpiCypher® CUTANA™ Direct -to-PCR CUT&Tag Protocol[16]

Both droplet and bulk samples were resuspended in 50 µL of tagmentation buffer, mixed by pipetting and incubated on a thermocycler (Bio-Rad, Hercules, CA) for 1 hour at 37°C. Following tagmentation, samples were washed with 50 µL of TAPS (Boston Bioproducts) buffer

to chelate carry-over divalent ions and resuspended in 5 μL of Release Buffer. Samples were vigorously vortexed and then incubated in a thermocycler for 1 hour at 58ºC. To quench the SDS, 15 μL of quenching buffer was added to each sample and vortexed to mix.

4.3.9 Amplification & Size Selection Purification

* Adapted from the EpiCypher® CUTANA™ Direct -to-PCR CUT&Tag Protocol.

To each sample, 25 μL of CUTANA High Fidelity 2X PCR Master Mix (Catalog No. 12-1018, EpiCypher, Inc, Durham, North Carolina) was added along with 2 μL of i5 primer and 2 μL of barcoded i7 primer (Integrated DNA technologies, Coral, IA). Working stocks for i5 and i7 primers were prepared beforehand to a concentration of 10 μM using ultra distilled water (Invitrogen™ UltraPure™ DNase/RNase-Free Distilled Water, Catalog No. 10-977-015, Fisher Scientific). Samples were incubated on a thermocycler with the following parameters: a) 5 minutes at 58ºC, b) 5 minutes at 72ºC, c) 45 seconds at 98ºC, d) 15 seconds at 98ºC, e) 10 seconds at 60ºC, f) steps d-e repeated for 14-21 cycles (dependent on input amount), g) 1 minute at 72ºC, h) hold at 4ºC. Following amplification, samples were purified using 1.5X AMPure beads (AMPure XP, Catalog No. A63880, Beckman Coulter, Brea, CA) following standard manufacturing instructions. Samples were eluted in 17 μL of 0.1X EB buffer, 2 μL were used for quantifying using Qubit dsDNA High Sensatory Assay (Thermo Fisher Scientific, Grand Island, NY), and up to 4 μL were used to analyze fragmentation patterns on an Agilent Bioanalyzer (Agilent Technologies, Santa Clara, CA).

4.3.10 Data Analysis

Quality of the sequencing reads was verified using FastQC and reads were trimmed using Trimmomatic. Utilizing Bowtie2, reads were aligned to the hg38 genome with default settings.

After identifying mappable reads, Bedtools was used to remove duplicate and low-quality reads. Spearman correlation assessment, heatmaps and PCA were calculated using deepTools with default parameters. Peak calling was performed with SEACR.

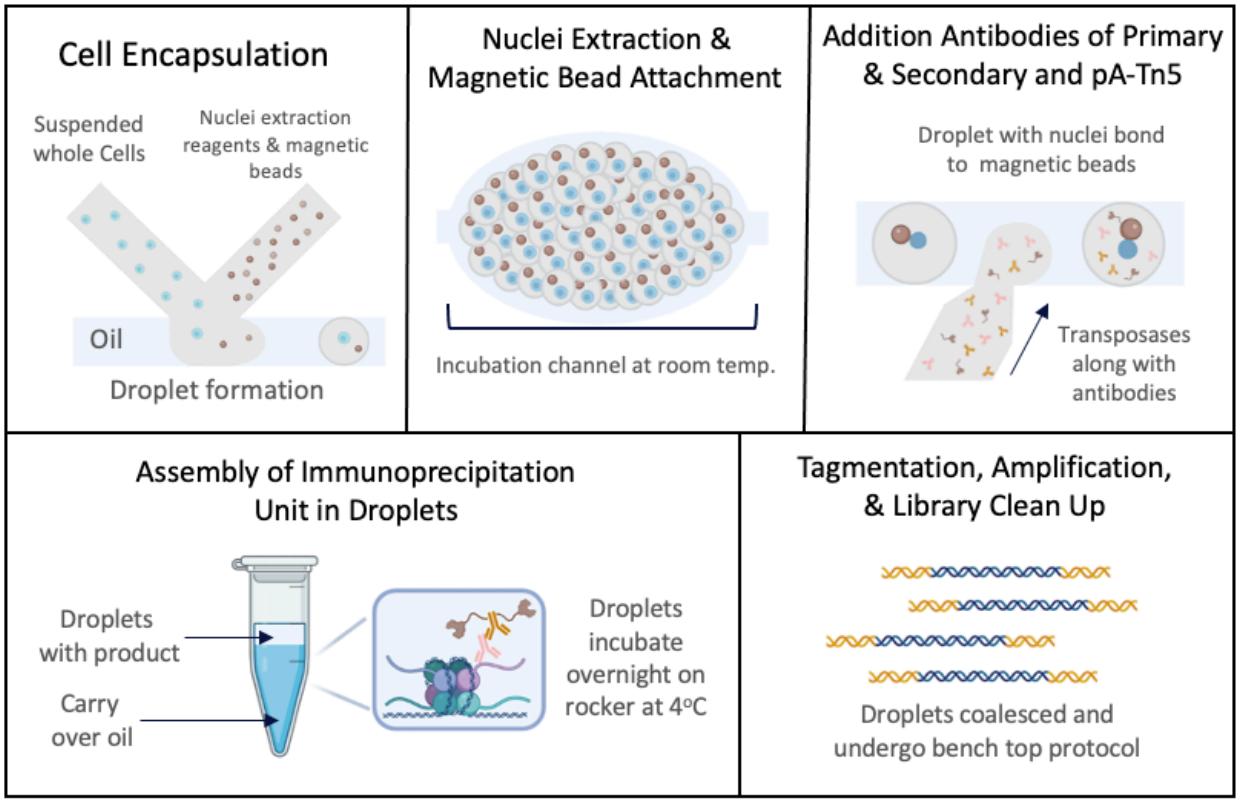

Figure 4.1 Flow chart depicting the different steps of the droplet integrated CUT&Tag (DropCUTT) protocol.

(a)

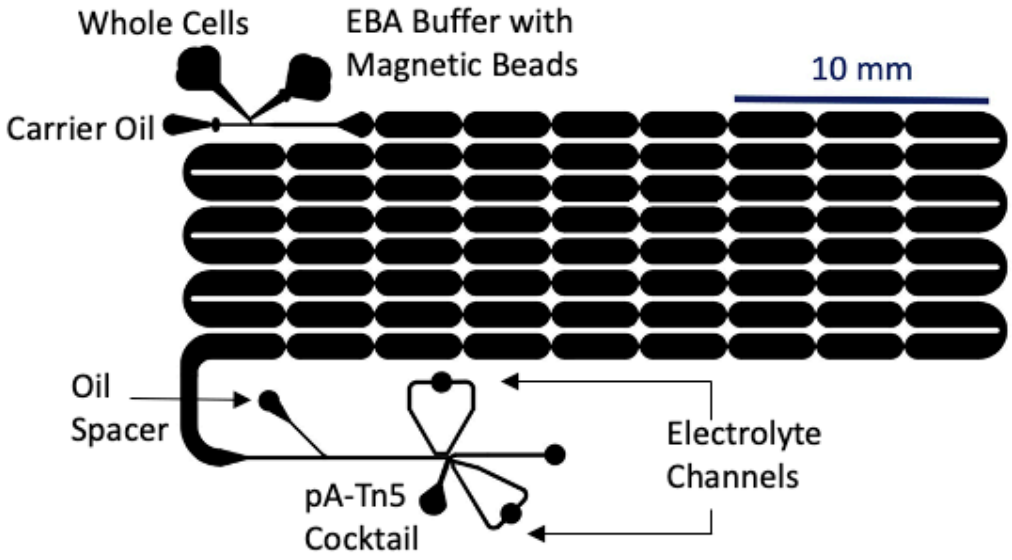

(b)

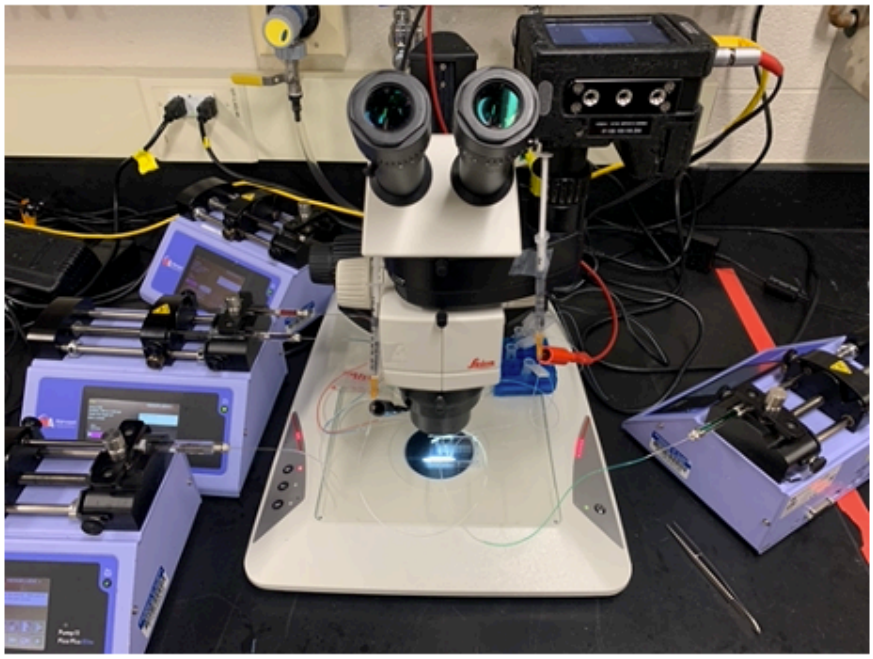

Figure 4.2 (a) Overview of microfluidic module and which port were used to introduce bioassay materials. (b) Complete set up for droplet integrated CUT&Tag.

4.4 Results and Discussion

4.4.1 Redesigning CUT&Tag Protocol for Fluidic Adaptation

To adapt this enzymatic tethering assay to a microfluidic platform, the CUT&Tag protocol needed to be modified in steps that would benefit from execution in micro droplets. Before transitioning to a microfluidic chip, bulk experiments needed to demonstrate appropriate tagmentation and ligation of adaptors with the integrated procedural changes. To condense this procedure, the initial goal was simultaneous assembly of the immunoprecipitation of the primary and secondary antibody to the target of interest. Within the conventional protocol, this consisted of two separate incubations (overnight & 1 hour), however simultaneous addition of both antibodies resulted in a single 1.5-hour incubation while still yielding the appropriate chromatin fragmentation at ~ 300 base pairs. Furthermore, the buffer conditions were redesigned for a single incubation in assembly buffer with both antibodies and the hybrid transposase, pAG-Tn5 (Figure 4.3a). As demonstrated in the electrophoresis gel, the redesigned protocol achieved the correct multiunit construct leading to a targeted digestion only within the immunoprecipitated samples for both H3K27me3 and H3K4me3 (Figure 4.3b). The conventional bulk assay has been redesigned to successfully assemble the three-tier immunoprecipitation unit (primary antibody-secondary antibody - pAG-Tn5) in a single incubation and achieved the proper fragmentation (~300 bp). These results confirmed that the adaptations made to the assay do not significantly alter the outcome in the traditional, bulk protocol.

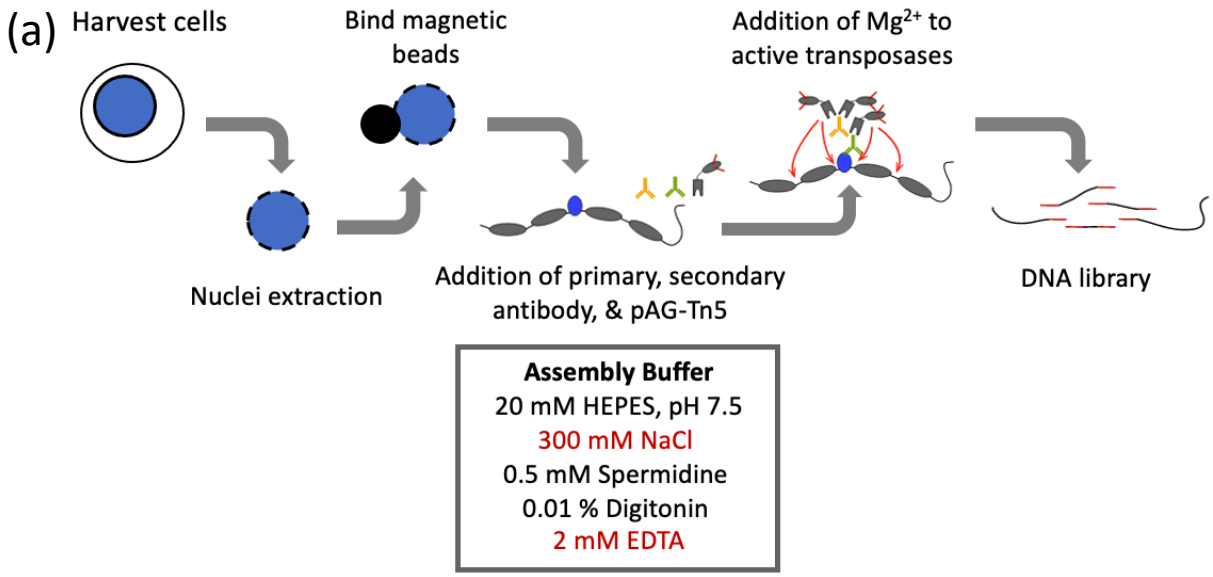

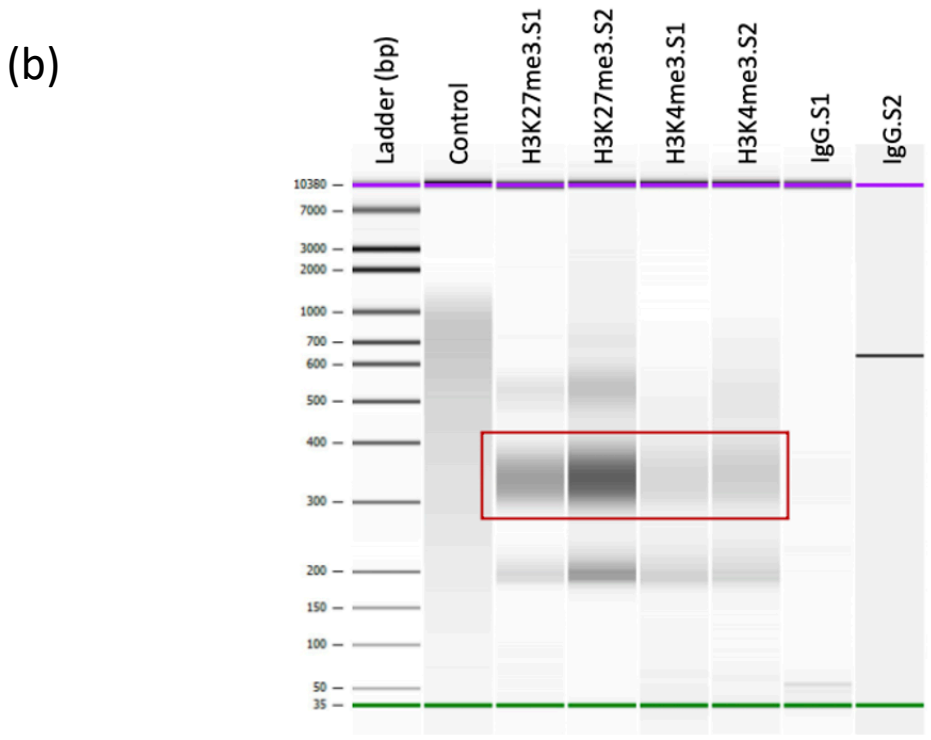

Figure 4.3 (a) Experimental protocol for condensing CUT&Tag protocol. All three components (primary antibody, secondary antibody, and pAG-Tn5) were incubated together in assembly buffer. (b) electropherogram of tagmented DNA, targeting H4K27me3 and H3K4me3. Targets were profiled in K562 cells with 250,000 cells per sample.

4.4.2 Translating Condensed CUT&Tag Protocol to Droplet Microfluidic Device

The MNase device was previously used for membrane lysis and chromatin digestion. Here, we expanded the device's functionality and utility by optimizing it to complete nuclei extraction and assembly of the three-tier immunoprecipitation unit. In this newly optimized protocol (Figure 4.1), whole cells and magnetic beads were introduced into the miniature chip in buffer conditions that extract nuclei and bind Concanavalin A magnetic beads for sample manipulation. Each droplet incubates through delay channels for three and a half minutes, concluding with injection of the three tier immunoprecipitation unit reagents (primary antibody, secondary antibody, pAG-Tn5). The droplets were then collected into an Eppendorf vial through an outlet channel and incubated overnight, allowing for the assembly of the 3-unit construct (primary antibody-secondary antibody - pAG-Tn5).

Initial microfluidic adaptations of the assay generated droplets containing nuclei bound to magnetic beads along with primary and secondary antibodies. The primary antibody identifies the target of interest, while the secondary antibody directs the binding of pAG-Tn5. The droplets would then incubate through the delay channels, and utilizing the pico injector, pAG-Tn5 was added to each (Figure 4.4a). Illustrated by the bioanalyzer data (Figure 4.4b), these droplet adaptations produce the correct tagmentation fragments, product peak at ~300 bp when using 100K K562 cells per sample. To incorporate further portions of the CUT&Tag protocol, the nuclei extraction, and bead attachment were condensed and automated into a single incubation. Extraction and bead activation buffer (EBA Buffer) was formulated and optimized to extract nuclei from whole cells and contain the necessary components to bind the Concanavalin A magnetic beads within a three-minute room temperature incubation (Figure 4.1). With these alterations, the DropCUTT procedure continued to yield appropriately tagmented fragments at

~300 bp when profiling H3K27me3 in 100K K562 cells. The droplet bioassay was also completed with 20K and 10K cell samples to test the adapted assay on device with lower cell inputs. The product peak resulted at ~300 bp (Figure 4.5), highlighting the range of cell inputs the DropCUTT protocol can work with. This is important for the eventual expansion into profiling rare cell types with minimal amounts.

With the correct fragmentation patterns confirmed, samples processed by DropCUTT were sequenced to validate compatibility with low-input samples and to ensure reproducibility of the primary antibody binding location across all sample inputs. It is important to validate that the peak at 300 bp is the correctly profiled DNA, to confirm the primary antibody is detecting chromatin regions the histone tail modification H3K27me3 is localized to. Three sequencing libraries were prepared from the previously mentioned sample inputs (100K, 20K, 10K cells per sample) in both the DropCUTT system and the bulk protocol for comparison. Profile tracks for H3K27me3 were generated from reads mapped to the human genome for direct comparison (Figure 4.7). Localization of peaks and peak shape is consistent across the various cell amounts and processing methods used, indicating good correlation between the DropCUTT and bulk procedures. IgG negative controls, absent of the primary antibody, have little to no signal, indicating that the primary antibody is effectively locating the histone tail modification of interest, which acts as the nucleation point for the assembly of the three-tier immunoprecipitation unite. Additionally, it communicates there is no arbitrary or off-target binding of the primary antibody and the additional components (pAG-Tn5 and secondary antibody) across the genome.

To evaluate the statistical dependency between data sets, Spearman correlation coefficients were calculated. This assessment coefficient essentially describes the relationship of two variables, in this case two sequencing data sets, using monotonic functions. A correlation

value of one occurs when identical monotonic functions are being compared. Therefore, the Spearman correlation value will be high, closest to one, when the two sequencing data sets are statistically similar. The Spearman correlation assessment (Figure 4.6) shows high correlation among droplet samples with an average value of 0.84 for H3K27me3 profiled across three sample input sizes. The samples prepared using the bulk protocol have a similar average coefficient value of 0.85, however when observing individual coefficients, they are numerically spread out. The quality of data produced is comparable between bulk and droplet processed samples and there is consistency across the sample input sizes as well. Overall, the Spearman correlation coefficients calculated suggest consistent, reproducible data is generated across replicates, processing methods, and cell amount used. Confidence in this microfluidic profiling bioassay is important as we transition to applying DropCUTT to clinical samples through campus collaborations.

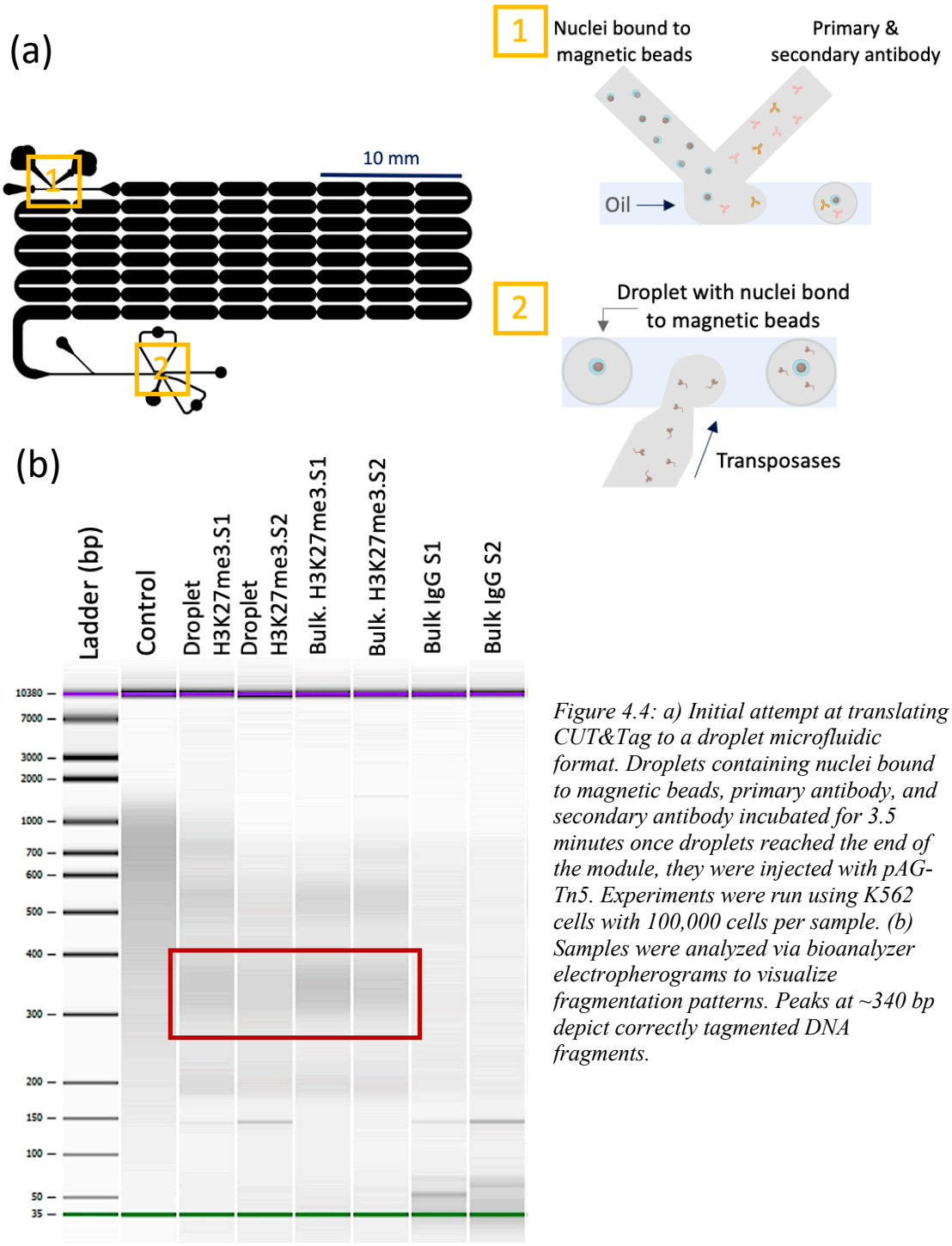

Figure 4.4: a) Initial attempt at translating CUT&Tag to a droplet microfluidic format. Droplets containing nuclei bound to magnetic beads, primary antibody, and secondary antibody incubated for 3.5 minutes once droplets reached the end of the module, they were injected with pAG-Tn5. Experiments were run using K562 cells with 100,000 cells per sample. (b) Samples were analyzed via bioanalyzer electropherograms to visualize fragmentation patterns. Peaks at ~340 bp depict correctly tagmented DNA fragments.

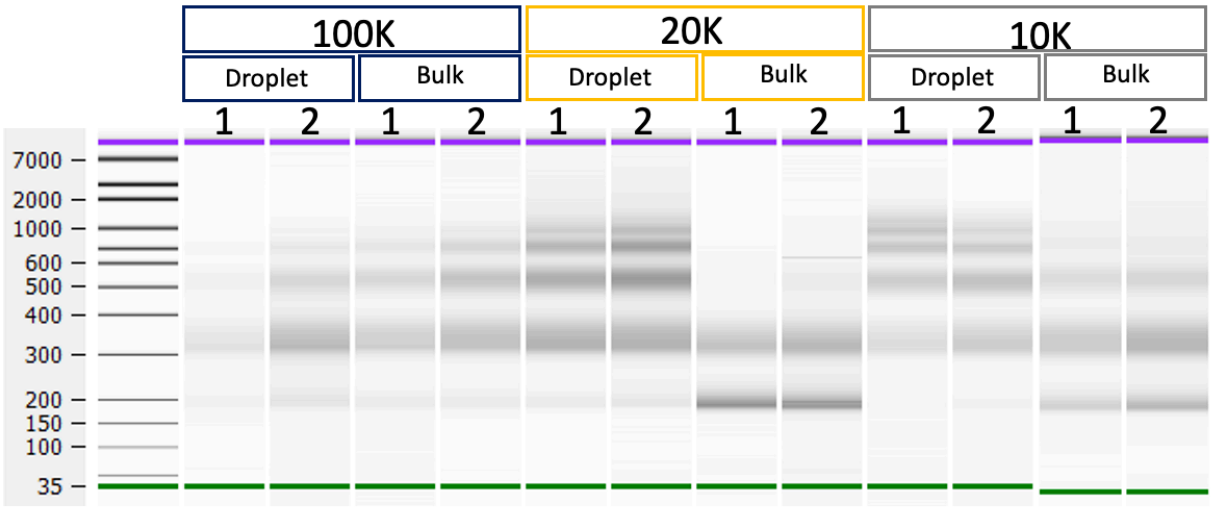

Figure 4.5: Bioanalyzer electropherogram visualizing fragmentation patterns of three input samples sizes (100K, 20K, 10K) processed using the DropCUTT system with bulk samples run in parallel. K562 cells were used at passage 48. Product peak bands can be observed at ~ 340 bp, for droplet and bulk samples. Negative IgG controls were run in parallel for both droplet and bulk processing. However, electropherogram profiles were not obtained because samples did not meet the minimum threshold concentration (0.5 ng/μL) to be loaded and analyzed through bioanalyzer.

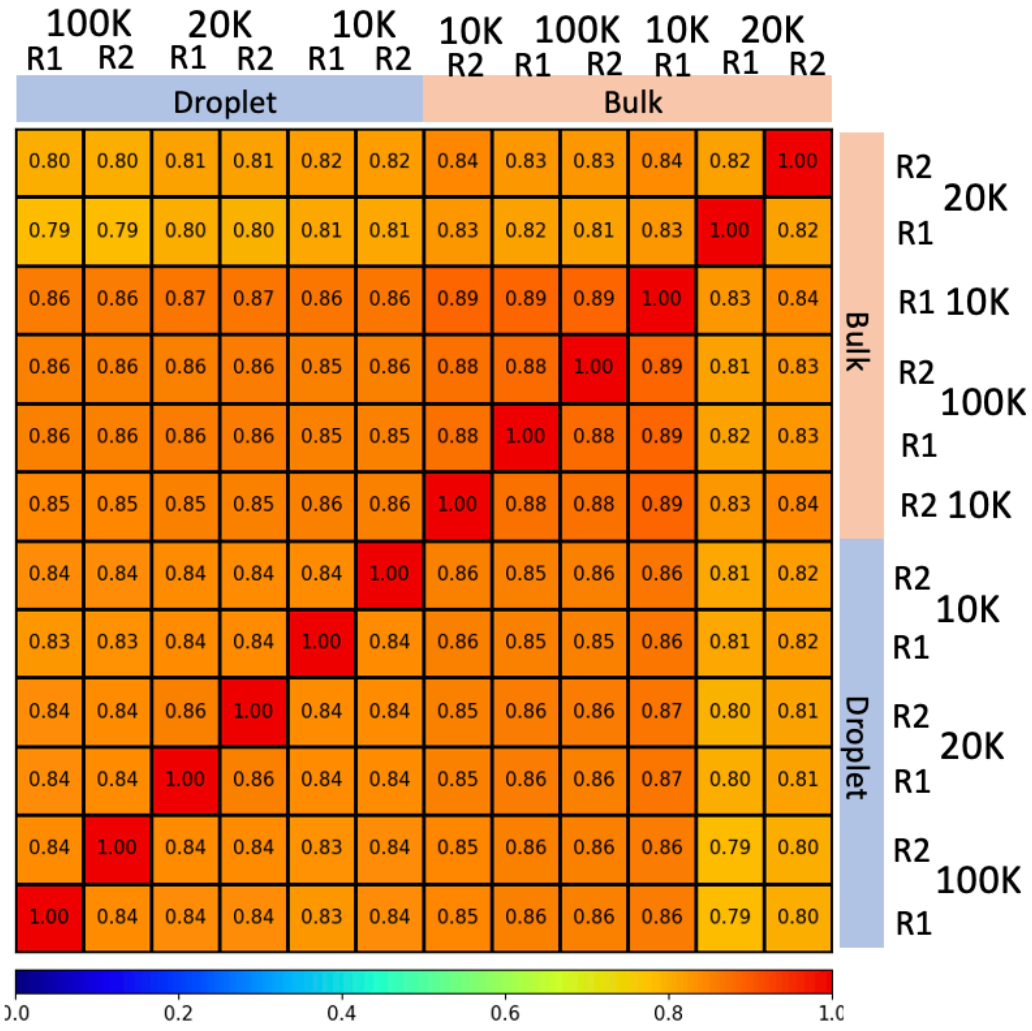

Figure 4.6 Spearman correlation assessment comparing quality of data for replicates and sample input size.

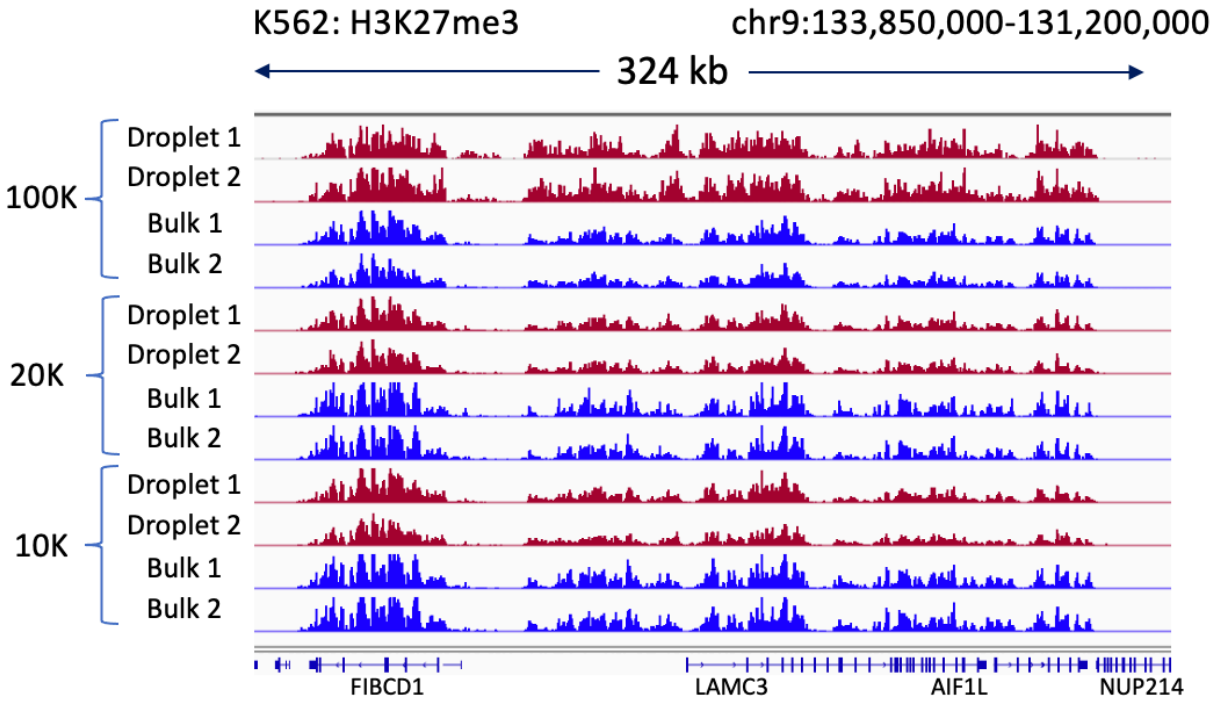

Figure 4.7 Profiling tracks for H3K27me3 at distinct input sizes (100K, 20K, 10K), localized at chromosome 9: 133,850,000-131,200,000 juxtaposing the processing methods (droplet vs. bulk). Peak localization and patterns are conserved across all samples indicating uniform processing and reproducibility of results through distinct variables.

4.4.3 Expanding DropCUTT profiling abilities to mouse glioma model

DropCUTT profiling abilities were expanded by profiling histone tail modifications in a glioma cell line. Mutated isocitrate dehydrogenase [1]7 ($IDH1^{R132H}$) is an early event in glioma development[18,19] that also aids the catalysis of α - ketoglutarate to (R)-2-hydroxyglutarate (2HG)[20,21]. The new product, 2HG, prohibits demethylation, leading to hypermethylation of DNA as well as histones[22]. The Castro lab from the Department of Pathology at the University of Michigan has developed a mouse glioma cell model from primary neurospheres (NS)[23], to study the impact of mutated isocitrate dehydrogenase 1 ($IDH1^{R132H}$) as well as in the wild type. Previous ChIP studies have observed higher levels of H3K27me3 and H3K4me3 in the mutated line (NPAI) compared to the wild type (NPA)[24]. Using the DropCUTT system, we worked to replicate the Castro lab's ChIP profiling data to observe how our microfluidic system compares to the gold standard for identifying loci associated with histone tail modifications of interest. Two targets were profiled, H3K27me3 and H3K4me3, in both the NPA and NPAI cell lines. Their fragmentation patterns were visualized using bioanalyzer (Figure 4.8). Profiles for H3K27me3 in both cell lines have product peak formation at ~340 bp. When targeting H3K4me3, a product peak forms at ~340 bp, but the predominant product peak is at ~200 bp. This could be due to 'nucleosome breaking' when open chromatin remodels and removes chromatin proteins for transcription, so linker DNA is accessible for tagmentation.

To ensure appropriate immunoprecipitation of the DropCUTT system with the NPA and NPAI cell lines, sequencing was performed, and bioinformatic processing done by our collaborator Ajay Larkin (Brandeis University). Profiling tracks were generated for samples targeting the histone tail modification, H3K4me3 in both the mutant (NPAI) and wild type (NPA) cell lines at the gene region *TGFB1* (Figure 4.9). Observing the transcription start site for

TGFB1, peak location is consistent across processing method as well as cell line. To ensure the peak location wasn't specifical to the DropCUTT system as well as the bulk procedure we compared our sequencing data sets to ChIP profiled data sets for H3K4me3 from the Castro lab[25]. The location of our peaks at the transcription start site of *TGFB1* also aligned with the location of the ChIP profiled samples. Lastly, Spearman correlation coefficients were calculated to observe the statistical similarities between sequencing data sets (Figure 4.10). Recall that identical monotonic functions (sequencing sets) yield a value of one, so when two sequencing data sets have high correlation, the coefficient calculated will be close to the value of one. When observing DropCUTT samples between droplet and bulk processing there is high correlation, mutant 0.97 and wild type 0.95. Comparing droplet to ChIP profiling data sets, the spearman coefficients calculated across the three biological replicates for the mutant cell line (C3, C1, C2) include 0.61, 0.87, 0.85, depicting statistical significance. Similarly for the wild type biological replicates (C54b, C2, C54a) the determined values include 0.89, 0.73, 0.72 illustrating that sequencing data generated through our DropCUTT system is comparable with data generated by the gold standard profiling assay ChIP. The fact that DropCUTT can generate reproducible data across a distinct model cell line as well as profile different targets demonstrates the versatility and adaptability of this automated system.

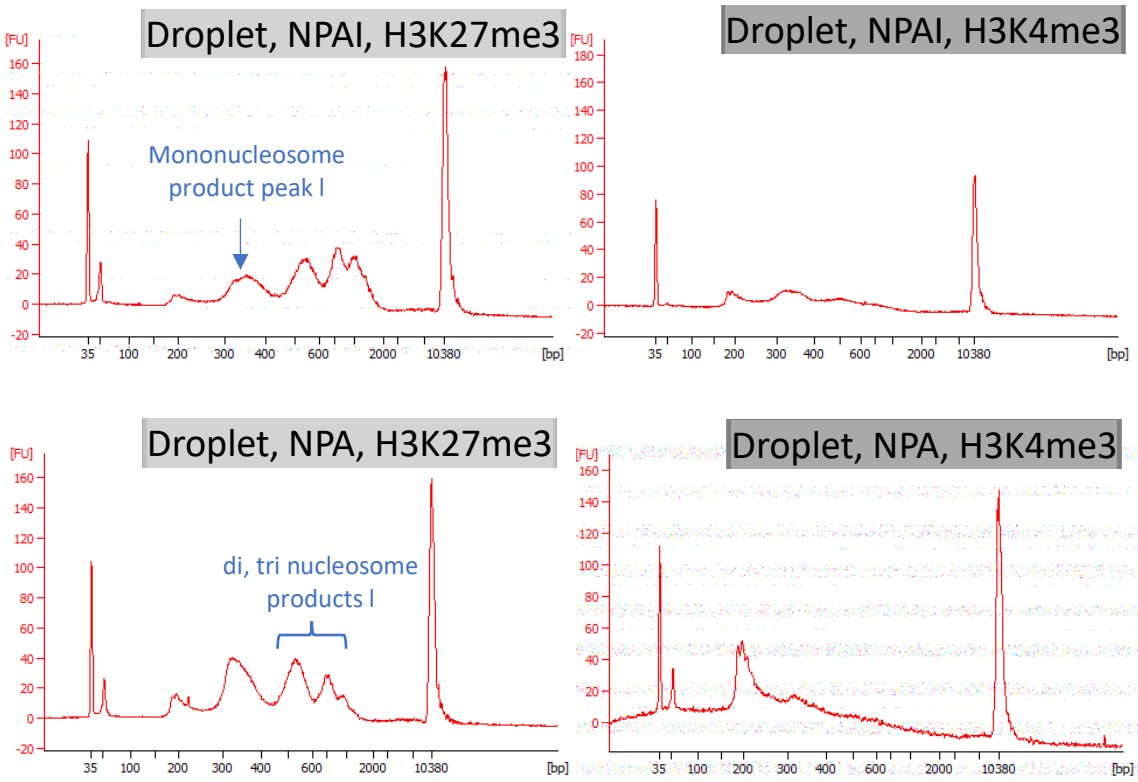

Figure 4.8 To further the application of DropCUTT, a mouse glioma cell model was profiled for H3K27me3 and H3K4me3. The NPA (wild type) and NPAI (mutant) cell lines were developed to study mutated isocitrate dehydrogenase 1 ($IDH1^{R132H}$), which hinders demethylation of histones, yielding higher amounts of these targets in the mutated cell line. The goal is to replicate previous ChIP data to compare DropCUTT to the goal standard for identifying associated loci with a target of interest. Above are the bioanalyzer electropherograms for the mutant and wild-type cell lines using 100,000 cells per sample. Negative IgG controls were run in parallel, however, not ran on bioanalyzer because samples did not meet the minimum threshold concentration (0.5 ng/μL) to be loaded.

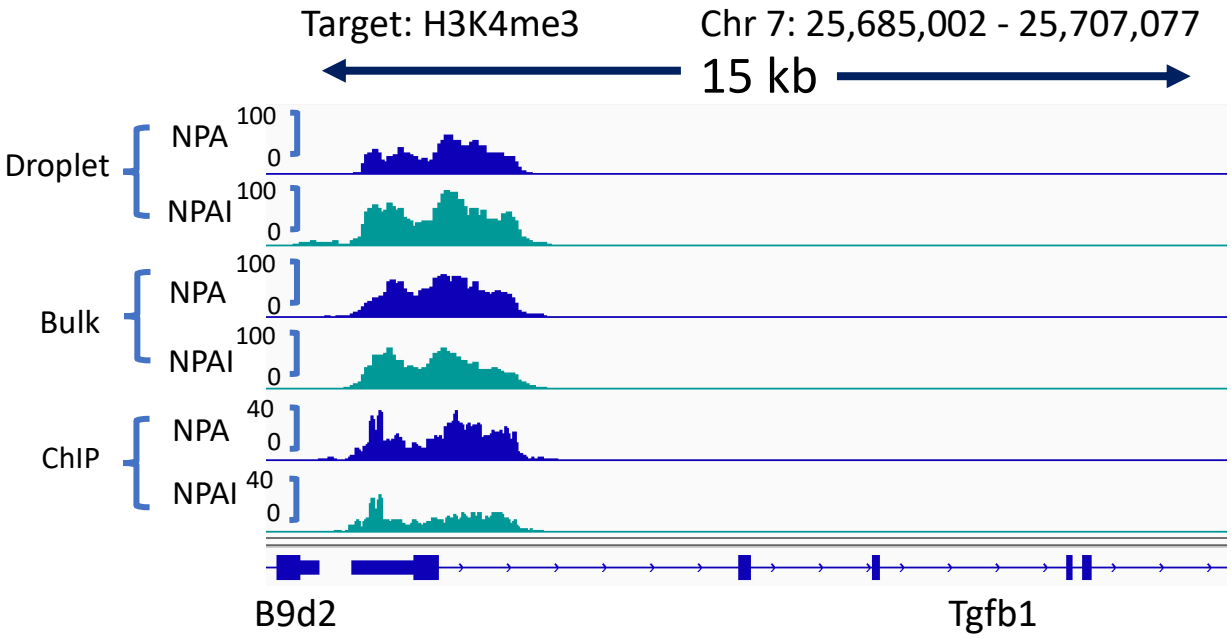

Figure 4.9 Profiling tracks for histone tail modification target H3K4me4 at Chr 7: 25,685002-25,707,077, gene region Tgfb1. Tracks compare the various processing methods (DropCUTT -droplet, bulk, and ChIP) utilizing 100K NPA and NPAI cells per sample. Placement of peaks at the TSS of Tgfb1is consistent across processing method as well as cell line, suggesting comparable profiling data is generated with the DropCUTT system to the conventional profiling assay ChIP.

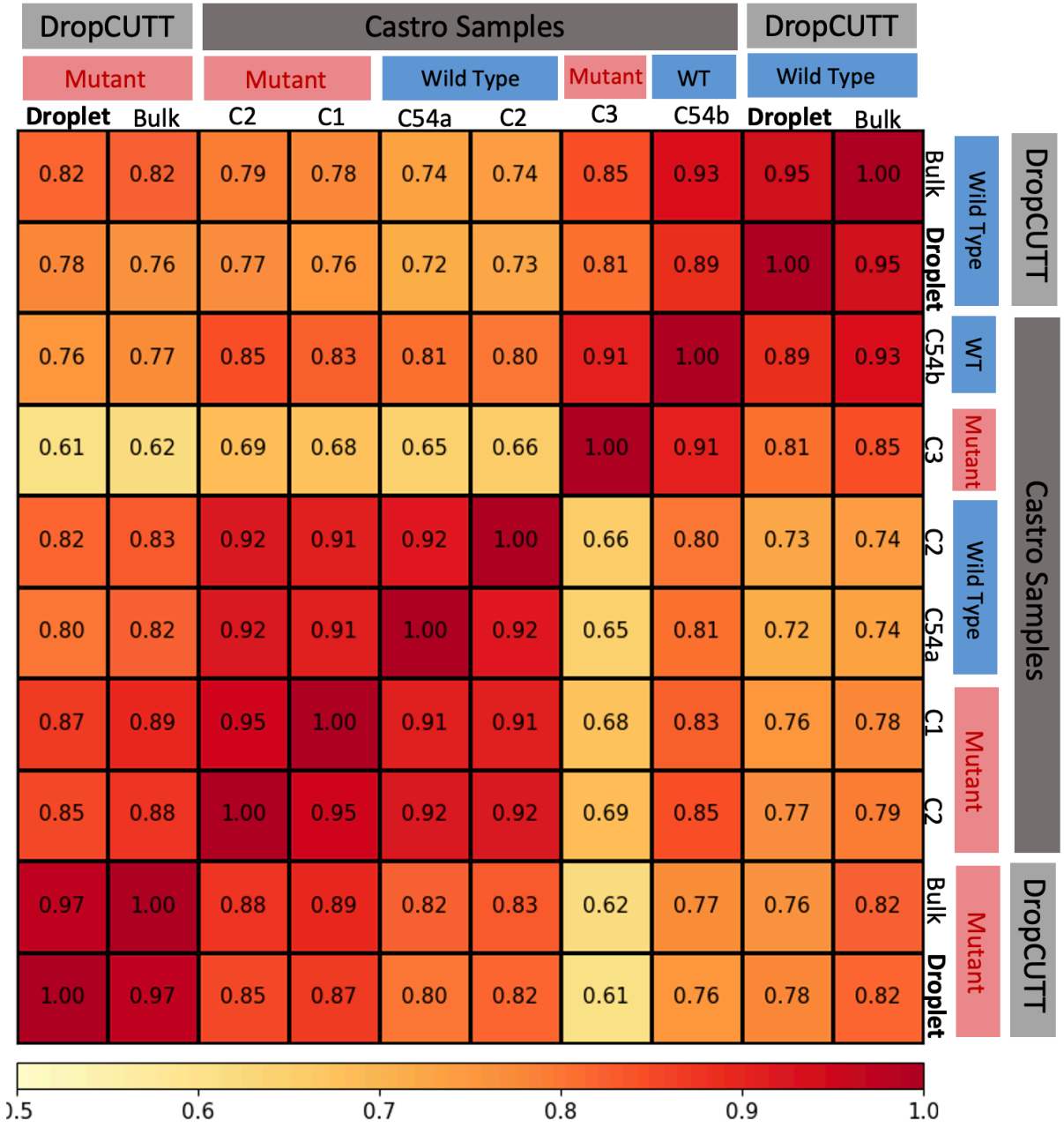

Figure 4.10 Calculated spearman correlation coefficients illustrating the statistical comparison between data sets generated through distinct processing methods across two cell line (NPA and NPAI) profiling the target H3K4me3.

4.5 Conclusion

In summary, the work in this chapter expands our droplet microfluidic platforms towards more uniform sample processing and higher throughput automation of enzymatic tethering assays. DropCUTT represents the first droplet microfluidic adaptation of the CUT&Tag protocol. It incorporates 2/3 of the assay in droplets, compared to previous microfluidic variations of profiling assays with minimal adaptability. With the automation of a significant portion of the protocol, this work is an effort to reduce the reliance on technical skills and improves the accessibility of CUT&Tag in research and clinical settings. The reduction of the assay time widens the technique's accessibility by reducing the time commitment needed to obtain meaningful data. Epigenetic technologies have vast clinical potential for patient diagnostics as well as understanding cell type specific chromatin landscapes. DropCUTT offers an accessible and dynamic opportunity to enable these studies.

Acknowledgments

We gratefully acknowledge the funding support from the National Science Foundation (NSF – Understanding the Rules of Life Epigenetics: 1921677). G.E.D. was also supported by the Rackham Merit Fellowship. G. Diaz and C. Cook (University of Michigan) participated in experiment design, device fabrication, and data collection. A. Larkin (Brandeis University) participated in experiment design and data analysis. We also thank the Castro lab (University of Michigan, Department of Pathology) for providing the NPAI and NPI cells for application experiments.

References

(1) Kornberg R.D. Chromatin structure: A repeating unit of histones and DNA. *Science,* **1974,** 184, 868–871.

(2) Boeger, H.; Griesenbeck, J.; Strattan, J.S.; Kornberg, R.D. Nucleosomes unfold completely at a transcriptionally active promoter. *Mol. Cell.*, **2003**, 11 (6), 1587-1598.

(3) Lee, C.-K.; Shibata, Y.; Rao, B., Strahl, B. D.; Lieb, J. D. Evidence for nucleosome depletion at active regulatory regions genome-wide. *Nat. Genet.,* **2004**, 36, 900–905.

(4) Hendrich, B.; Bickmore, W. Human diseases with underlying defects in chromatin structure and modification. *Hum. Mol. Genet.,* **2001**, 10, 2233–2242.

(5) Wu, C. The 5′ ends of *Drosophila* heat shock genes in chromatin are hypersensitive to DNase I. *Nature*, **1980**, 286 (5776), 854-860.

(6) Song, L.; Crawford, G.E. DNase-seq: a high-resolution technique for mapping active gene regulatory elements across the genome from mammalian cells. *Cold Spring Harbor Protocols*, **2010**, 2010 (2), pdb prot5384.

(7) Giresi, P.G.; Lieb, J.D. Isolation of active regulatory elements from eukaryotic chromatin using FAIRE (Formaldehyde Assisted Isolation of Regulatory Elements). *Methods*, **2009**, 48 (3), 233-239.

(8) Buenrostro, J.D.; Giresi, P.G.; Zaba, L.C.; Chang, H.Y.; Greenleaf, W.J. Transposition of native chromatin for fast and sensitive epigenomic profiling of open chromatin, DNA-binding proteins and nucleosome position. *Nat. Methods*, **2013**, 10 (12), 1213-1218.

(9) Carnell S.C.; Bowen A.; Morgan E.; Maskell D.J.; Wallis T.S.; Stevens M.P. Role in virulence and protective efficacy in pigs of Salmonella enterica serovar Typhimurium

secreted components identified by signature-tagged mutagenesis. *Microbiology,* **2007**, 153, 1940–1952.

(10) Naumann T.A.; Reznikoff W.S. Tn5 transposase with an altered specificity for transposon ends. *J. Bacteriol.,* **2002**, 184, 233–240.

(11) Hennig, B.P.; Velten, L.; Racke, I.; Tu C.S.; Thoms, M.; Rybin, V.; Besir, H.; Remans, K.; Steinmetz, L.M. Large-Scale Low-Cost NGS Library Preparation Using a Robust Tn5 Purification and Tagmentation Protocol. *G3,* **2018**, 8. 79–89.

(12) Herron, P.R.; Hughes, G.; Chandra, G.; Fielding, S.; Dyson, P.J. Transposon Express, a software application to report the identity of insertions obtained by comprehensive transposon mutagenesis of sequenced genomes: Analysis of the preference for in vitro Tn5 transposition into GC-rich DNA. *Nucleic Acids Res.,* **2004**, 32, e113.

(13) Tan, L.; Xing, D.; Chang, C.H.; Li, H.; Xie, X.S. Three-dimensional genome structures of single diploid human cells. *Science,* **2018**, 361, 924–928.

(14) Kaya-Okur, H.S.; Wu, S.J.; Codomo, C.A.; Pledger, E.S.; Bryson, T.D.; Henikoff, J.G.; Ahmad, K.; Henikoff S. CUT&Tag for efficient epigenomic profiling of small samples and single cells. *Nat. Commun.,* **2019**, 10, 1930.

(15) Kaya-Okur, H.S.; Janssens, D.H.; Henikoff, J.G. *et al*. Efficient low-cost chromatin profiling with CUT&Tag. *Nat. Protoc.,* **2020**, 15, 3264–3283.

(16) CUTANA™ Direct-to-PCR CUT&Tag Protocol– Methods Overview, *EpiCypher*.

(17) Santos-Rosa, H.; Schneider, R.; Bannister, A.J.; Sherriff, J.; Bernstein, B.E.; Emre, N.C.T.; Schreiber, S.L.; Mellor, J.; Kouzarides, T. Active genes are tri-methylated at K4 of histone H3. *Nature*, **2002**, 419, 407–11.

(18) Parsons, D.W.; Jones, S.; Zhang, X.; *et al*. An integrated genomic analysis of human glioblastoma multiforme. *Science*, **2008**, 321, 1807–1812.

(19) Louis, D.N.; Perry, A.; Reifenberger, G.; von Deimling, A.; Figarella-Branger, D.; Cavenee, W.K.; Ohgaki, H.; Wiestler, O.D.; Kleihues, P.; Ellison, D.W. The 2016 World Health Organization Classification of Tumors of the Central Nervous System: A summary. *Acta. Neuropathol*., **2016**, 131, 803–820.

(20) Dang, I.; White, D.W.; Gross, S.; Bennett, B.D.; Bittinger, M.A.; *et al*. Cancer-associated IDH1 mutations produce 2-hydroxyglutarate. *Nature*, **2009**, 462, 739–744.

(21) Xu, W.; Yang, H.; Liu, Y.; *et al*. Oncometabolite 2-hydroxyglutarate is a competitive inhibitor of α-ketoglutarate-dependent dioxygenases. *Cancer Cell,* **2011**, 19, 17–30.

(22) Figueroa, M. A.; Abdel-Wahab, O.; Lu, C.; Ward, P.S.; *et al*. Leukemic IDH1 and IDH2 mutations result in a hypermethylation phenotype, disrupt TET2 function, and impair hematopoietic differentiation. *Cancer Cell*, **2010,** 18(6), 553-67.

(23) Nunez, F. M.; Gauss, J. C.; Mendez, F.M.; *et al*. Genetically Engineered Mouse Model of Brainstem High-Grade Glioma. *STAR Protocols,* **2020**, 1, 100165.

(24) Núñez, F. J.; Mendez, F.M.; Kadiyala, P.; Alghamri, M.S.; *et al*. IDH1-R132H acts as a tumor suppressor in glioma via epigenetic up-regulation of the DNA damage response. *Sci. Transl. Med*., **2019**, 11, eaaq1427.

(25) Alghamri, M.S.; McClellan, B.L.; Avvari, R.P. *et al*. G-CSF secreted by mutant IDH1 glioma stem cells abolishes myeloid cell immunosuppression and enhances the efficacy of immunotherapy. *Science Advances*, **2021**, 7, eabh3243.

Chapter 5 Conclusion

Dependable and user-friendly bioassays are needed in clinical and diagnostic settings to monitor the epigenome for the progression of certain diseases and cancers. Nonetheless, conventional epigenetic and chromatin profiling assays developed for research have limitations that make them incompatible with medical screenings.[1] The multidisciplinary field of droplet microfluidics can be utilized to streamline and automate epigenetic and chromatin profiling assays but also alleviate the constraints that limit their transition into medical and diagnostic screening[2]. Principally, this field allows for low inputs because microfluidic modules can process cells individually in monodisperse droplets. Microfluidic adaptation also permits reliable reproducibility by strengthening sample processing uniformity and efficient incubations through conventional mixing to increase reagent interactions. Thence, the projects that construct this thesis strive to progress the automation of profiling assays through the field of droplet microfluidics and are motivated by their future implementations within medical and clinical environments.

The reported work expands the capabilities of the Bailey lab's microfluidic modules to adapt more significant procedural segments and expand the functionality of published modules for translating assays for which these modules were not developed. Previous chapters discuss advancements towards automating chromatin profiling assays, such as ChIP[3], as well as the novel enzymatic tethering assays, CUT&RUN[4] and CUT&Tag[5]. Including previous efforts, four epigenetic profiling assays have been translated to a droplet microfluidic format utilizing the MNase module[6]. This speaks to the versatility, robustness, and adaptability of this design to

tackle biological procedures. Through the use of two microfluidic modules, two-thirds of the ChIP protocol was adapted to a droplet format. The protocol was validated by profiling a panel of histone tail modification in two distinct cell lines (HeLa and MWCL-1). Moreover, novel enzymatic tethering assays, CUT&RUN and CUT&Tag, were also automated. Droplet integrated CUT&RUN consolidated two individual incubations into one to construct multi-part complexes and was validated through qPCR analysis. Working off CUT&RUN procedural alterations, DropCUTT was verified through sequencing data for input independence by profiling the epigenetic modification H3K27me3 in three sample inputs (100K, 20K, 10K). Additionally, its applicability was expanded to profile H3K4me3 within mouse model glioma cell lines (NPA and NPAI)[7]. This work addresses challenges and procedural optimization for translating benchtop protocols to a microfluidic format. Promising strides were achieved; however, more work must be completed to elevate reproducible assay performance, expand utility into clinical sample screening, and ultimately expand beyond proof of concept.

5.1.1 Continuing Adaption of Chromatin Immunoprecipitation Procedure

Chromatin immunoprecipitation (ChIP) is the gold standard for epigenetic profiling assays, utilizing antibodies to enrich DNA binding proteins and identify their position on the genome. Chapter 2 showcases our work to translate ChIP to a droplet microfluidic format by developing three distinct modules that address sequential segments of the benchtop protocol. The initial module, previously published MNase[6], breaks the cellular and nuclear membranes and digests chromatin into nucleosome length fragments (~150 base pairs). However, the module's second half was redesigned to deliver quenching buffer and functionalized magnetic beads to probe for the target of interest. The succeeding module CAR-Wash[8] compressed the washing of the sample with four distinct wash buffers onto a single module. A third module was constructed to liberate the genomic fragments where the targeted proteins sit from the antibody functionalized Dynabeads. A panel of histone tail modification targets (H3K4me3, H3K27me3, H3K27ac, H3K4me, H3K36me3, CTCT) were profiled in two cell lines (HeLa and MWCL-1). Numerous variables were optimized in the droplet as well as bulk protocols to improve target pull-down efficiency. Ultimately, two-thirds of the ChIP protocol was effectively translated to a droplet microfluidic format. Through analysis of quantitative polymerized chain reactions (qPCR) and calculating ΔΔCt values for a positively and negatively associated gene, we demonstrate effective pull-down of histone tail modifications H3K27me3 and H3K4me3 in HeLa cells as well as H3K4me3 and H3K27ac in MWCL-1.

While ChIP is an effective protocol to investigate genomic regions where chromatin proteins are positioned, the protocol can be labor-intensive and time consuming. The work in Chapter 2 addresses these limitations through droplet microfluidic automation, which reduces operation time from 4-5 days to ~ 2 days. However, further development is needed to expand the

system's prospects. Final optimization is needed for the cylindrical heater to undertake the chromatin liberation protocol segment. Proteinase K and RNase A concentrations must be cemented within a single incubation to maximize reproducible DNA recovery. Furthermore, the end portion of the CAR-Wash module needs to be redesigned to incorporate a pico injector that would incorporate Proteinase K and RNase A into the resegmented droplets and feed directly into the cylindrical heater. To progress the capabilities of ChIP, multiplexity of targets profiled from an initial sample input is necessary. This could be achieved utilizing two distinct types of beads, magnetic and polystyrene, where each is functionalized with a different antibody and simultaneously added to the digested chromatin samples. Following the immunoprecipitation portion, the magnetic beads would be isolated using a magnetic rack, and the polystyrene beads through centrifugation. Figure 5.1 is preliminary qPCR data profiling H3K4me3 and H3K27me3 from the same input sample (HeLa, 250K cells per sample). Both targets show enrichment in their regions of enrichment (H3K4me3 -Brg1 and H3K27me3 – MYT1) and minimal enrichment within regions of depletion as well as among the negative controls. Additional work is needed to increase the enrichment signal and test different combinations of targets being profiled. Lastly, distinct digestion methods such as sonication and site-specific restriction enzymes need to be explored to incorporate the profiling of transcription factors and chromatin proteins. This additional development would elevate the application of droplet ChIP by increasing data generation from limited sample input and enhancing experiment efficiency.

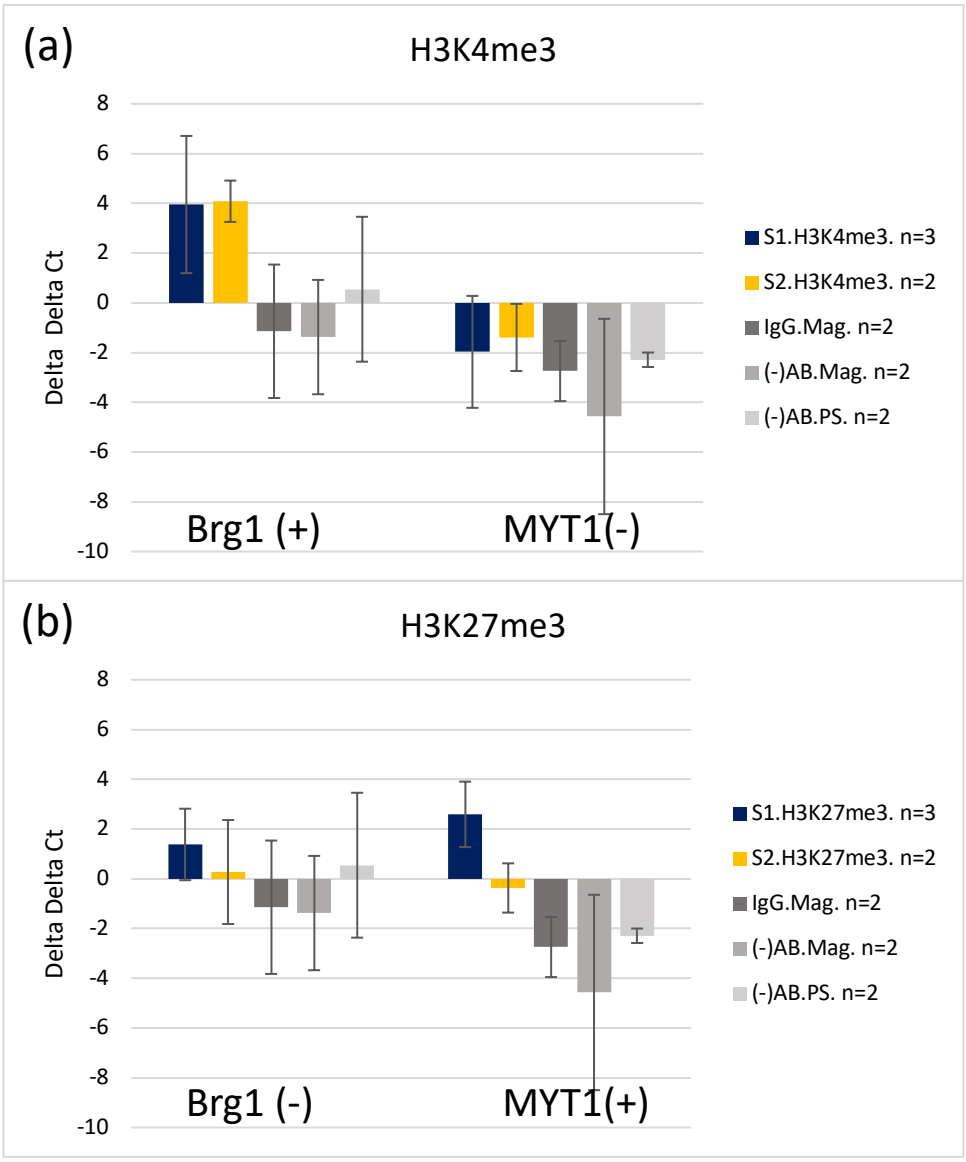

Figure 5.1 Preliminary enrichment profiles for bulk ChIP experiment targeting H3K4me3 and H3K27me3 from the same input sample (250K HeLa cells per sample). Both targets (blue) reach the enrichment threshold of 2.2 in their regions of enrichment (H3K3me 3- Brg1, H3K27me3 – MYT1). Yellow bars are enrichment signals for targets from separate input samples. Grey bars are negative controls, magnetic beads coated with IgG (IgG. Mag.), bare magnetic beads ((-)AB Mag), and bare polystyrene beads ((-)AB PS).

5.1.2 Enzymatic Tethering Assays for Clinical and Diagnostic Screening

Chapters 3 and 4 showcase our attempts to harness the potential of enzymatic tethering assays and combine their novelty with droplet microfluidics to streamline the procedures for epigenetic profiling. Initial proof of concept studies demonstrate encouraging results that our droplet-integrated protocols for CUT&RUN and CUT&Tag can efficiently pull-down histone tail modifications. In order to advance DropCUTT's progress and application, further experimental studies are needed that focus on adapting additional portions of the benchtop protocol on device, incorporating crosslinked as well as clinically preserved input materials, and transitioning fabrication to commercially compatible materials.

A significant portion of microfluidic bioassays do not advance beyond proof-of-concept experiments. As a means to mitigate this possibility and demonstrate the versatility of our integrated droplet systems, more profiling targets must be screened through varying cell inputs. Epigenetic target of interest, H3K27me3 produces promising enrichment using 100K cells per sample for droplet-integrated CUT&RUN and with DropCUTT using 100K, 20K, and 10K cells. H3K27me3 is an abundant target often recommended as a positive control to include in an experimental setup. To test the limits of the DropCUTT and CUT&RUN systems, we are working on profiling H3K27ac, H3K36me3, and CTCF. Preliminary data, utilizing the DropCUTT system to profile these targets, has been collected using 50,000 K562 cells per sample, and bioanalyzer fragmentation patterns were obtained. To confirm targets were adequately profiled using CUT&Tag, a defined nucleosomal pattern of bands at approximately 180 base pairs apart (150 bp, 360 bp, and 540 bp) after library preparation is expected on an electropherograms[9]. However, the predominant product peak should be at ~360 bp due to nucleosome-length digestion producing ~150 bp fragments, plus the addition of sequencing

adaptors ~180 bp-long. The band pattern is observed in the bioanalyzer electropherograms of all three targets (Figure 5.1). When considering the intensity of this fragmentation pattern, it is notable that the peaks are poorly resolved from one another. Explanations for this could include nonspecific fragmentation due to premature pAG-Tn5 activity. Additionally, because these targets are predominantly associated with active transcription and euchromatin, linker DNA is possibly being tagmented alongside nucleosomes and blending the fragmentation patterns. This increases variability within the expected fragmentation bands (150 bp, 360 bp, and 540 bp).

Additional module alterations are recommended to further the droplet integration of DropCUTT. In the previous chapter, the procedure for DropCUTT consists of incubating droplets in a microfluidic module, then collecting the droplets into an Eppendorf tube for overnight incubation. This overnight incubation at 4°C facilitates the simultaneous assembly of the three-tier immunoprecipitation unit in droplets. However, it would be helpful if this incubation occurred on device. Adding an incubation chamber to the MNase design would allow facile transportation of droplet samples and decrease sample loss due to droplets staying in outlet tubing. Variations of an on-device incubation chamber can be observed in Figure 5.2. Version 1 brought challenges during treatment with Aquapel, and so the shape of the incubation chamber was redesigned into a teardrop (Version 2). A photomask has been purchased for this new incubation chamber however, moving forward, a master will need to be fabricated and the design tested, initially by treating the module with Aquapel, then by noting if the droplets can be contained within the chamber and efficiently recovered following incubation.

Moving forward, DropCUTT would benefit from expanding usage into crosslinked cell inputs, multiplexity of the procedure to profile multiple targets of interest from one initial input and transitioning towards commercially acceptable fabrication materials. Within clinical settings,

long-term sample storage includes formaldehyde crosslinking[10] to conserve interactions between chromatin proteins and chromatin fibers. The original CUT&Tag protocol was developed to work with native cell conditions. While procedural alterations have been made to incorporate crosslinked samples[11], additional work is needed to observe the reproducibility of DropCUTT processing with fixed cell populations for distinct targets at a variety of cell amounts. Furthermore, multiplexing of DropCUTT is needed to maximize the utility of the initial sample input. As previously mentioned, sample acquisition within clinical settings is limited, and the multiplexity of this assay would increase the extraction and generation of sequencing data abundantly. Lastly, to progress the potential commercialization of this automated protocol, microfluidic module fabrication would need to move towards commercial materials such as poly (methyl methacrylate) (PMMA) and cyclic olefin polymer (COP)[12] with surface treatments to generate hydrophobic microchannels[13,14]. Fortunately, the Bailey lab has experience transitioning PDMS fabricated structures for droplet manipulation to thermoplastic fabrication[15].

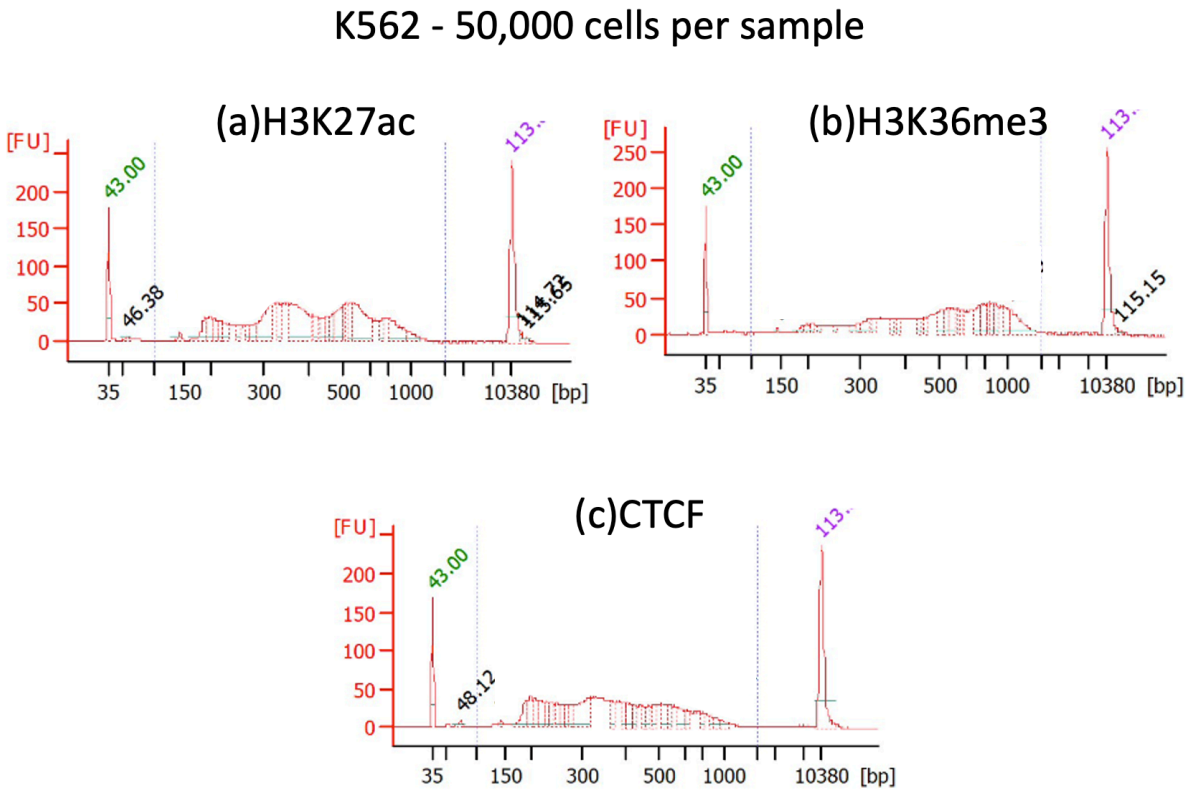

Figure 5.2 Chromatin fragment analysis through Bioanalyzer for additional targets (H3K27ac, H3K36me3, CTCF) to demonstrate DropCUTT's ability to profile versatile targets. H3K27ac is a target associated with active transcription however is scarce throughout the genome. H3K36me3 is a clinically relevant target and transcription factor CTCF, which mitigates architectural chromatin loops and is associated with transcriptional activation and repression.

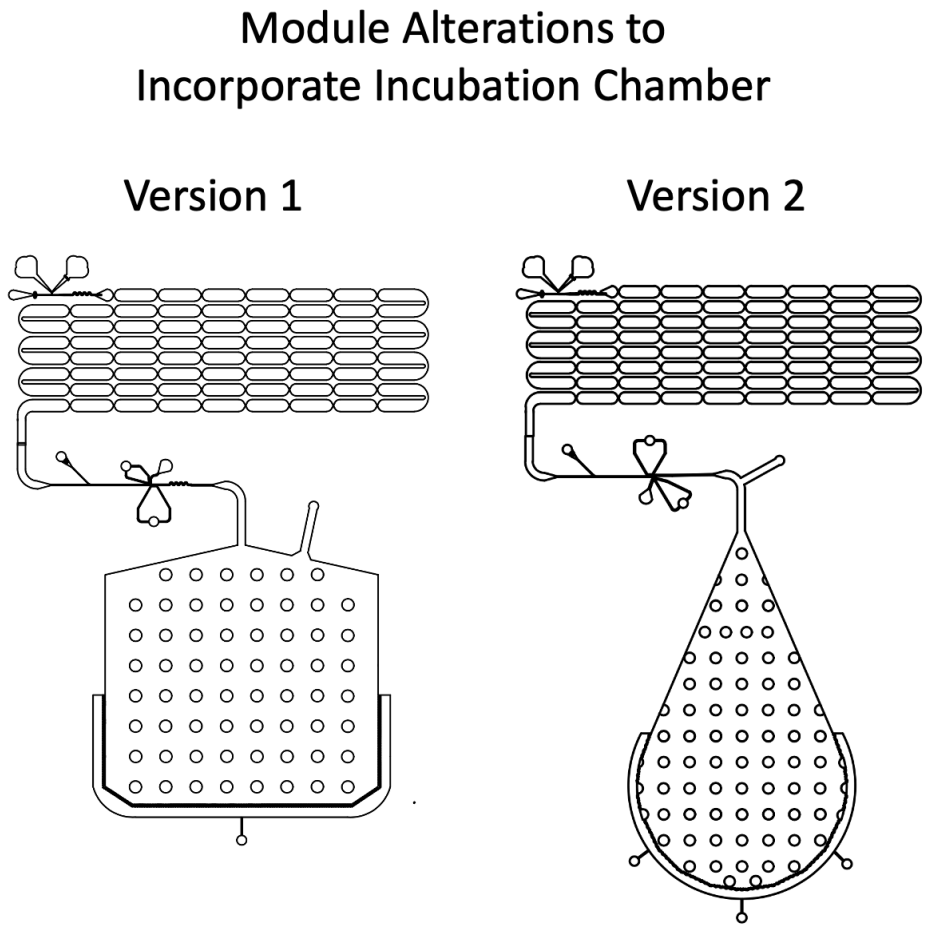

Figure 5.3 Variations of incubation chamber on DropCUTT microfluidic module. The addition of a reservoir would allow droplets to continue incubating on device through the simultaneous assembly of the immunoprecipitation unit.

5.1.3 Tangible Utility of Droplet Microfluidic Technologies

Droplet microfluidics made its initial literature presence in 1997[16], and the field has been around for over two decades. Within this time, two distinct periods have characterized the growth and establishment of this research field. The initial stage of this technology centered on emergence, specifically establishing functional components[17,18], controllable compartmentalization[19], and simplistic applications within biology and chemistry[20]. The second stage has empowered the impact and utility of droplet microfluidics to enable innovative research. Recent advantages include high-throughput experimentation, increasing experiment efficiency, and rapid production of large-scale, high-quality data sets[21]. The droplet microfluidics field has matured and significantly impacted single-cell experimentation[22] and small volume detection[23]. Droplet based single-cell RNA-Seq platforms, Drop-Seq[24] and inDrop[25], yield the ability to integrate and profile gene expression patterns within heterogeneous cell populations. This application has been immensely successful through commercialization by 10X Genomics[26]. Similarly, due to its user-friendly operation, digital droplet PCR (ddPCR), capitalized on by Bio-Rad[27], has also had a significant impact and rapid adaptation. This platform segregates a nucleic acid sample into millions of droplets, and a signal is only generated within droplets containing the targeted sequence[28,29]. Droplet technologies are advancing and becoming an instrumental tool in undertaking complex chemical and biological applications however, growing pains are foreseen.

While droplet technologies are exciting, follies are limiting broader applications. Manufacturing of microfluidic chips can be expensive due to intricate, multi-channel size and three-dimensional structures. Typically, construction and assembly is performed in particle-controlled cleanrooms by highly skilled technicians utilizing complex machinery. To overcome

these high costs, exploration into microfluidic fabrication utilizing 3D printing is underway[30]. Additionally, the operation of devices can be complicated. Generating droplets requires using an expensive gas pressure system or multiple syringes on costly pumps. There is, however, work into developing fluid manipulation without pumps to increase implementation outside of lab environments.

Droplet microfluidic platforms tackle complex experiments and procedures through strategic combinations of functional components. The automation of epigenetic and chromatin profiling assay is an emergence of the current state of droplet technologies, and the work in this thesis exemplifies this advancement. Droplet integrated ChIP, along with DropCUTT, progresses experimental efficiency by combining individual time-consuming incubations and transitioning them into droplets on device. Furthermore, DropCUTT works to increase the amount and quality of data generated from small cell amounts by going as low as 10K cells per sample and still generating next-generation sequencing data. Coupling droplet microfluidic with profiling assays has excellent potential and impact within the landscapes of clinical epigenetics but also towards systematically implementing epigenetic biomarker profiling within clinical and diagnostic screening.

References

(1) Dirks, R.A.M.; Stunnenberg, H.G.; Marks, H. Genome-wide epigenomic profiling for biomarker discovery. *Clin. Epigenet.*, **2016**, 8, 122.

(2) Deng, C.; Naler, L.B.; Lu, C. Microfluidic epigenomic mapping technologies for precision medicine. *Lab Chip*, **2019,** 19, 2630.

(3) Collas, P. The Current State of Chromatin Immunoprecipitation. *Mol. Biotechnol.*, **2010**, 45(1), 87-100.

(4) Skene, P.J.; Henikoff, S. An efficient targeted nuclease strategy for high-resolution mapping of DNA binding sites. *eLife,* **2017**, 6, e21856.

(5) Kaya-Okur, H.S.; Janssens, D.H.; Henikoff, J.G. *et al*. Efficient low-cost chromatin profiling with CUT&Tag. *Nat. Protoc.,* **2020**, 15, 3264–3283.

(6) Xu, Y.; Doonan, S.R.; Ordog, T.; Bailey, R.C. A droplet microfluidic platform for efficient enzymatic chromatin digestion enables robust determination of nucleosome positioning. *Lab Chip*, **2018**, 18, 2583-2592.

(7) Núñez, F. J.; Mendez, F.M.; Kadiyala, P.; Alghamri, M.S.; *et al*. IDH1-R132H acts as a tumor suppressor in glioma via epigenetic up-regulation of the DNA damage response. *Sci. Transl. Med*., **2019**, 11, eaaq1427.

(8) Doonan, S. R.; Lin, M.; Bailey, R.C. Droplet CAR-Wash: continuous picoliter-scale immunocapture and washing. *Lab Chip*, **2019**, 19, 1589.

(9) Gaffney, D.J.; McVicker, G.; Pai, A. A.; Fondufe-Mittendorf, Y. N.; Lewellen, N.; Michelini, K.; Widom, J.; Gilad, Y.; Pritchard, J. K. Controls of Nucleosome Positioning in the Human Genome. *PLoS Genet*., **2012**, 8, e100303.

(10) Hoffman, E.A.; Frey, B. L.; Smith, L.M.; Auble, D. T. Formaldehyde crosslinking: a tool for the study of chromatin complexes. *J Biol Chem.,* **2015**, 290 (44), 26404–26411.

(11) CUTANA™ Direct-to-PCR CUT&Tag Protocol– Methods Overview, *EpiCypher*.

(12) Nge, P.N.; Rogers, C.I.; Woolley, A.T. Advances in microfluidic materials, functions, integration, and applications. *Chem. Rev*., **2013**, 113, 2550 - 2583B.

(13) Subramanian, B.; Kim, N.; Lee, W.; Spivak, D.A.; Nikitopoulos, D.E.; McCarley, R.L.; Soper, S.A. Surface Modification of Droplet Polymeric Microfluidic Devices for

the Stable and Continuous Generation of Aqueous Droplets. *Langmuir*, **2011**, 27, 7949 —7957.

(14) Hwang, S.J.; Tseng, M.C.; Shu, J.R.; Yu, H.H. Surface modification of cyclic olefin copolymer substrate by oxygen plasma treatment. *Surf. Coat. Technol.*, **2008**, 202, 3669 —3674.

(15) Sohore, V.; Doonan, S.R.; Bailey, R.C. Droplet microfluidics in thermoplastics: device fabrication, droplet generation, and content manipulation using integrated electric and magnetic fields. *Anal. Methods*, **2018**, 10, 4264.

(16) Kawakatsu, T.; Kikuchi, Y.; Nakajima, M. Preparation of micron-scale monodisperse oil-in-water microspheres by microchannel emulsification. *J. Am. Oil Chem. Soc.*, **1997**, 74, 317 —321.

(17) Ren, K.; Zhou, J.; Wu, H. Materials for microfluidic chip fabrication. *Acc. Chem. Res.*, **2013**, 46, 2396– 2406.

(18) Günther, A.; Jensen, K. F. Multiphase microfluidics: from flow characteristics to chemical and materials synthesis. *Lab Chip,* **2006**, 6, 1487– 1503.

(19) Baret, J.-C. Surfactants in droplet-based microfluidics. *Lab Chip,* **2012**, 12, 422-433.

(20) Solvas, X. C. I.; deMello, A. J. Droplet microfluidics: recent developments and future applications. *Chem. Commun.*, **2011**, 47, 1936 —1942.

(21) Ding, Y.; Howes, P.D.; DeMello, A.J. Recent Advances in droplet Microfluidics. *Anal. Chem.,* **2020**, 92 (1), 132-149.

(22) Joensson, H. N.; Svahn, H. A. Droplet Microfluidics-A Tool for Single-Cell Analysis. *Angew. Chem., Int. Ed.,* **2012**, 51 (49), 12176-12192.

(23) Zhu, Y.; Fang, Q. Analytical detection techniques for droplet microfluidics—A review. *Anal. Chem. Acta.,* **2013**, 787, 24– 35.

(24) Macosko, E.Z.; Basu, A.; Satija, R.; Nemesh, J.; Shekhar, K.; Goldman, M.; Tirosh, I.; *et al*. Highly Parallel Genome-wide Expression Profiling of Individual Cells Using Nanoliter Droplets. *Cell*, **2015**, 161, 1202 —1214.

(25) Klein, A. M.; Mazutis, L.; Akartuna, I.; Tallapragada, N.; Veres, A.; Li, V.; Peshkin, L.; Weitz, D. A.; Kirschner, M. W. Droplet barcoding for single cell transcriptomics applied to embryonic stem cells. *Cell*, **2015**, 161, 1187 —1201.

(26) 10X Genomics, https://www.10xgenomics.com/products/single-cell-gene-expression, (accessed October 2022)

(27) BioRad, Bio-Rad, www.bio-rad.com/en-ch/applications-technologies/droplet-digital-pcr-ddpcr-technology, (accessed October 2022)

(28) Kiss, M.M.; Ortoleva-Donnelly, L.; Beer, N.R.; Warner, J.; Bailey, C.G.; Colston, B.W.; Rothberg, J. M.; Link, D.R.; Leamon, J.H. High-Throughput Quantitative Polymerase Chain Reaction in Picoliter Droplets. *Anal. Chem.*, **2008**, 80, 8975 —8981.

(29) Schaerli, Y.; Wootton, R.C.; Robinson, T.; Stein, V.; Dunsby, C.; Neil, M.A.; French, P.M.; deMello, A. J.; Abell, C.; Hollfelder, F. Continuous-Flow Polymerase Chain Reaction of Single-Copy DNA in Microfluidic Microdroplets. *Anal. Chem.*, **2009,** 81, 302 —306.

(30) Waheed, S.; Cabot, J.M.; Macdonald, N.P.; Lewis, T.; Guijt, R.M.; Paull, B.; Breadmore, M. C. 3D printed microfluidic devices: enablers and barriers. *Lab Chip*, **2016**, 16, 1993 —2013.

(31) Zhao, B.; Cui, X.; Ren, W.; Xu, F.; Liu, M.; Ye, Z.G. A Controllable and Integrated Pump-enabled Microfluidic Chip and Its Application in Droplets Generating. *Sci. Rep.*, **2017**, 7, 11319.

Appendices

Appendix A

Additional Targets Profiling with Droplet Integrated Chromatin Immunoprecipitation (ChIP) System

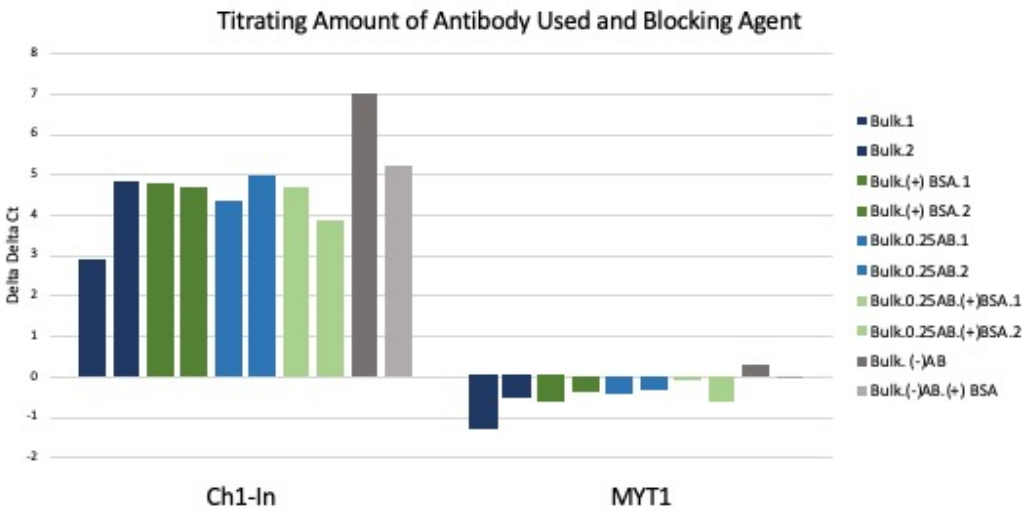

Appendix Figure A.1: qPCR enrichment profiles for H3K4me (Catalog No.ab8895, Abcam), 250K HeLa cells per sample, utilizing blocking agent bovine serum albumin (BSA) and decreasing the amount of antibody used to minimize nonspecific binding to magnetic beads. Alterations were insufficient as both negative controls, (-) AB and (-)AB(+)BSA, have a high amount of enrichment in the region of enrichment (Ch1-In).(-)AB – bare magnetic beads.*

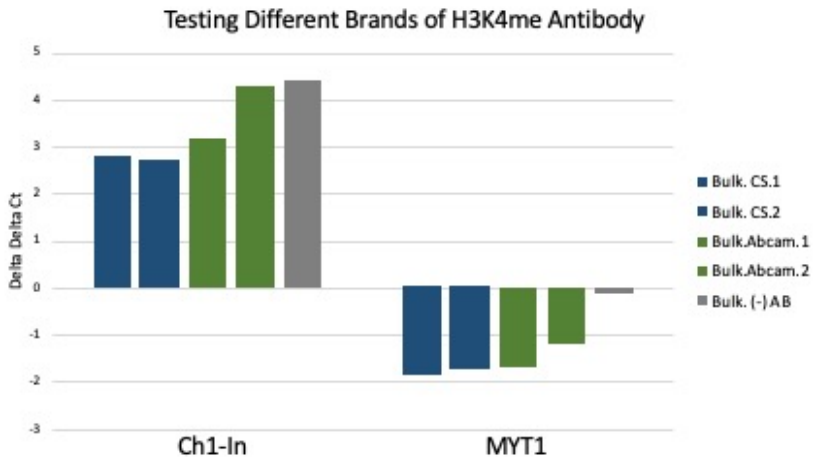

Appendix Figure A.2: Enrichment profiles for H3K4me, 250K HeLa cells per sample, utilizing different antibody vendors to increase immunoprecipitation efficiency above nonspecific binding to magnetic beads. The vendors tested (Cell Signaling Technologies, Catalog No. and Abcam, Catalog No. ab8895) were ineffective as the negative controls, (grey: (-) AB), has higher enrichment than the immunoprecipitated samples (blue and green).

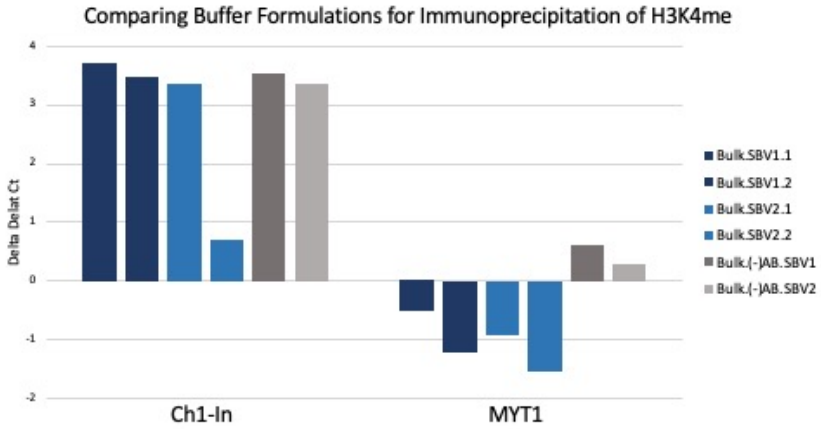

Appendix Figure A.3: Enrichment signals for H3K4me (Catalog No. ab8895, Abcam), 250K HeLa cells per sample, in two buffer formulations – Stop Buffer Version 1 (SBV1) as listed in the materials section (Chapter 2) and Stop Buffer Version 2 (SBV2) does not incorporate sodium dodecyl sulfate (SDS). Buffer changes were insufficient as the negative controls (grey: (-) AB. SBV1 and (-) AB, SBV2) continued to have significant signal in the region of enrichment (Ch 1-In).

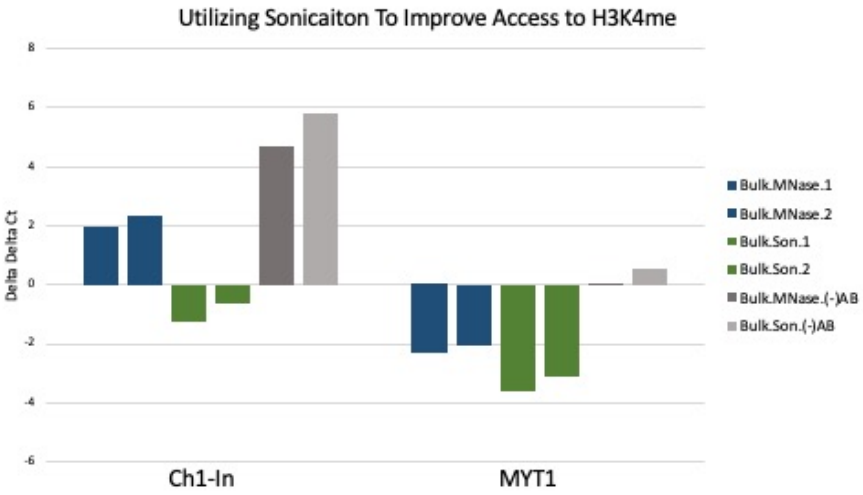

Appendix Figure A.4: Enrichment signals for H3K4me (Catalog No. ab8895, Abcam), 250K HeLa cells per sample. Chromatin shearing was performed utilizing sonication and MNase, to compare the pulldown efficiency of H3K4me. Shearing methods were unsuccessful as the negative controls (grey: MNase (-) AB and Son. (-) AB) have higher signals in the region of enrichment (Ch 1-In).

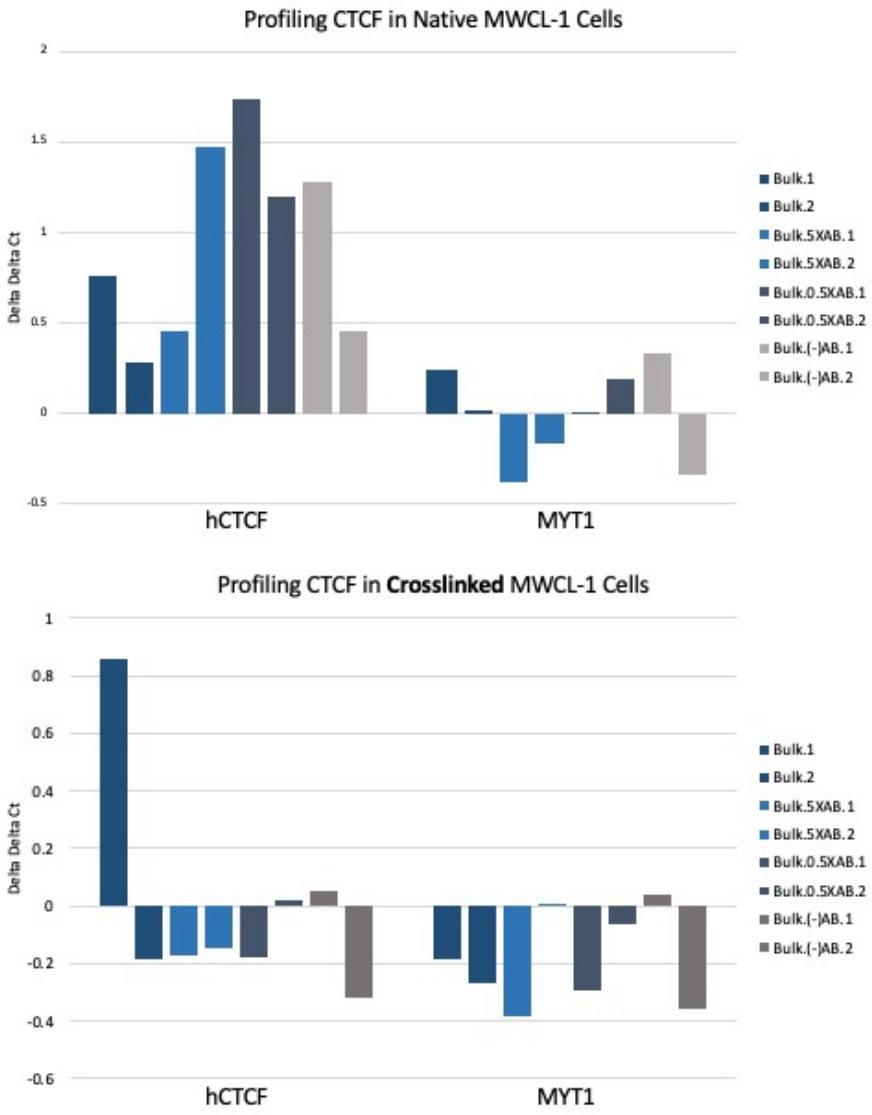

Appendix Figure A.5: Enrichment signals for CTCF (Catalog No. 3418T, Cell Signal Technology), 250K MWCL-1 cells per sample, in native and crosslinked conditions. Antibody amounts were titrated to increase the immunoprecipitation pull-down. As the antibody amount decreased, delta delta Ct signals increased when profiled in native conditions. In fixed samples, titrating the amount of antibody did not yield an effective pull-down of CTCF.

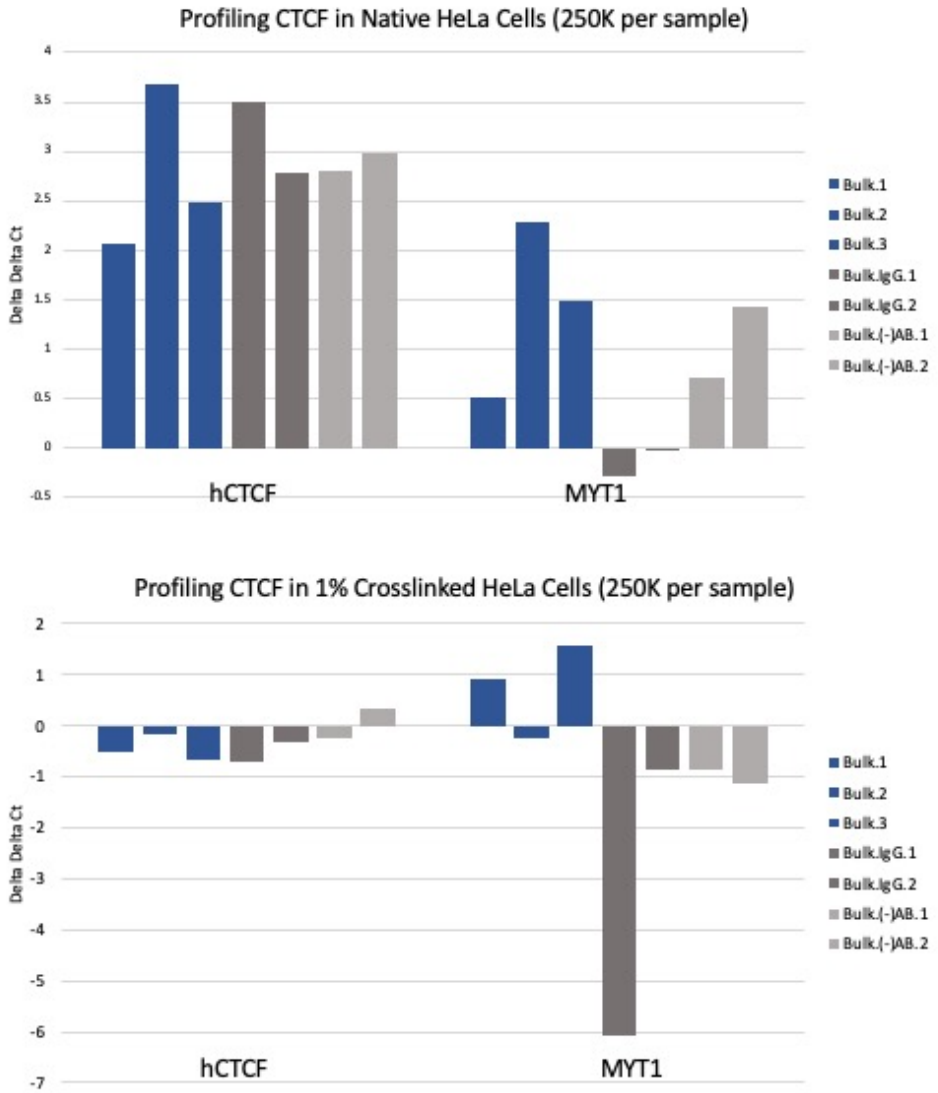

Appendix Figure A.6: Enrichment signals for CTCF (Catalog No. 3418T, Cell Signal Technology), 250K HeLa cells per sample, in native and fixed conditions. While an adequate amount of signal was calculated, this data is inconclusive as the negative controls (grey) also yield significant enrichment in the region of enrichment (hCTCF), suggesting the pull-down is not specific to the presence of the CTCF antibody.

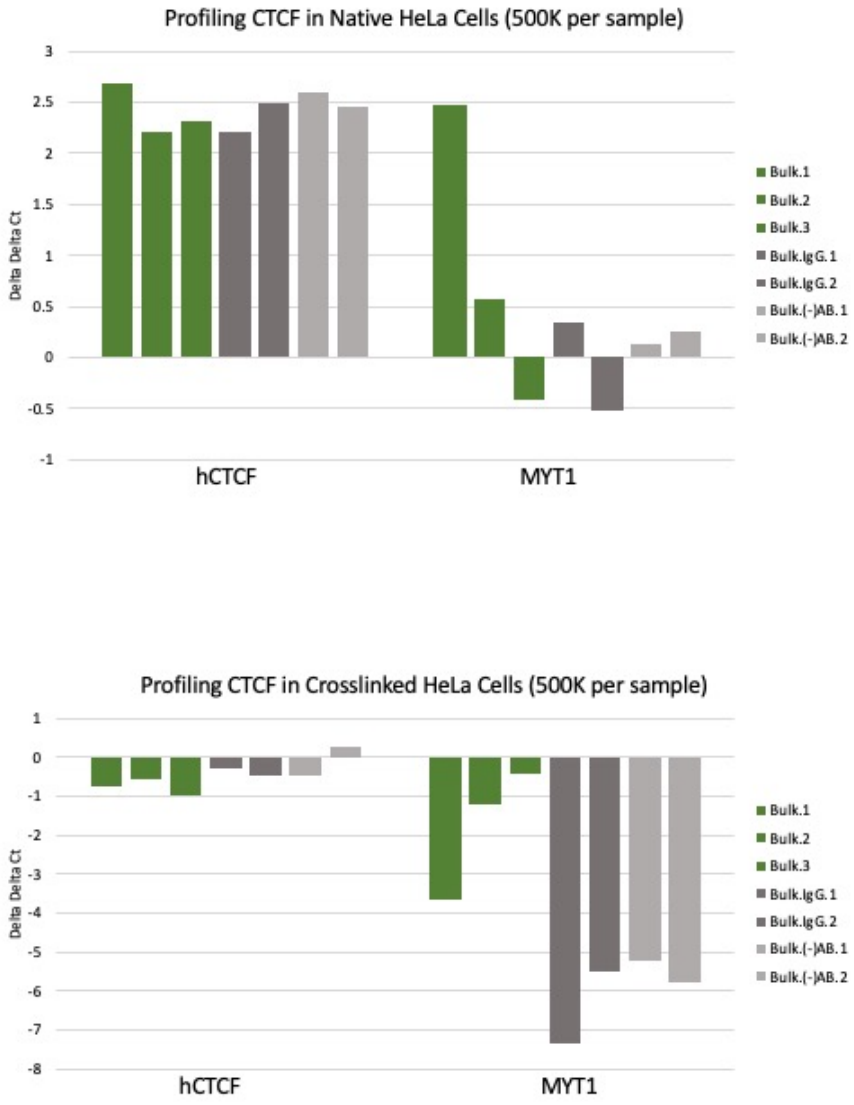

*Appendix Figure A.7: Enrichment signals for CTCF (Catalog No. 3418T, Cell Signal Technology), **500K** HeLa cells per sample, in native and fixed conditions. Increasing the number of cells used does not yield appropriate enrichment for CTCF in fixed or native conditions.*

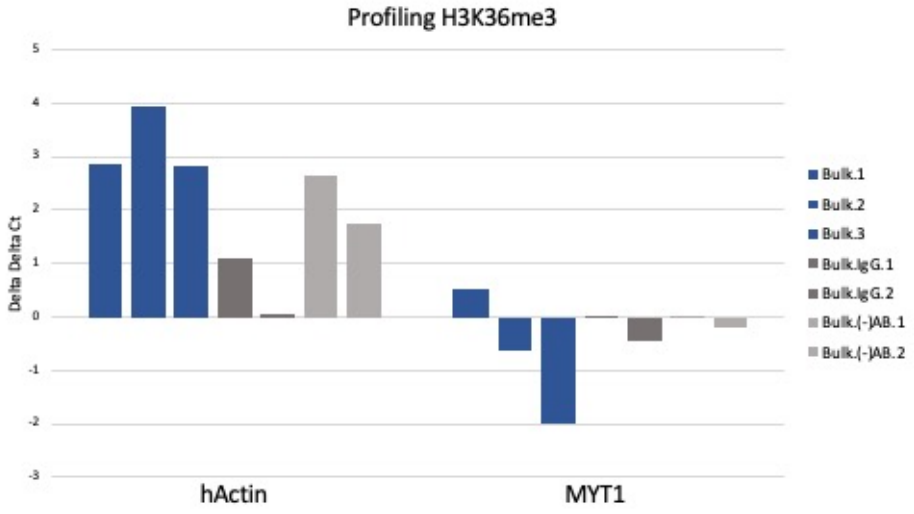

Appendix Figure A.8: Enrichment profiles for H3K36me3 (Catalog No. 61102, Active Motif), 250K HeLa cells per sample. All three replicates yielded comparable delta delta Ct values. The negative IgG controls, IgG, have minimal signal in the enrichment region, hActin. However, the bare bead negative controls, (-) AB, have comparable signal with the immunoprecipitated samples in the enrichment region.

Appendix B

Further Optimization of the CUT&RUN Protocol for Droplet Microfluidic Adaptation

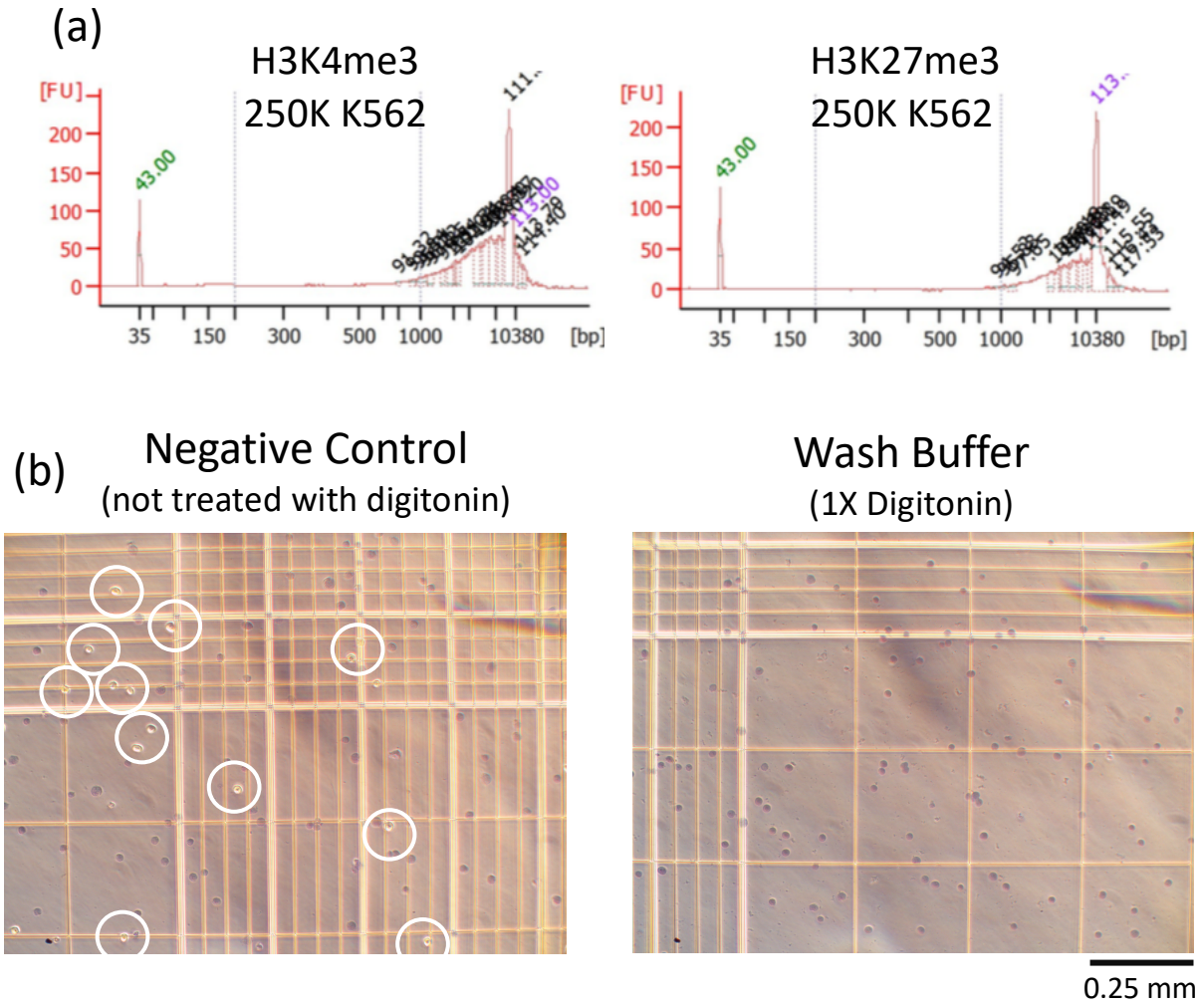

Appendix Figure B.1: (a) Initial attempt at running CUT&RUN protocol utilizing 250K K562 cells per samples profiling histone tail modifications, H3K4me3 (n=1) and H3K27me3 (n=1). Bioanalyzer electropherograms suggest no chromatin digestion occurred. The product peak for both targets of interest is not present at ~ 150 bp. Instead, DNA fragments are between 1,000 and 10,000 bp. (b) Testing whether digitonin permeabilizes K562 cell membrane utilizing trypan blue stain according to manufactures instructions. Cells were visualized on a hemocytometer. Left – K562 cells treated with wash buffer without digitonin. Right – K562 cells treated with wash buffer containing 1X digitonin. This suggests that the wash buffer containing digitonin permeated the cell membrane because trypan blue entered the cells, and that is why cells appear as blue dots (Right).

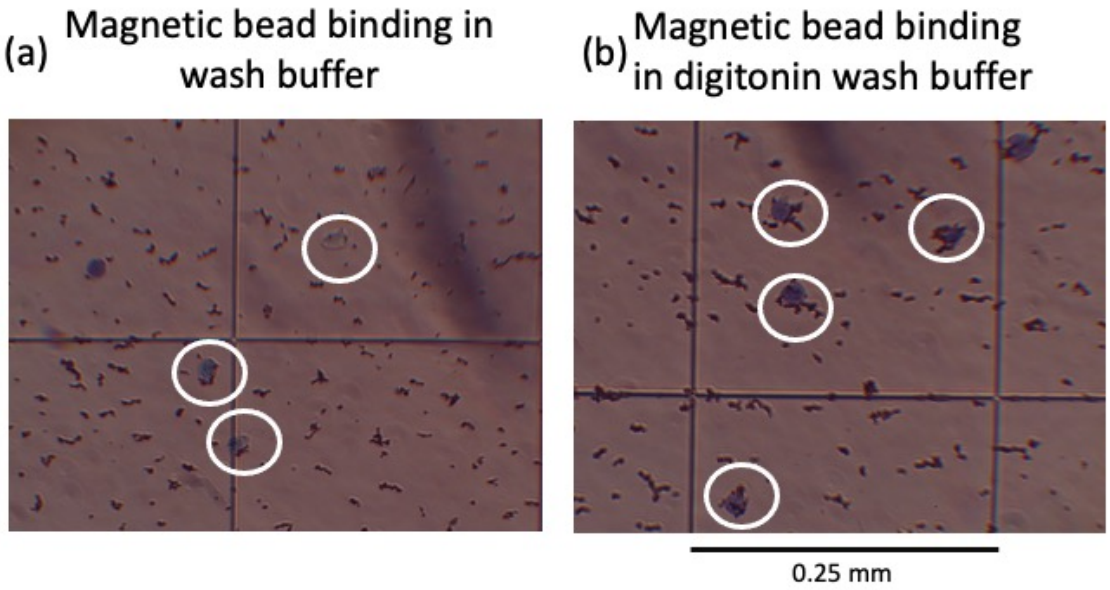

Appendix Figure B.2: Two initial incubations were combined when condensing the CUT&RUN protocol - permeabilization of cells and attachment of concanavalin A magnetic beads. (a) Simultaneous incubation in wash buffer allowed the binding of magnetic beads to K562 cells. However, cells were not efficiently permeabilized. (b) Simultaneous incubation in digitonin wash buffer adequately permeabilized cells and allowed the binding of magnetic beads to cells. Interestingly, beads form larger aggregates with the addition of digitonin in the wash buffer.

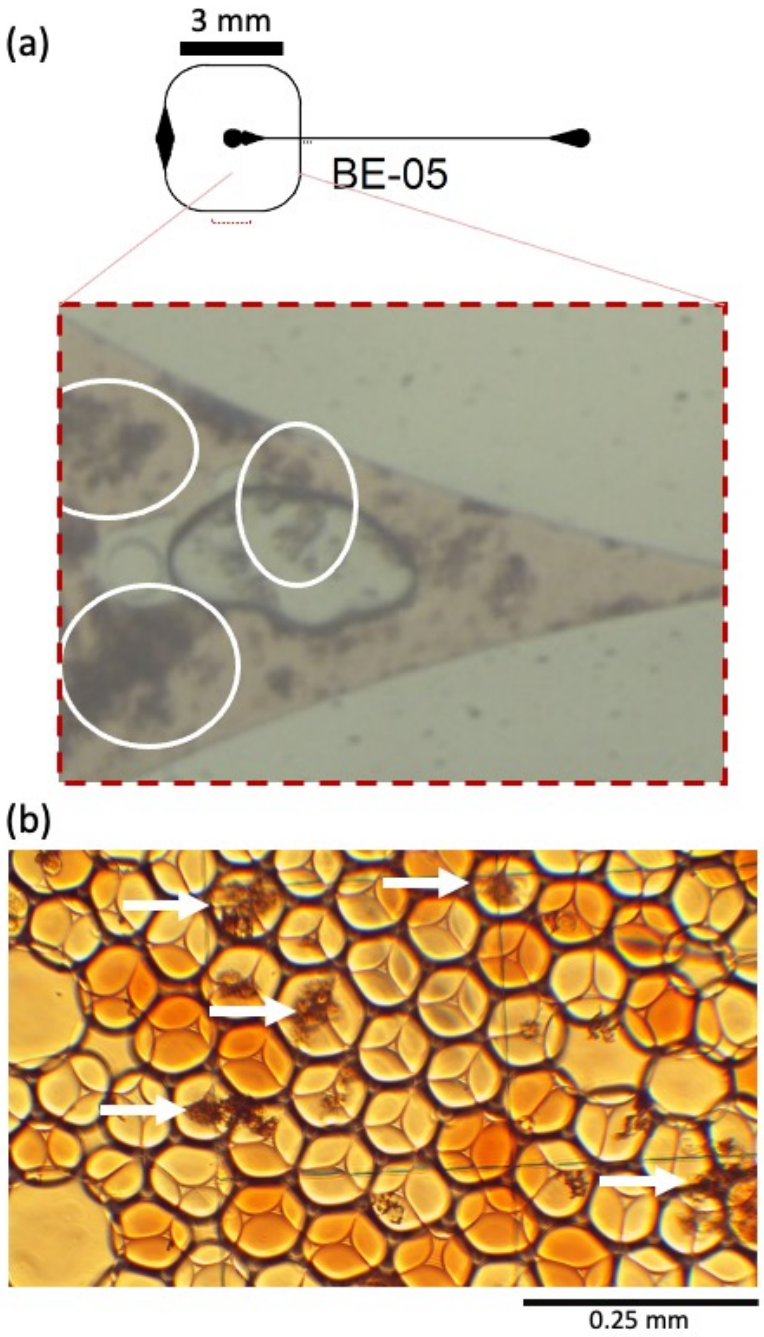

Appendix Figure B.3: (a) Microfluidic module design utilized to emulsify bead-cell sample. During extensive run time, bead-cell units formed aggregates and nonspecifically interacted with PDMS channel walls. (b) Droplets generated with large aggregates (white arrows) tend not to be uniform in size.

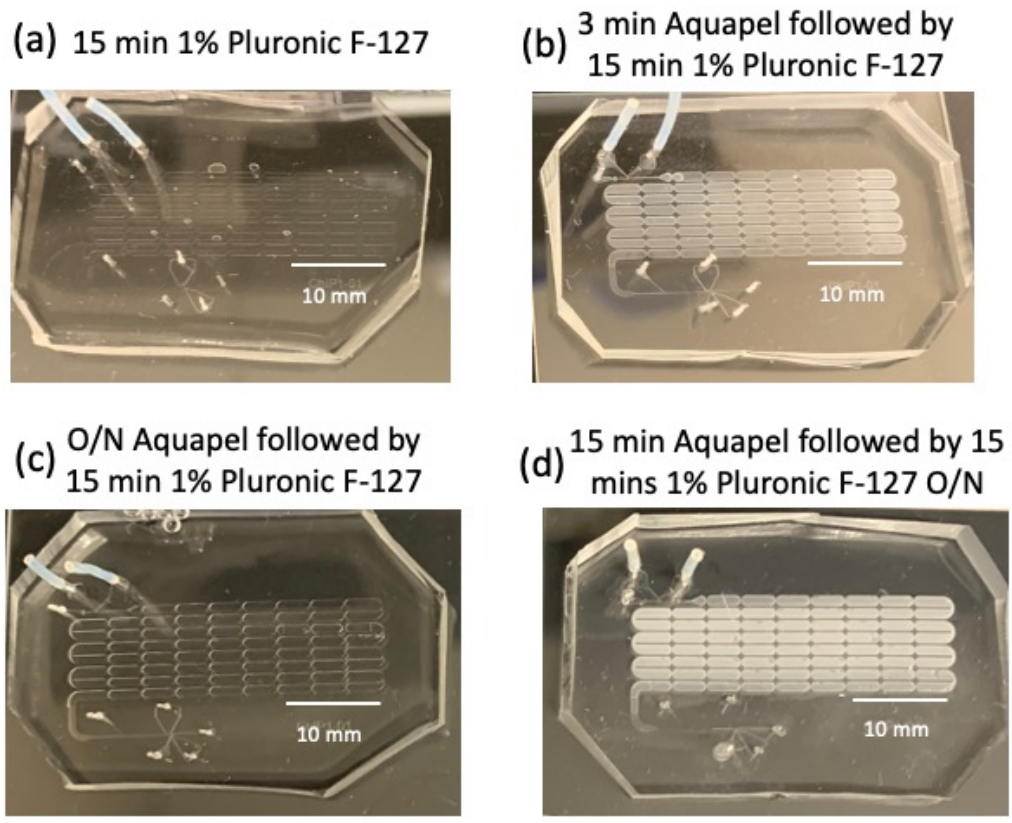

Appendix Figure B.4: Additional surface treatments tested on MNase module to reduce the nonspecific binding of bead-cell unit to the PDMS microchannel walls. (a) Microfluidic module treated with 1% Pluronic F-127 suspended in PBS for 15 minutes. (b) Module initially treated with Aquapel for 3 minutes, flushed with air, then treated with 1% Pluronic F-127 suspended in PBS for 15 minutes. (c) Module treated overnight with Aquapel; this was sufficient time for Aquapel to evaporate. Then treated with 1% Pluronic F-127 suspended in PBS for 15 minutes. (d) Module treated with Aquapel for 15 minutes, flushed with air, then treated with 1% Pluronic F-127 suspended in PBS overnight.

Appendix C

Supplementary Optimization and Development of DropCUTT

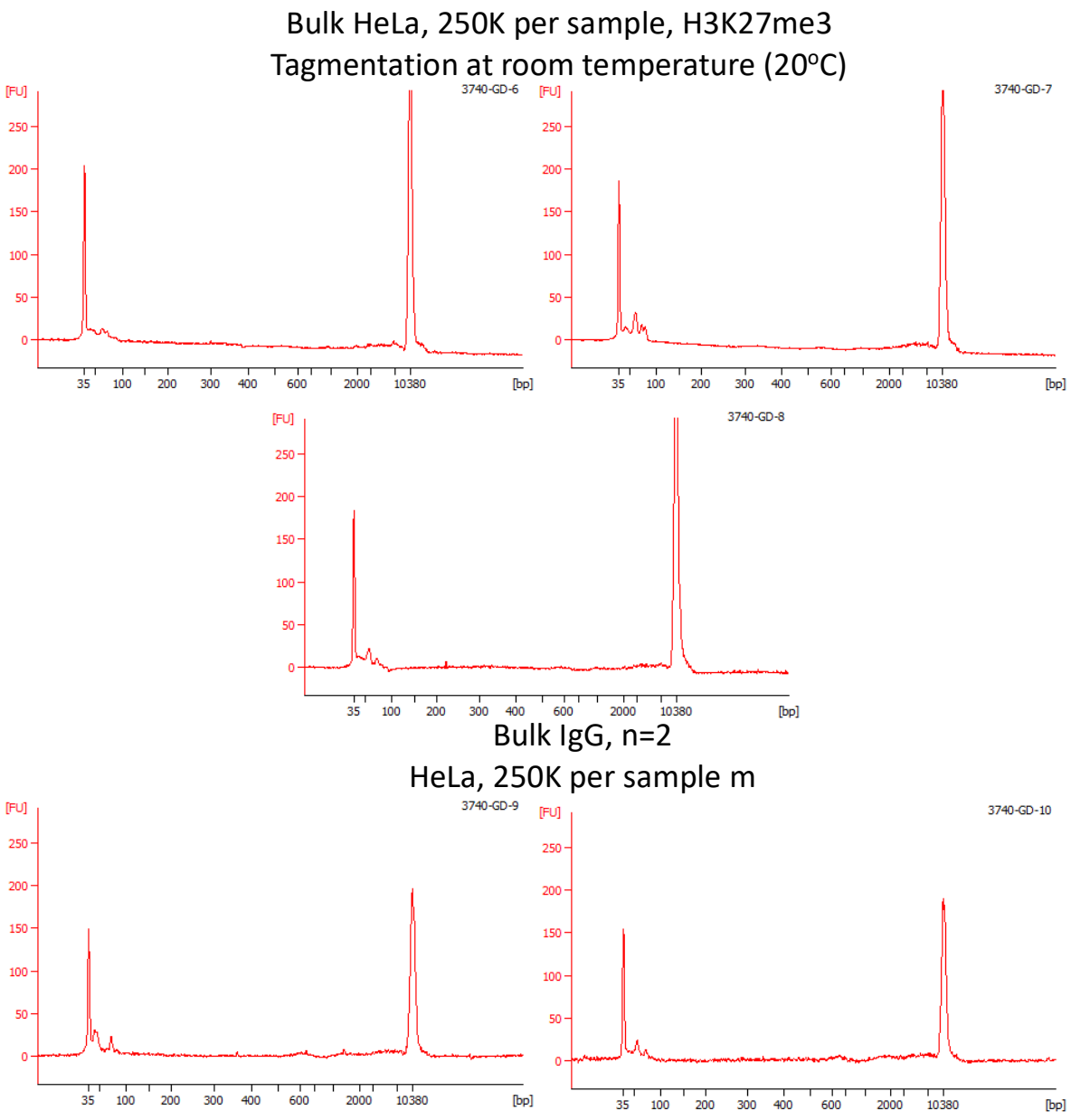

Appendix Figure C.1 Bioanalyzer fragmentation patterns for HeLa cells were processed with the EpiCypher CATANA CUT&Tag protocol, tagmentation ran at room temperature (20°C) for one hour instead of at 37°C. Each sample contained 250K HeLa cells, the target of interest was H3K27me3 (n=3), and additional IgG (n=2) controls were run in parallel. The tagmentation step requires the addition of the divalent ion (Mg2+) as well as heating

(37°C) to cut the double-stranded DNA and ligate on partial adaptors. This is confirmed because there is no product peak formation at 300 bp in the samples that underwent tagmentation at room temperature.

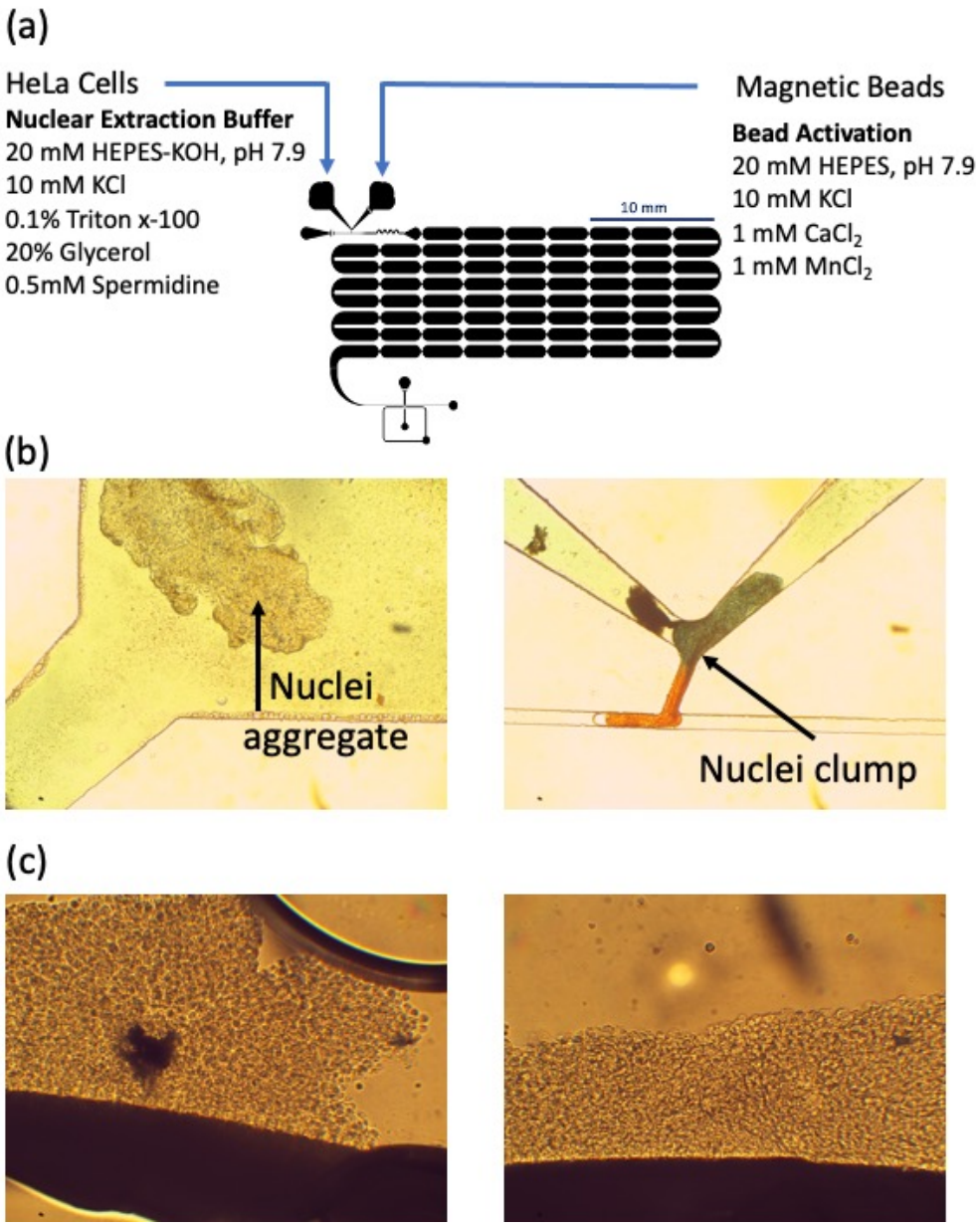

Appendix Figure C.1: (a) Experiment schematic for an initial attempt at delivering HeLa cells in Nuclear Extraction Buffer onto the MNase module. (b)The nuclei extraction occurred rapidly at room temperature while waiting to be loaded onto the microfluidic device - nuclei aggregated and formed clumps that clogged the droplet generator. (c) To confirm, nuclei were extracted at room tempura in bulk for 5 minutes, then pelleted (3 minutes, 600xg). Bulk-extracted nuclei were then visualized and compared to aggregates on MNase modules.

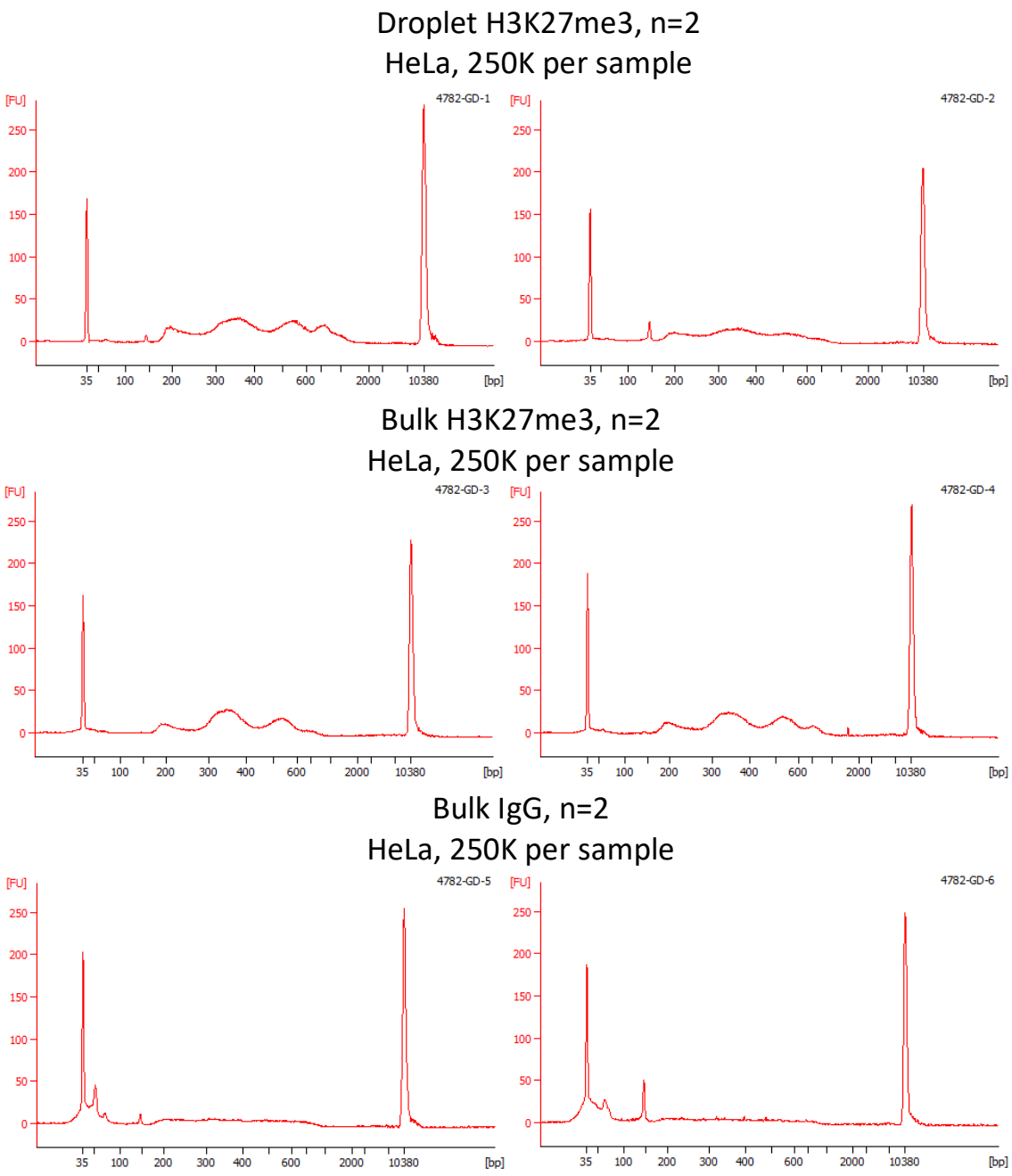

Appendix Figure C. 2: DropCUTT experiment with initial formulation for Extraction Bead Activation (EBA) Buffer (20 mM HEPES pH 8, 10 mM KCl, 1 mM CaCl2, 1 mM MnCl2, 0.5 mM Spermidine, 0.1% Triton X-100, 20% Glycerol, and Roche cOmpleteTM EDTA-free Protease Inhibitor) as well as Antibody Buffer (20 mM HEPES pH 7.5 , 1mM NaCl, 0.5 mM Spermidines, 0.01% Digitonin, 2 mM EDTA, and Roche cOmpleteTM EDTA-free Protease Inhibitor, source: EpiCypher CATANA CUT&Tag protocol). Each sample contains 250K HeLa cells, the target of interest was H3K27me3 (n=2), and additional bulkm(n=2) and IgG (n=2) controls were run in parallel. The desired fragmentation pattern is apparent for both the bulk and droplet samples.

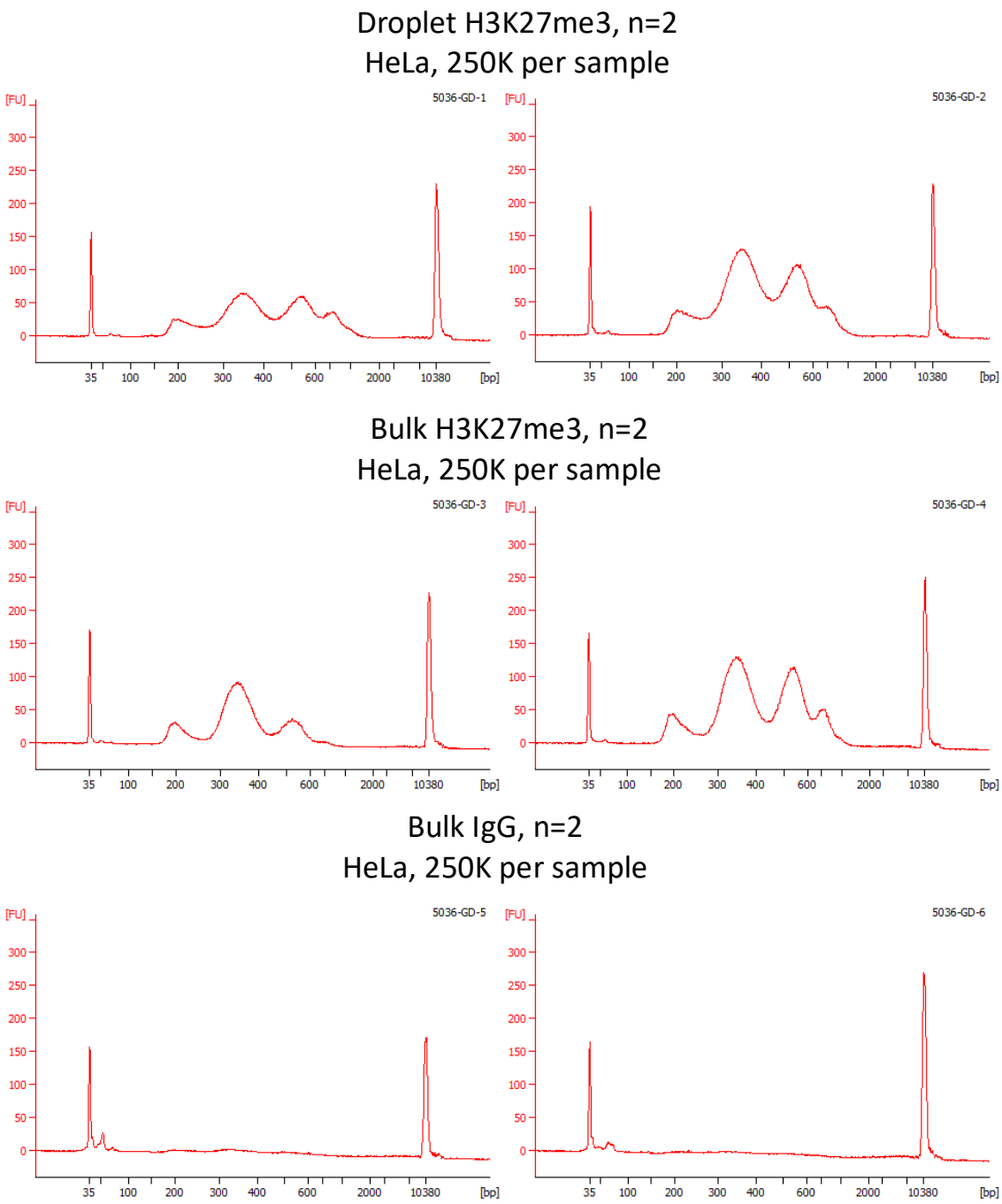

Appendix Figure C. 3: Digestion patterns for K562 cells when EDTA is increased 3X in Antibody Buffer to chelate carryover divalent ions from EBA Buffer. Each sample contains 250K HeLa cells, the target of interest was H3K27me3 (n=2), and additional bulk (n=2) and IgG (n=2) controls were run in parallel. Increasing the amount of EDTA to chelate divalent ions discouraged premature tagmentation and improved peak definition. A significant product peak formed across the droplet and bulk samples at ~300 bp.

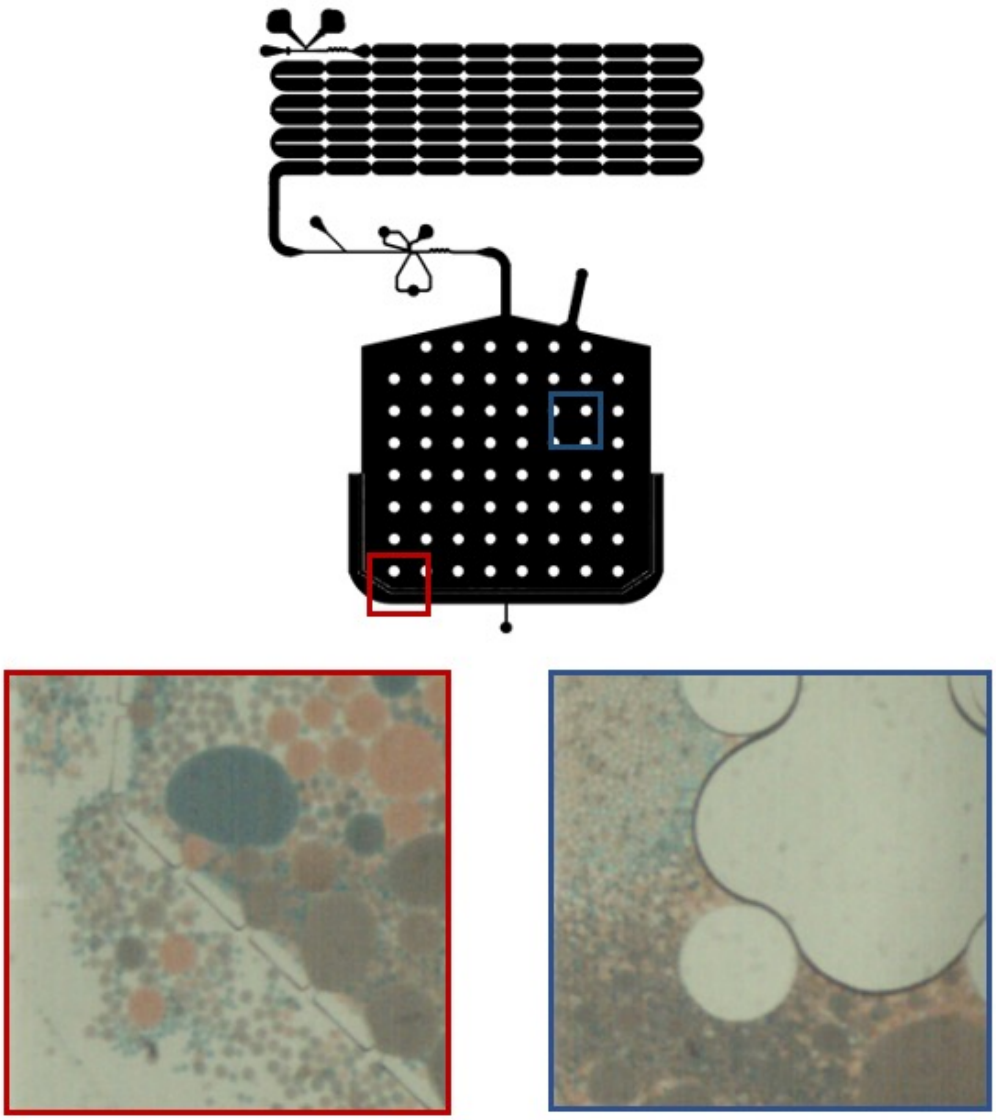

Appendix Figure C.4: Schematic of the MNase module with additional incubation chamber to incorporate the assembly of the three-tier immunoprecipitation unit on device. Practical challenges arose with this initial design. Treating the chamber with aquapel to produce a hydrophobic coating proved challenging as it could not be equally distributed. Additionally, the barrier meant to keep droplets contained within the chamber, while the carrier oil proceeded to waste, did not contain the droplets, and they proceeded to travel into the waste stream.

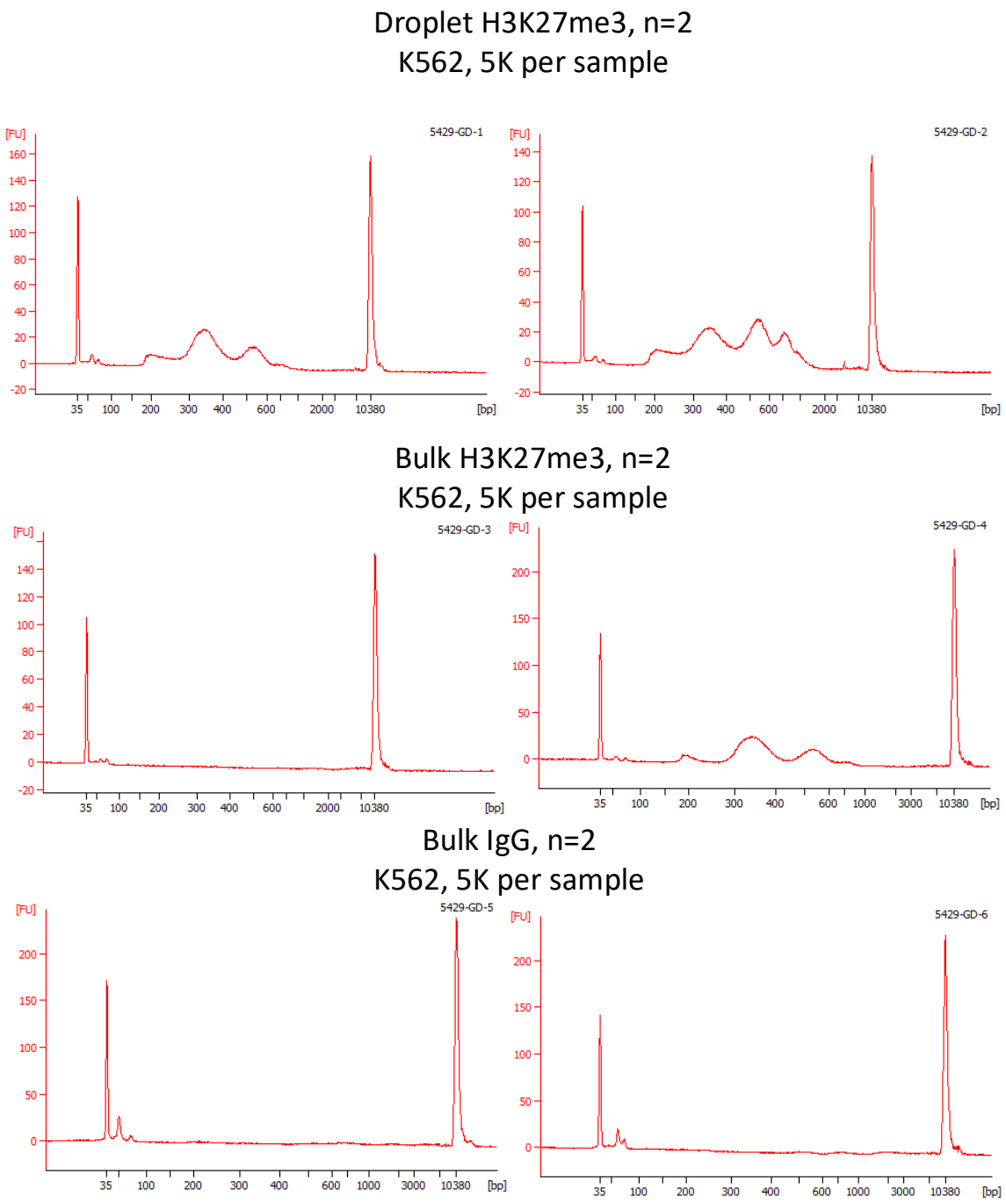

Appendix Figure C.5: Chromatin digestion profiles for DropCUTT with 5,000 K562 cells per sample. The target of interest was H3K27me3 (n=2). Additional bulk (n=2) and IgG (n=2) controls were run in parallel. Utilizing 5,000 cells per sample produced a product peak at ~300bp for the droplet-processed samples. However, results were inconsistent for the bulk samples.

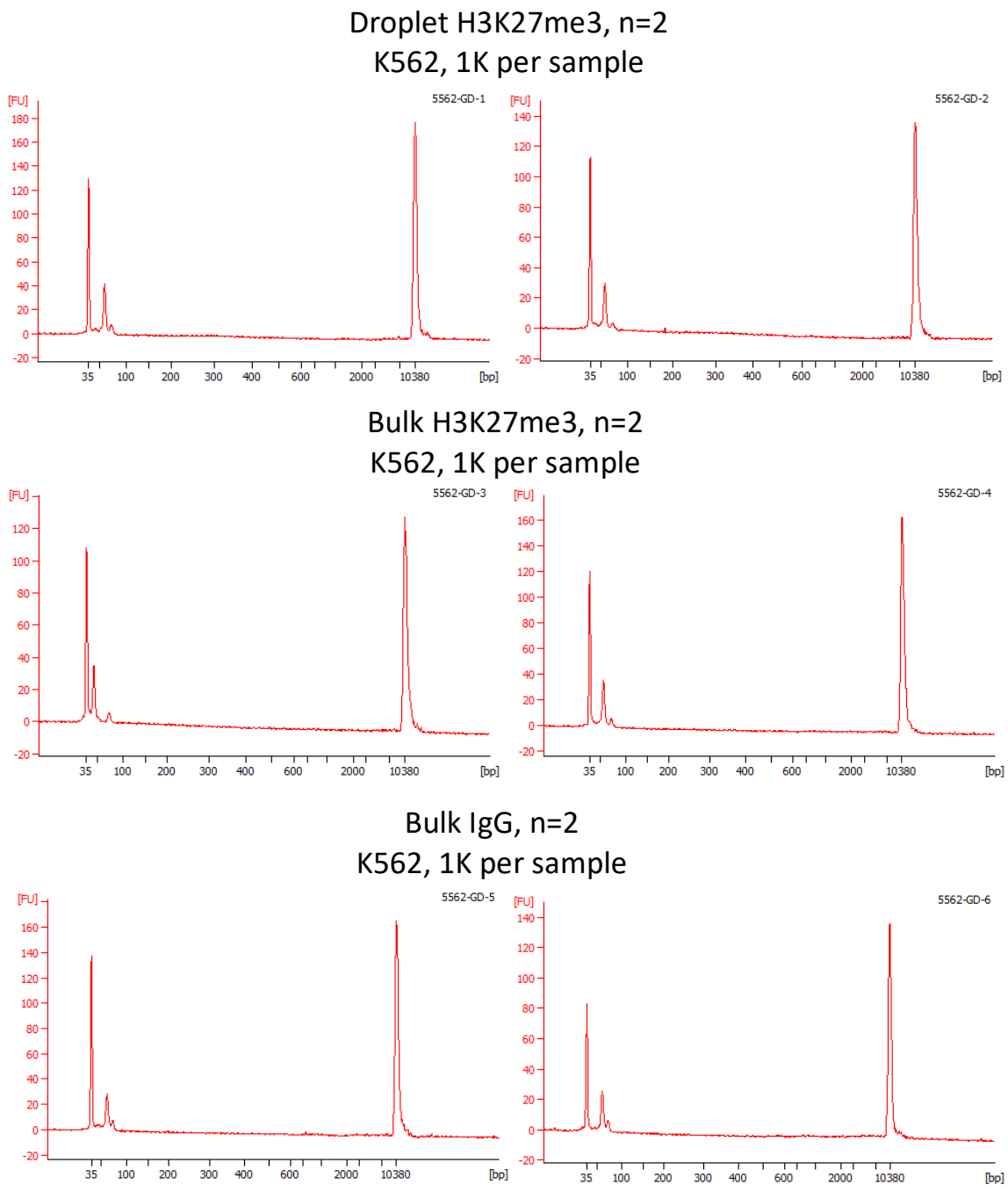

Appendix Figure C.6: Digestion profiles for DropCUTT with 1,000 K562 cells per sample. Utilizing this number of cells for both the droplet and bulk methods is not enough to yield the appropriate fragmentation patter or product peak. The target of interest was H3K27me3 (n=2), additional bulk (n=2) and IgG (n=2) controls were run in parallel.

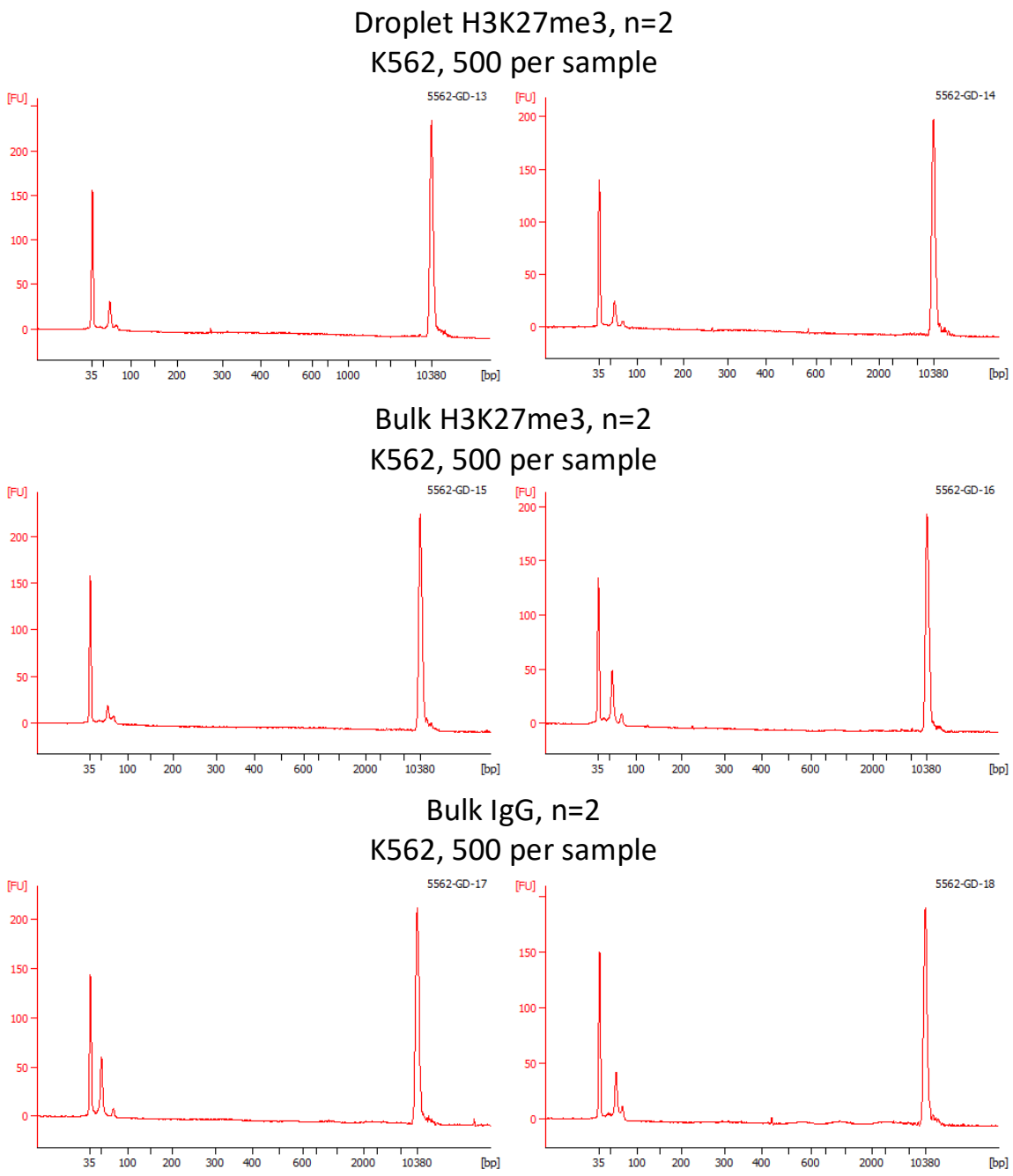

Appendix Figure C.7: Digestion profiles for DropCUTT with 500 K562 cells per sample. Utilizing this number of cells for droplet and bulk methods is insufficient to yield tagmented DNA of the appropriate fragmentation or product peak. The target of interest was H3K27me3 (n=2), additional bulk (n=2) and IgG (n=2) controls were run in parallel.

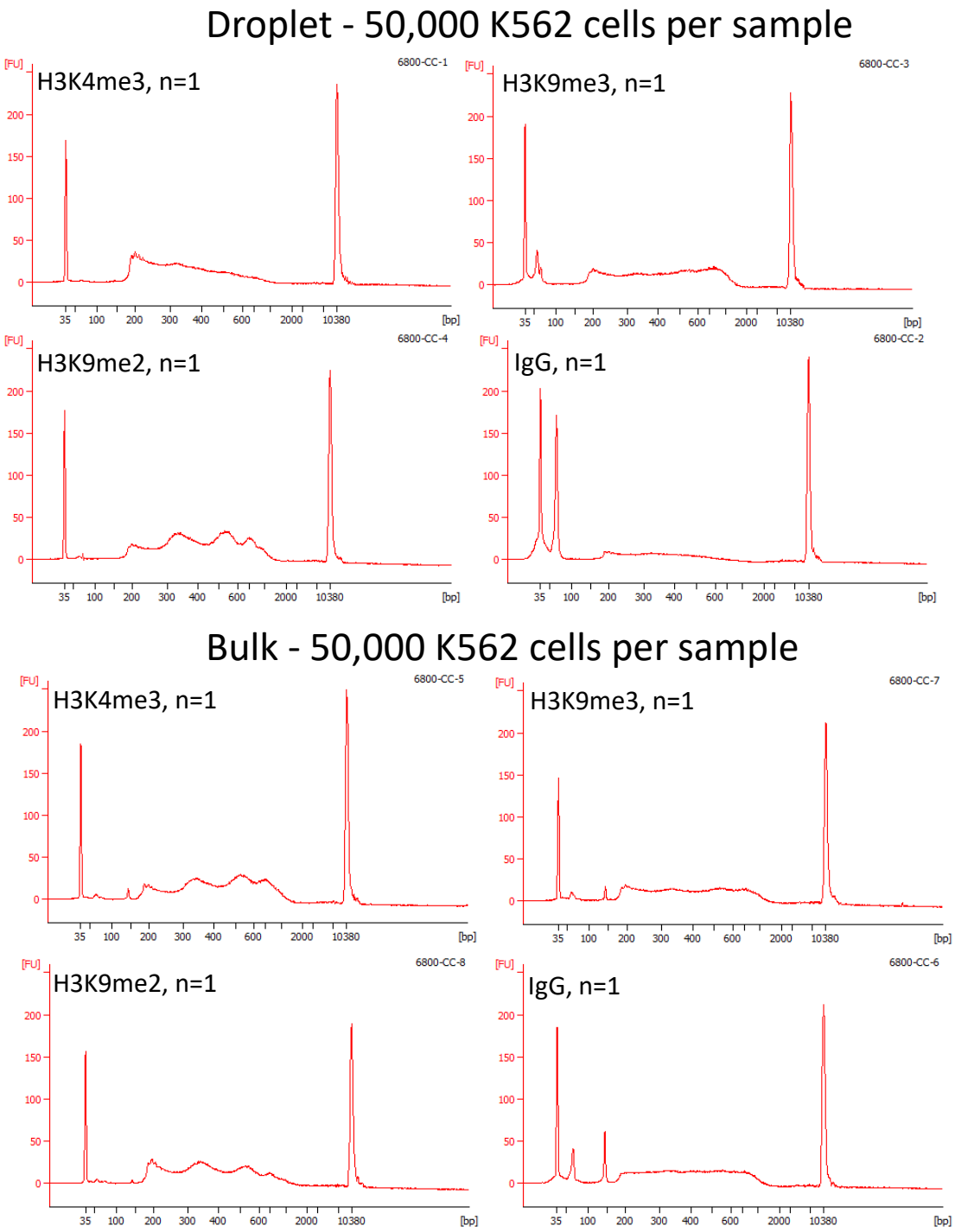

Appendix Figure C.8: Electrophoresis patterns for additional targets profiled with DropCUTT. Each sample contained 50,000 K562 cells and the targets of interest included H3K4me3 (n=1), H3K9me2 (n=1), and H3K9me3 (n=1), additional bulk (n=1) and IgG (n=1) controls were run in parallel. While it is promising that all three targets profiled have product peaks at ~300 bp, additional optimizations are needed.

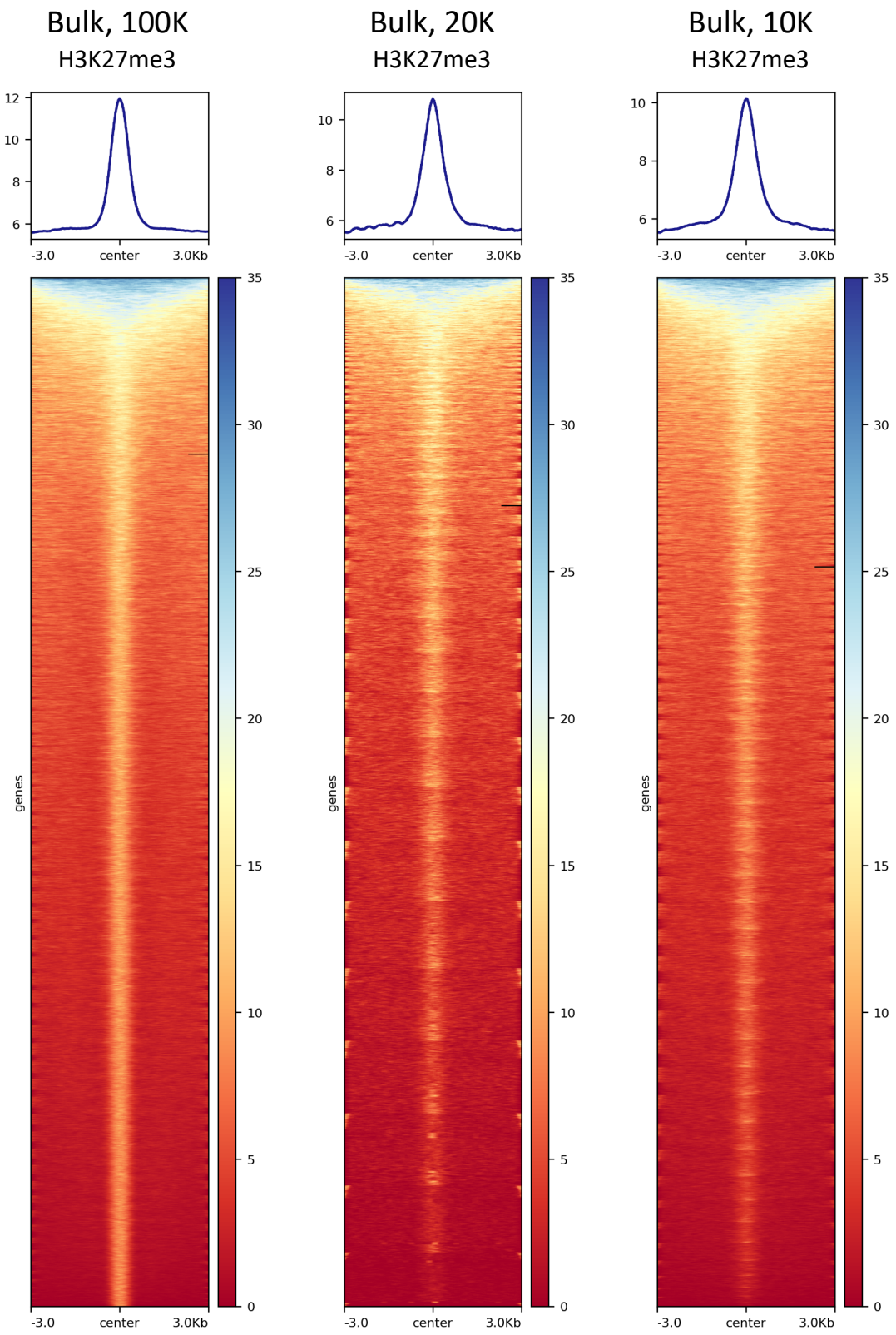

Appendix Figure C.9: Heat maps for the bulk sample process (100K, 20K, 10K per sample) depict the peak distribution for each sample in a 6 kb window. Legend portrays peak intensity.

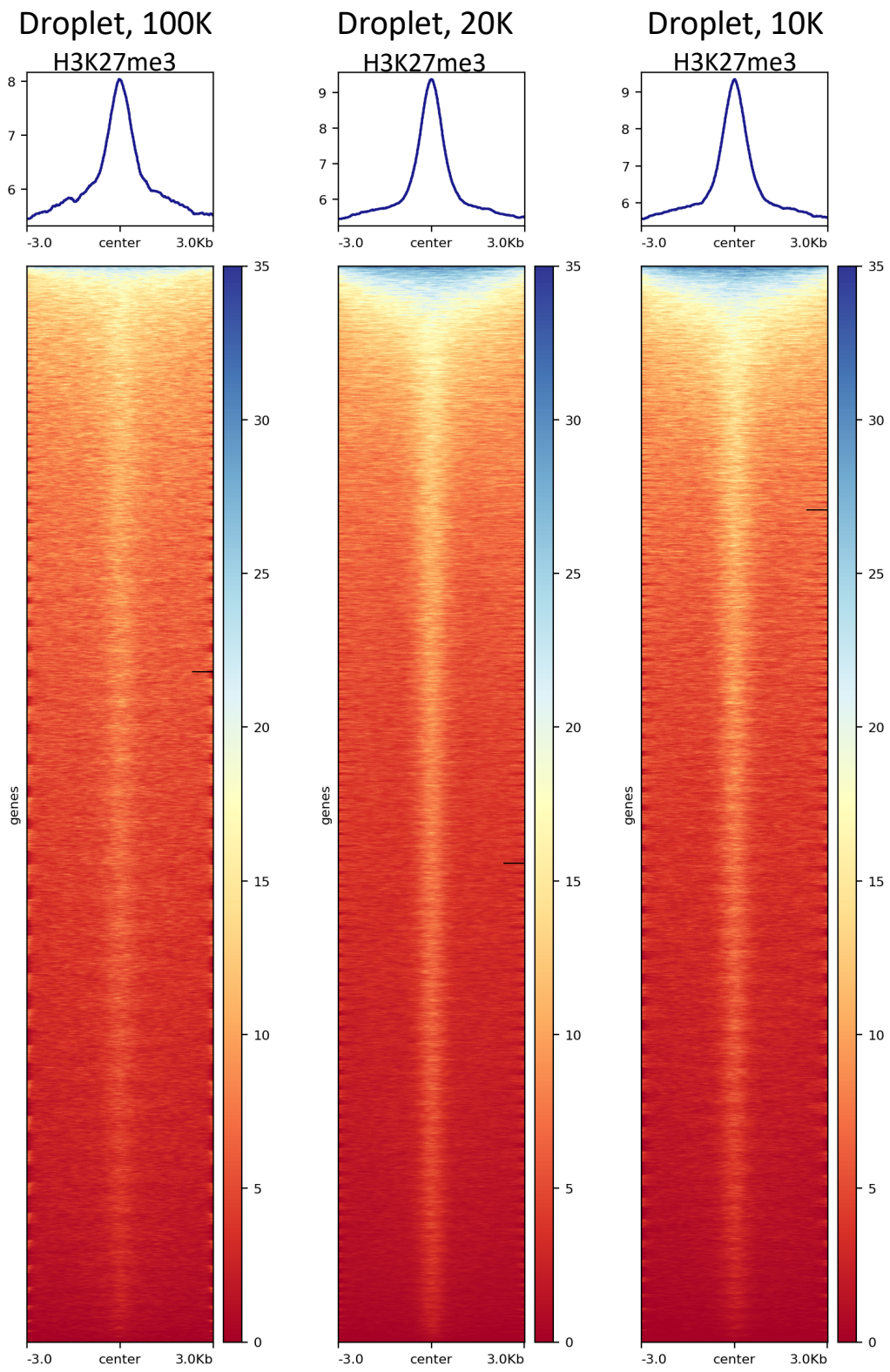

*Appendix Figure C. 10: Heat maps for the **droplet** sample process (100K, 20K, 10K per sample) depict the peak distribution for each sample in a 6 kb window. Legend portrays peak intensity.*

i5 Adaptors	Sequence	Barcode
i5_1	AATGATACGGCGACCACCGAGATCTACACTAGATCGCTCGTCGGCAGCGTCAGATGTGTAT	CTAGATCG
i5_1.2	AATGATACGGCGACCACCGAGATCTACACCTCTCTATTCGTCGGCAGCGTCAGATGTGTAT	CTCTCTAT
i5_1.3	AATGATACGGCGACCACCGAGATCTACACTATCCTCTTCGTCGGCAGCGTCAGATGTGTAT	TATCCTCT
i5_1.4	AATGATACGGCGACCACCGAGATCTACACAGAGTAGATCGTCGGCAGCGTCAGATGTGTAT	AGAGTAGA
i5_1.5	AATGATACGGCGACCACCGAGATCTACACGTAAGGAGTCGTCGGCAGCGTCAGATGTGTAT	GTAAGGAG

Appendix Table C.1: Sequences for i5 indexes along with their specific barcodes. Different combinations of primers were used to obtain sequencing data for Chapter 4.

i7 Adaptors	Sequence	Barcode
i7_1	CAAGCAGAAGACGGCATACGAGATTCGCCTTAGTCTCGTGGGCTCGGAGATGTG	TCGCCTTA
i7_2	CAAGCAGAAGACGGCATACGAGATCTAGTACGGTCTCGTGGGCTCGGAGATGTG	CTAGTACG
i7_3	CAAGCAGAAGACGGCATACGAGATTTCTGCCTGTCTCGTGGGCTCGGAGATGTG	TTCTGCCT
i7_4	CAAGCAGAAGACGGCATACGAGATGCTCAGGAGTCTCGTGGGCTCGGAGATGTG	GCTCAGGA
i7_5	CAAGCAGAAGACGGCATACGAGATAGGAGTCCGTCTCGTGGGCTCGGAGATGTG	AGGAGTCC
i7_6	CAAGCAGAAGACGGCATACGAGATCATGCCTAGTCTCGTGGGCTCGGAGATGTG	CATGCCTA
i7_7	CAAGCAGAAGACGGCATACGAGATGTAGAGAGGTCTCGTGGGCTCGGAGATGTG	GTAGAGAG
i7_8	CAAGCAGAAGACGGCATACGAGATCCTCTCTGGTCTCGTGGGCTCGGAGATGTG	CCTCTCTG
i7_9	CAAGCAGAAGACGGCATACGAGATAGCGTAGCGTCTCGTGGGCTCGGAGATGTG	AGCGTAGC
i7_10	CAAGCAGAAGACGGCATACGAGATCAGCCTCGGTCTCGTGGGCTCGGAGATGTG	CAGCCTCG
i7_11	CAAGCAGAAGACGGCATACGAGATTGCCTCTTGTCTCGTGGGCTCGGAGATGTG	TGCCTCTT
i7_12	CAAGCAGAAGACGGCATACGAGATTCCTCTACGTCTCGTGGGCTCGGAGATGTG	TCCTCTAC
i7_2.13	CAAGCAGAAGACGGCATACGAGATCAGATCCAGTCTCGTGGGCTCGGAGATGTG	TGGATCTG
i7_2.14	CAAGCAGAAGACGGCATACGAGATACAAACGGGTCTCGTGGGCTCGGAGATGTG	CCGTTTGT
i7_2.15	CAAGCAGAAGACGGCATACGAGATACCCAGCAGTCTCGTGGGCTCGGAGATGTG	TGCTGGGT
i7_2.16	CAAGCAGAAGACGGCATACGAGATCCCAACCTGTCTCGTGGGCTCGGAGATGTG	AGGTTGGG
i7_2.17	CAAGCAGAAGACGGCATACGAGATCACCACACGTCTCGTGGGCTCGGAGATGTG	GTGTGGTG
i7_2.18	CAAGCAGAAGACGGCATACGAGATGAAACCCAGTCTCGTGGGCTCGGAGATGTG	TGGGTTTC
i7_2.19	CAAGCAGAAGACGGCATACGAGATTGTGACCAGTCTCGTGGGCTCGGAGATGTG	TGGTCACA
i7_2.20	CAAGCAGAAGACGGCATACGAGATAGGGTCAAGTCTCGTGGGCTCGGAGATGTG	TTGACCCT
i7_2.21	CAAGCAGAAGACGGCATACGAGATTGTCCGCGGTCTCGTGGGCTCGGAGATGTG	CGCGGACA
i7_2.22	CAAGCAGAAGACGGCATACGAGATATATGGAAGTCTCGTGGGCTCGGAGATGTG	TTCCATAT
i7_2.23	CAAGCAGAAGACGGCATACGAGATAACGAATTGTCTCGTGGGCTCGGAGATGTG	AATTCGTT
i7_2.24	CAAGCAGAAGACGGCATACGAGATTCGACGCCGTCTCGTGGGCTCGGAGATGTG	GGCGTCGA
i7_2.25	CAAGCAGAAGACGGCATACGAGATCACTTTGTGTCTCGTGGGCTCGGAGATGTG	ACAAAGTG
i7_2.26	CAAGCAGAAGACGGCATACGAGATTTCAAGTAGTCTCGTGGGCTCGGAGATGTG	TACTTGAA
i7_2.27	CAAGCAGAAGACGGCATACGAGATGCTATCACGTCTCGTGGGCTCGGAGATGTG	GTGATAGC
i7_2.28	CAAGCAGAAGACGGCATACGAGATAATCTACTGTCTCGTGGGCTCGGAGATGTG	AGTAGATT
i7_2.29	CAAGCAGAAGACGGCATACGAGATCCGGCAATGTCTCGTGGGCTCGGAGATGTG	ATTGCCGG
i7_2.30	CAAGCAGAAGACGGCATACGAGATCTTAGCAAGTCTCGTGGGCTCGGAGATGTG	TTGCTAAG

Appendix Table C.2: Sequences for i7 indexes along with their specific barcodes. Different combinations of primers were used to obtain sequencing data for Chapter 4.